1-1-1989

Optical imaging of IRAS galaxies : the evolution of infrared- bright galaxies.

Beverly Joy Smith
University of Massachusetts Amherst

OPTICAL IMAGING OF IRAS GALAXIES:
THE EVOLUTION OF INFRARED-BRIGHT GALAXIES

A Dissertation Presented

by

BEVERLY JOY SMITH

Submitted to the Graduate School of the

University of Massachusetts in partial fulfillment

of the requirements for the degree of

Doctor of Philosophy

February, 1989

Department of Physics and Astronomy

OPTICAL IMAGING OF IRAS GALAXIES: THE EVOLUTION OF INFRARED-BRIGHT GALAXIES

A Dissertation Presented

by

BEVERLY JOY SMITH

Approved as to style and content by:

Susan G. Kleinmann

Susan G. Kleinmann, Chair

Suzan Edwards, Member

Barry R Holstein

Barry Holstein, Member

David van Blerkom

David van Blerkom, Member

Judith S. Young

Judith Young, Member

Robert B Hallock

Robert Hallock, Department Head

Department of Physics and Astronomy

Acknowledgements

There are many people whom I would like to thank—first, and most importantly, my advisor, Susan Kleinmann, who was always ready with suggestions, and encouragement, and a joke; who always seemed to have time no matter how busy she was. She made this thesis possible. The other members of my committee, Judy Young, David van Blerkom, Suzan Edwards, and Barry Holstein, also have given me many helpful suggestions on this project.

I am indebted to John Huchra for providing me with redshifts, and to Jim Condon, for the use of his computer code. I am also grateful to the staff at Kitt Peak for their help over the years, especially Dean Hudek, George Wills, Jeannette Barnes, and Ed Anderson. I would also like to give thanks to Linda and Lowell Tacconi-Garman, who set up the word processor macro which made printing this out easy, and to Steve Resch, for his patient help in measuring positions on the Grant Machine. I would like to thank Beth Berry, Steve Lord, and my father Robert Smith for their careful reading of this thesis, and also Nick Devereux and Steve Schneider for helpful comments. I am also grateful to Sally Rule, Denise Kuzmeskus, Jackie Golonka, Terry Gryzbowski, and Sandy Ostrowski for all their help with travel forms and other miscellaneous details. I would also like to thank all the wonderful people I have met in this department, and my parents for all their encouragement.

This work was supported in part by AFOSR grants #85-0057, and #88-0070 the general investigator program at IPAC, and a Sigma Chi grant-in-aid of research.

ABSTRACT

OPTICAL IMAGING OF IRAS GALAXIES:

THE EVOLUTION OF INFRARED-BRIGHT GALAXIES

FEBRUARY 1989

BEVERLY JOY SMITH, B.A., BROWN UNIVERSITY

Ph.D., UNIVERSITY OF MASSACHUSETTS

Directed by: S.G. Kleinmann

Gravitational interactions play an important role in galaxy evolution, both in causing rapid structural changes in individual galaxies, and in changing the overall properties of galaxies over the age of the Universe. Galaxy interactions have also been linked to high far-infrared luminosities and Seyfert activity. In this thesis, the relationship between far-infrared luminosity and interactions is explored by means of an I-band CCD imaging survey of a 60 μm flux-limited sample of 275 galaxes. The galaxies in this sample are classified as interacting or non-interacting based on the information in these images. The definition of an interacting pair used here is: the companion galaxy must have at least 1/4 the I–band luminosity of the infrared galaxy, the separation between the two must be less than three times the larger radius, and the velocity difference for the two galaxies must be less than 500 km/s. It is found that 56 of these galaxies are interacting, 198 are non-interacting, and 21 are ambiguous. The interacting galaxies have an average 60 μm luminosity of ~6 times that of the non-interacting galaxies, consistent with numerical models of interacting galaxies.

The 60 μm luminosity functions $\phi(L)$ of interacting galaxies and of non-interacting galaxies are then derived. Non-interacting galaxies dominate the luminosity function at low luminosities, while interacting dominate at high luminosities. The luminosity function of non-interacting galaxies drops off fairly steeply at $L > 10^{10}L_o$ ($\phi(L) \propto L^{-2.1}$), while that of interacting galaxies is flatter ($\phi(L) \propto L^{-1.2}$). There are ~5 times as many non-interacting galaxies as interacting galaxies having L(60) > L(MILKY WAY), and ~100 times more having $L(60) > 2 \times 10^8 L_o$. The derived luminosity functions of interacting and non-interacting galaxies are used to predict 60 μm source counts in deeper surveys.

Assuming the I-band light ratio approximates the mass ratio, the 60 μm luminosity is compared with mass ratio and with pair separation. It is found that the mean luminosity of pairs with separation greater than 3 times the radius is similar to that of galaxies without bound companions, suggesting that encounters between galaxies with separations greater than three times the radius do not greatly enhance the star formation rate. Additionally, low mass companions (m_1/m_2) are not found to greatly enhance the far-infrared luminosity.

TABLE OF CONTENTS

LIST OF TABLES

LIST OF FIGURES

CHAPTER I

INTRODUCTION

A. Overview

The role played by gravitational interactions between galaxies in the evolution of galaxies is just starting to be understood. Galaxy interactions have been cited as the cause of such varied phenomenon as galaxy bridges and tails (Toomre and Toomre 1972), Seyfert activity (Roos 1981; Kennicutt and Keel 1984), star formation bursts (Larson and Tinsley 1977; Condon *et al.* 1982; Bushouse 1986), high far-infrared luminosity (Lonsdale *et al.* 1984), and efficient use of the available gas supply in star formation (Young *et al.* 1986; Sanders *et al.* 1986). Interactions and mergers have also been suggested as a reason for statistical evolution of the properties of extragalactic sources, for example, the transformation of spirals into ellipticals by means of merging galaxies (Toomre 1977), the observed evolution of quasars (Roos 1985), and the evolution of the far-infrared luminosity function $\phi(L)$ of galaxies (Hacking, Condon, and Houck 1987; hereafter HCH). The luminosity function is defined as the number density of galaxies per magnitude as a function of luminosity.

In this thesis, the relationship between far-infrared luminosity and interactions is investigated by means of a detailed study of a 60 μm selected sample of galaxies. To classify the galaxies as interacting or non-interacting, optical images in a deep red color (I–band, $\lambda_{eff} \sim 8500Å$) were obtained using the Kitt Peak 2.1m telescope.

These images are necessary because the Palomar Observatory Sky Survey (POSS) plates have too poor spatial resolution to determine whether the galaxies are interacting or non-interacting. The galaxies in the sample are classified as interacting or non-interacting based on the information in these images, and the 60 μm luminosity functions of interacting galaxies and of non-interacting galaxies are derived. Finally, these luminosity functions are applied in the evolutionary models by HCH.

A study of this nature became possible when the Infrared Astronomical Satellite (IRAS) was launched in 1983, giving an unbiased view of the infrared sky for the first time. Thus, this introduction opens with a discussion of previous IRAS results on galaxies. Then, previous work on the evolution of infrared galaxies is discussed, followed by an outline of this project.

B. Review of IRAS Results on Galaxies

IRAS was launched in January 1983 and operated until November 1983, when the cryogenic helium supply used to cool the telescope was depleted. The satellite contained a 0.6m telescope, and had detectors that operated at four wavelengths: 12, 25, 60, and 100 μm. The IRAS *Point Source Catalog* (1985; hereafter PSC) contains ~150,000 stars, ~22,000 galaxies, and ~70,000 non-stellar galactic objects. It is complete to ~0.6 Jy at 60 μm for point source objects (Chester 1985).

Initial analyses of the IRAS data showed that the sources detected at 12 and 25 μm were mostly stars, those at 60 μm were predominantly galaxies, while the majority of high latitude sources at 100 μm were due to interstellar dust in the Milky Way (Rowan-Robinson *et al.* 1984). The ratio of the far-infrared fluxes (25 μm/60 μm, 60 μm/100 μm) differs dramatically for stars and galaxies. Figure 1, reproduced from Smith, Kleinmann, Huchra, and Low (1987; hereafter SKHL), shows the location in the log (F(100)/F(60))–log (F(60)/F(25)) plane of the 86 objects in a 60 μm flux-limited sample. Stars generally have flux densities which decrease with increasing wavelength, while the flux densities of galaxies tend to increase with increasing wavelength.

Most of the galaxies detected by IRAS were found to be spirals, irregulars, or peculiar galaxies; relatively few elliptical galaxies were detected (de Jong *et al.* 1984). The infrared emission from galaxies has generally been attributed to the absorption and re-radiation by interstellar dust grains of optical and ultraviolet photons originating from O and B stars (*c.f.*, Rieke and Lebofsky 1979). Thus, the far-infrared flux has been used as a measure of recent star formation in normal galaxies (Young *et al.* 1986). In Seyfert galaxies and in quasars, contributions to the ultraviolet radiation field from an active nucleus may also be significant (Miley, Neugebauer, and Soifer 1985). It has been suggested that active nuclei may also contribute to the infrared flux in the most infrared-luminous galaxies discovered by

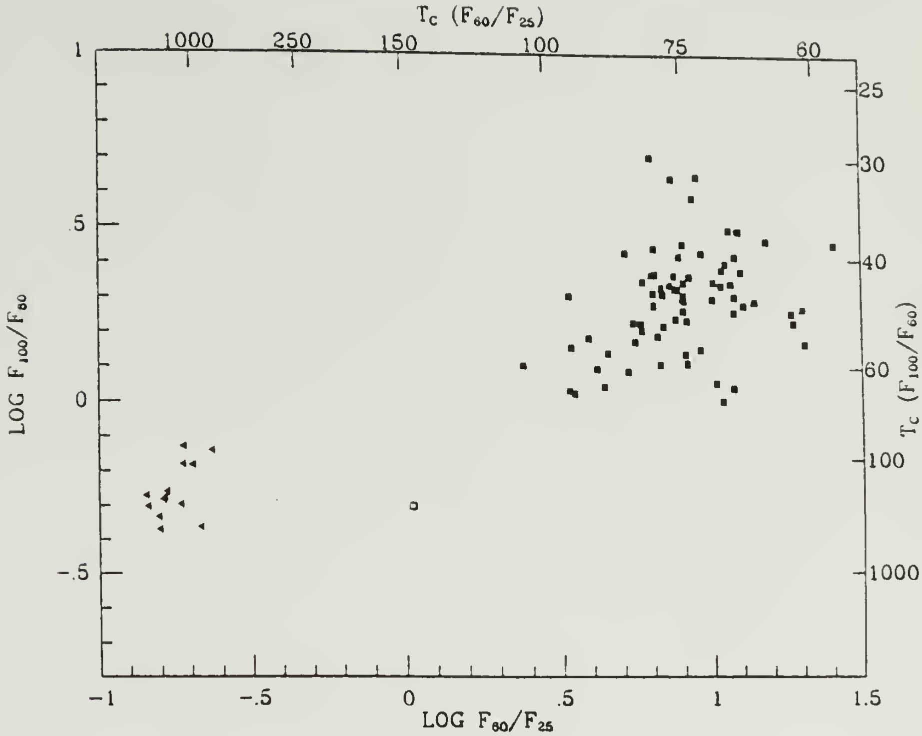

Figure 1. The location in the log (F(100)/F(60))–log (F(60)/F(25)) plane of the 86 objects in a 60 μm flux-limited sample. This Figure is reproduced from SKHL. The filled squares are galaxies, the triangles are stars, and the open square is a planetary nebula. This Figure also gives a color temperature corresponding to each flux ratio, calculated by fitting the two relevant flux densities to a blackbody.

IRAS, even when no optical signature of Seyfert or quasar activity is present (Becklin 1986; Becklin and Wynn- Wynn-Williams 1986; DePoy 1986).

Several groups of researchers (SKHL; Lawrence *et al.* 1986; Soifer *et al.* 1986, 1987; Vader and Simon 1986) have derived the 60 μm luminosity function $\phi(L)$ of galaxies. SKHL found that high luminosity galaxies tend to be found in pairs, while low luminosity galaxies are generally isolated spirals. This led to their suggestion that the galaxies which form the 60 μm luminosity function come from two distinct populations, normal spiral galaxies and interacting galaxies. Further, ~35% of a complete 60 μm flux-limited sample of galaxies are interacting, compared to ~6% of an optically selected sample (Lonsdale *et al.* 1984). This is probably due to induced star formation in interactions, as interacting galaxies have anomalous optical colors (Larson and Tinsley 1978), higher Hα fluxes than isolated galaxies (Bushouse 1986), and higher $L(IR)/M(H_2)$ than isolated galaxies (Young *et al.* 1986; Solomon and Sage 1988). Interactions may also induce non-thermal nuclear activity (Kennicutt and Keel 1984), which may also increase the far-infrared luminosity.

C. Previous Studies on the Evolution of IRAS Galaxies

In addition to the full sky survey, IRAS made deeper, pointed observations in selected regions of the sky. The full sky survey provides a measure of $\phi(L)$ in the local Universe (a galaxy of luminosity $10^{10} L_o$ can be seen to 250 $(100/H_o)$ Mpc or z = 0.05 at the limit of the PSC, where H_o is the Hubble constant); the pointed observations can be used to study the change in $\phi(L)$ with increasing redshift.

Previously, searches for evolution of extragalactic sources have been done using optical (Koo 1985; 1986), radio (Schmidt 1972a, b, c; Condon 1984), near-infrared (Lebofsky and Eisenhart 1986; Eisenhart and Lebofsky 1987), and X-ray (Stocke *et al.* 1983; Gioia *et al.* 1984) surveys. The availability of the IRAS data has now made it possible to measure the evolution of a far-infrared selected sample. An IRAS sample has an advantage over optical surveys because of uniform sky coverage, insensitivity to reddening, insensitivity to surface brightness gradients, high characteristic luminosity L_*, and sensitivity to interactions.

The deepest 60 μm survey available at present was obtained from over 1000 IRAS scans of a 6.25 deg^2 region near the north ecliptic pole (Hacking and Houck 1987). Co-addition of this data and point source extraction yielded a sample of 98 objects to a flux limit of F(60) ~ 50 mJy, ten times fainter than the PSC. They estimate that this sample is ~80% complete at 50 mJy. They found that 80% of the 60 μm sources have an optical galaxy visible on the POSS plates ($B \leq 18^1/2$) within the IRAS error box. The other 20% of the sources may be optically faint galaxies below the level of the POSS plates. The average infrared-selected galaxy has L(60)/L(B) ~ 3 (Soifer *et al.* 1984), thus, at F(60) ~50–100 mJy, it would have B ~ 18. This suggests that galaxies with high L(IR)/L(B) such as those discovered by Houck *et al.* (1985) would not be visible on the POSS plates at these 60 μm flux levels. However, there is also a possibility that some of these sources are actually galactic dust clouds. These clouds, generally called infrared cirrus (Low *et al.* 1984), mimic the infrared colors of galaxies, and dominate the sky at 100 μm. Cirrus also appears at 60 μm. Hacking and Lonsdale (1989) are currently undergoing an optical spectroscopy survey of the sources in this survey, to determine optical identification and redshifts. The Hacking and Houck (1987) sample is confusion-limited, meaning that a 60 μm survey made with the IRAS beamsize could not go to levels fainter than ~50 mJy, because sources will not be resolved (Hacking 1987).

HCH compared this data with results of four different evolutionary models. The models used include one in which it is assumed that no evolution occurs, two in which it is assumed that the density (but not the luminosity) of galaxies evolves, and one in which it is assumed that only the luminosity evolves. Pure density evolution assumes that only the density of galaxies varies with redshift; the luminosities, spectral energy distributions, and the shape of the luminosity function do not change. The density evolution models assume that $\phi(L,z) = \phi(L,z{=}0)(1+z)^n$, where n = 6 and 7, respectively. A choice of n = 6 is deduced from a collision model with relative velocities between galaxies that remain constant with time, and n = 7 is derived from a collision model where relative velocities decrease with the expanding universe (HCH). Their luminosity evolution model is the best-fit evolutionary model to radio galaxy source counts from Condon (1984); in this case, the luminosity varies with redshift, but the shape of the luminosity function does not change. This is expressed by $\phi(L,z) = \phi(\frac{L}{(1+z)^n},z{=}0)$, where n = −4 for radio galaxies.

HCH found that the 60 μm galaxy counts are a factor of two higher than the non-evolving model would predict, using H_o = 100 km/s/Mpc. The density evolution models fall slightly below the source counts, while the results of luminosity evolution lie slight above the source counts.

D. This Study

If a higher density of interacting and merging galaxies in the early universe is assumed (Toomre 1977; Roos 1985), and far-infrared emission is linked to interactions and mergers, the excess 60 μm source counts seen in the Hacking and Houck (1987) sample may be due to an increase in the number of interactions and mergers with lookback time. However, the contributions of non-interacting galaxies to the deep source counts must be taken into account, independently of the change in the merger rate of galaxies. HCH did not separate the effects of interacting and non-interacting galaxies on the source counts, because the relative contributions of interacting and of non-interacting galaxies to the local 60 μm luminosity function were unknown. In the present study, the local 60 μm luminosity function is separated into that of interacting galaxies and that of non-interacting galaxies, by using I–band imaging to distinguish interacting galaxies. These two contributions are then treated differently in a revised version of the HCH evolutionary model, in that the luminosity function of non-interacting galaxies is kept constant, while that of interacting galaxies is evolved.

The assumption that the non-interacting galaxy component does not evolve rapidly is justified by noting that the average isolated galaxy has a 60 μm luminosity of $10^{10}L_{o}$, and thus would lie at a redshift of ~0.15 at the 50 mJy flux limit of the deepest IRAS survey (Hacking and Houck 1987). Optical studies (Butcher and Oemler 1984; Koo 1985) show little evidence for a change in the optical colors of galaxies within this redshift range, suggesting little systematic change in the stellar population and in average star formation rate. Thus one would expect that the far-infrared properties also are not changing over the epoch that these galaxies are visible to IRAS.

The evolution of the merger rate of galaxies is expected to be a fairly steep function of redshift, with $\rho(\text{mergers}) \propto (1 + z)^n$, where $n \cong 5-7$ (Toomre 1977; Roos 1985; HCH). A galaxy at the average luminosity of the interacting galaxies in this sample would lie at z ~ 0.4 at the Hacking and Houck (1987) 50 mJy limit. At this redshift, the density of interacting galaxies is thus predicted to increase by a factor of ~5–10 from the local value.

To separate interacting galaxies from non-interacting galaxies, it was first necessary to obtain high quality images for a flux-limited sample. Apparent blue magnitudes for the galaxies in the SKHL sample ranged from 12th to 19th magnitude, with optical diameters from several arcminutes to 5 arcseconds, thus it was not always possible to determine structure from the POSS plates. This motivated the current study, a deep I-band (λ_{eff} ~ 8500Å) imaging survey of a complete 60 μm flux-limited sample of 275 galaxies, using the Kitt Peak 2.1m telescope. This deep red filter is an optimum means of measuring the mass distribution, as I-band emission generally traces the old stellar population and is less affected by extinction than shorter wavelength emission (Boroson, Strom, and Strom 1983; Schweizer 1976). Further, recent studies (Bothun *et al.* 1988; Pierce and Tully 1988) show that the Tully-Fisher relationship (Tully and Fisher 1977), which relates absolute magnitude to HI line width, is as good or better in I-band than in B ($\lambda_{eff} \sim 4400$Å) or H ($\lambda_{eff} \sim 1.6\ \mu m$) band, supporting the use of I-band to trace the mass in a galaxy. The Tully-Fisher relationship is based on the fact that the HI line width is a function of the kinematic mass of a galaxy.

These images provide evidence of interaction, and make it possible to classify the galaxies into two groups, interacting and non-interacting. The working definition of an interacting galaxy pair used here is: the companion galaxy must have at least 1/4 the I–band luminosity of the infrared galaxy, the separation between the two must be less than three times the larger radius, and the velocity difference for the two galaxies must be less than 500 km/s. Redshifts for these galaxies were obtained from the literature or were provided by J. Huchra (private communication), and improved IRAS photometry was obtained from the Add Scan Program at the Infrared Processing and Analysis Center (IPAC). Two luminosity functions are then constructed. These luminosity functions are then used in conjunction with the model from HCH to model the deep IRAS source counts.

The organization of this thesis is as follows: Chapter II discusses the galaxy sample selection, the observations, and the data. A detailed discussion of the definition of interaction follows in Chapter III, and the sample galaxies are classified accordingly. Examples of different kinds of galaxies are also shown in Chapter III. In Chapter IV, the definition of interaction is statistically tested, by examining the range of far-infrared luminosities as a function of interaction parameters, and the separated luminosity function is given. The model is then discussed in Chapter V, and compared with the the HCH models and the deep IRAS data. Finally, the conclusions are given in Chapter VI.

CHAPTER II

THE SAMPLE AND OBSERVATIONS

A. The Sample

The sample consists of the 275 galaxies brighter than 2 Jy at 60 μm which lie in the regions listed in Table 1. These regions were chosen so as to be out of the galactic plane ($|b^{II}| > 20°$) to minimize confusion with galactic sources, and north of $\delta = -20°$, to be observable from Kitt Peak. The survey covers 5078 deg^2 of the sky. These regions do not contain any of the major local galaxy clusters, such as Coma, Hercules, or Virgo. Thus, the surface density of galaxies, 0.055 ± 0.003 deg^{-2}, is lower than the density 0.067 ± 0.003 deg^{-2} for the survey carried out by SKHL of a similar flux-limited sample, because that sample included Coma. For comparison, an extrapolation of the relationship between optical source counts and blue magnitude given by Tyson and Jarvis (1979) shows that a blue magnitude-limited sample complete to $m_B \sim 10.5$ would have an equivalent surface density of ~0.05 deg^{-2}. The infrared sample extends deeper in space; an F(60) > 2 Jy survey has a median redshift of ~5000 km/s (SKHL), while a $m_B \leq 10.5$ sample would have a median redshift of ~600 km/s, extrapolating from Sandage and Tammann (1981).

The galaxies in this sample were selected from two different IRAS catalogs, the PSC (version 2; 1985) and the IRAS Small Scale Structure Catalog (1986; hereafter SSSC). The PSC lists 264 galaxies brighter than 2 Jy in these regions. Stars were avoided by using a flux ratio criteria of F(12) < 3 F(60) in selecting galaxies from these catalogs. For unresolved objects, the PSC is statistically complete to ~0.6 Jy (Chester 1985). However, there is a bias against extended sources: the flux from extended galaxies may be underestimated in the PSC, because the software used to extract point source objects from the raw IRAS data used a point source template with a full width half maximum of 1.5′ at 60 μm (IRAS Explanatory Supplement 1986). This means that some galaxies that should be in this sample may appear in the PSC with F(60) < 2 Jy, or not appear in it at all.

To minimize the incompleteness problem due to extended sources, three different approaches were taken. First, the SSSC was searched. This catalog, derived from the same IRAS satellite data as the PSC, was created with an 8′ template. Use of this catalog in addition to the PSC partially solves the problem of finding extended galaxies missed in the PSC; however, it is not ideal for two reasons. First, the SSSC is not statistically complete at 60 μm flux levels as low as 2 Jy. Second, there is a problem with confusion with galactic objects, as the sources in the SSSC, even at high galactic latitudes, are predominately galactic. The confusing sources are either warm dust clouds emitting in the far-infrared, generally known as galactic cirrus (Low *et al.* 1984), or stellar sources embedded in molecular clouds. For this study, SSSC sources with no optical counterparts on the POSS plates were judged to be cirrus, and were excluded from the sample. This means that if a class of galaxies with low optical surface brightness and high infrared flux exist, and these galaxies subtend angles > 1′ on the sky, they may be erroneously eliminated by this criterion. However, there is no concrete evidence for such a class of galaxies at present; a comprehensive study of the far-infrared properties of galaxies with low optical surface brightness could address this question.

Out of the 299 sources listed in the SSSC above 2 Jy in the selected regions of the sky, only 19 had extragalactic counterparts visible on the POSS plates. Of these, nine were already in the sample, so ten galaxies were added to the sample.

The second approach to the problem of incompleteness was to search two optically selected samples of extended galaxies for galaxies which may have been missed by the SSSC, since the SSSC is not statistically complete to the 2 Jy limit of this study. The first catalogue is the IRAS Atlas of Optically Large Galaxies (Rice *et al.* 1986), which contains the total IRAS fluxes of 85 galaxies with optical diameters greater than 8′ from the *Second Reference Catalogue of Bright Galaxies* (de Vaucouleurs, de Vaucouleurs, and Corwin 1976); the second is an overlapping survey by Young *et al.* (1988), which contains total infrared fluxes of 182 optically bright galaxies with optical diameter $\Theta > 2'$. A search through these catalogs yielded no additional galaxies with F(60) > 2 Jy in the selected regions of the sky.

The third approach was to search an optically-selected catalog (the Uppsala General Catalogue of Galaxies, Nilson 1973; hereafter UGC) for galaxies which appear in the PSC at 60 μm flux densities between 1.5 and 2 Jy. The original IRAS database was used to obtain improved measurements of these galaxies. This was accomplished using the Add-Scan program at the Infrared Processing and Analysis Center (IPAC), which co-adds all the available IRAS data, and makes it possible to obtain the total flux of the galaxy for galaxies with angular sizes less than ~4′. The Add-Scan program gives a one-dimensional scan through a source, obtained by summing all available data. Co-addition also provides more sensitivity, often yielding measurements of the 25 and 12 μm fluxes in cases where only upper limits are listed in the PSC. Add-Scans were obtained for the 45 galaxies which appear in the PSC with 1.5 Jy < F(60) < 2 Jy, are associated with UGC galaxies, lie in the selected regions of the sky, have optical diameters > 1′, and are not in the Young *et al.* (1988) sample. The corrections ranged from 10% to 20%. Four were found to have total 60 μm fluxes > 2 Jy. They were added to the sample, bringing the total sample size to 277.

Add-Scans were also obtained for ~30% of the SSSC and PSC sources in the sample, to check for extended emission and cirrus. For one of the sources which was in the SSSC but not in the PSC, the Add-Scan data showed lower flux densities than the SSSC values (below 2 Jy at 60 μm). Another source appeared in the PSC at F(60) > 2 Jy, but had an integrated Add-Scan value of < 2 Jy. These sources were thus eliminated from the sample, bringing the final sample size to 275 galaxies.

B. Optical Identification and Optical Data

The 275 selected IRAS galaxies are listed in Table 2, along with their PSC positions. This Table also list the PSC associations with optically catalogued galaxies, and the UGC morphological types of these galaxies, when available. In addition, a brief description of the appearance in the I-band images (see Section D) is also given.

Table 3 lists the optical properties of the subset of 140 IRAS galaxies from Table 2 which are either in pairs or are individual galaxies with pronounced tails or distortions, since these may be merger remnants (*c.f.*, Toomre and Toomre 1972). Column 1 gives the PSC name; columns 2–7 give the PSC position, column 8 gives the optical name, if it has been previously catalogued. This Table also gives the optical position of the associated optical galaxies, and the position(s) of its companion(s) in columns 9–14. Column 14 gives each heliocentric velocity; column 15 gives the blue magnitude; and the last column lists the literature reference for the data. For the galaxies with companions visible on the POSS plates, optical positions were obtained from SKHL, Dressel and Condon (1976), Peterson (1973), Kojoian *et al.* (1981), or were measured from the POSS plates using the Grant machine at N.O.A.O. The SKHL and Grant machine measurements have accuracies of ~1"; those of Kojoian *et al.* (1981) are accurate to ~2", and the Dressel and Condon (1976) and Peterson (1973) results are accurate to ~4".

For 79 of the pairs in Table 3, only one optical galaxy lies within the IRAS positional error box (~30" × 10"), thus there is no uncertainty in the optical identification. In these cases, the optical identification has been marked with an asterisk. However, in the remaining 61 cases, two or more optical galaxies lie within the the error box, leading to an uncertainty in the identification of the IRAS source. For 17 of these pairs, follow-up 10 μm observations were made of each galaxy in the pair. When only one of the possible optical sources was detected at 10 μm, that was presumed to be the 60 μm identification. The 10 μm measurements were obtained by S. Willner (private communication), or as part of this study (see Section F). Five galaxies were detected, and are thus assumed to be the optical identification, and are also marked with an asterisk. These galaxies are distinguished in the notes column in Table 3. Note also that, for three resolved pairs, both galaxies in the pair are listed independently in the PSC above 2 Jy, and are thus counted separately in the sample.

In this study, it is assumed that the IRAS flux comes from only one galaxy in a pair when the pair is unresolved by the IRAS beam. To estimate how much error is introduced in the study by this assumption, a study of the relative 60 μm fluxes of galaxies in pairs is needed. From an investigation of an optically-selected set of 133 pairs which were resolved by IRAS, Haynes and Herter (1988) find that in only 14 cases were both galaxies detected by IRAS at 60 μm above the PSC limit of 0.5 Jy, compared to 70 pairs in which only one galaxy was detected. Thus, if these pairs had been unresolved, ~20% of the detected pairs would have had significant contributions to the 60 μm flux from both galaxies. Further, out of the set of resolved pairs in the current study (69 pairs), only 3 pairs have both members above the 2 Jy limit (4%). Also, Joseph *et al.* (1984) found, in a study of 28 interacting pairs, that near-infrared colors suggestive of star formation bursts never appeared in both galaxies in a pair. These results suggest that the assumption that the flux comes from a single galaxy in an unresolved pair may cause errors in the flux in, at most, ~12 cases in the current study, or ~4% of the total sample, if the unresolved pairs are similar to the resolved pairs and to the pairs in these other samples.

In these unidentified cases, the galaxy which is presumed from this study to be the identification is the first one listed. These choices are based on proximity to the IRAS position. In all but one of these cases, both possible optical counterparts fall at the same redshift, so the optical identification is irrelevant in determining the 60 μm luminosity. The one source (IRAS 00537+1337) where the two possible optical counterparts have different redshifts is discussed at length in Chapter III.

Table 3 also gives heliocentric velocities and blue magnitudes for each galaxy. Velocities are from SKHL, Huchra *et al.* (1983), Nilson (1973), Palumbo *et al.* (1983), Sanders *et al.* (1987), J. Huchra (private communication), or from this work (see Section E). Individual references are listed in the last column. All but one of the galaxies identified with infrared sources have redshifts available. This source, IRAS 03521+0028, is discussed at length in Chapter III.

Blue magnitudes for galaxies brighter than m_B = 15.7 magnitudes are from the Zwicky Catalog (Zwicky *et al.* 1961), and are accurate to ~0.3 magnitudes (Huchra 1976). For fainter galaxies, the blue magnitudes are eye estimates from J. Huchra (private communication) and are estimated to be accurate to ± 0.5 magnitudes.

C. Infrared Data

Table 4 lists 12, 25, 60, and 100 μm infrared flux densities for the 275 sample galaxies. At wavelengths where the source is not detected, 3σ upper limits to the fluxes are given. All flux densities were scaled to be consistent with the PSC calibration scale (Helou 1988). Thus, for the galaxies which are common to both the SKHL sample and this sample, the flux densities given here differ slightly from the values listed in SKHL.

The data listed in Table 4 were obtained from the Add Scan program, the PSC, the SSSC, or from the literature. Individual references are listed in the last column. For unresolved sources, the flux density listed in the Table refers to the peak value in the median scan for the Add Scan data. For sources in which the integrated flux density exceeded that of a point source with the same peak flux by 15%, the flux density is the integrated flux density from the median scan.

The flux densities in Table 4 have been corrected to the rest frame of the galaxy (K-corrected), and corrected for the shape of the spectral energy distribution within the IRAS 60 μm bandpass (color-corrected). Table 4 includes the percentage correction to the original flux density. The color-corrections are necessary because the flux densities given in the IRAS catalogs were calculated assuming an intrinsic spectral energy distribution of λ^{-1} within the bandpass. However, for galaxies, the spectral energy distribution is better approximated by a blackbody of temperature of 30K < T < 80K at far-infrared wavelengths. For more details on this correction procedure, see Appendix.

D. CCD Observations and Reductions

I-band images of the sample galaxies were obtained with a Texas Instruments CCD array mounted at the Cassegrain focus of the 2.1m telescope at Kitt Peak National Observatory during the nights of November 13, 17, and 18, 1986, February 5-7, and 9, 1987, and September 12-16, 1987. The images have a field of view of 2.5′ × 2.5′. The data were binned on the chip in 2 × 2 pixel summations, yielding a pixel resolution of 0.39". The chip was preflashed for 5 seconds, to avoid nonlinearity at low flux levels. To avoid non-linearity at high flux levels, integration times were limited so that the peak count from the galaxy would be ~6000 counts. These generally ranged from five to ten minutes. Objects with small angular size were generally observed several times, to search for faint tidal structures at low flux levels. Detailed information on the observations is given in Table 5.

To determine pixel-by-pixel variations in sensitivity, bias frames and dome flats were taken each night. A bias frame is a zero second exposure taken with the shutter closed, to determine the zero level response all over the chip. A dome flat is a short

(15 second) exposure of an illuminated white patch on the inside of the telescope dome. The average bias frame was subtracted from each image, and then the images were divided by the average dome flat. Bad pixels and bad channels were removed from the data by interpolation from surrounding pixels. After cleaning the images, multiple images of an object were added to increase the signal to noise ratio. In this process, the images were registered by centroids of unsatuated stars in the frame.

Fields near globular clusters previously measured by Christian *et al.* (1985) were observed two or three times each night for flux calibration purposes. Each field had ~6 available standard stars. Airmass corrections were determined from comparison of observations at different zenith angles.

Due to the proximity of the moon to many of these fields on the nights that the observations were made, the sky background was often uneven over an image. This lead to decreased calibration accuracy. The dispersion in the calibration of the standard stars in a field was sometimes as large as 0.2 magnitudes. Furthermore, four out of the 12 nights were partially cloudy, so ~20% of the images could not be calibrated at all. However, these images are quite adequate for classifying interacting and non-interacting galaxies, and in determining the relative brightness of galaxies in pairs.

E. Optical Spectroscopy

Optical longslit spectra of a number of companion galaxies to the galaxies in this sample were obtained in order to determine redshifts and confirm physical association with the IRAS source. These were obtained with the Gold Spectrograph CCD Camera on the Kitt Peak 2.1m telescope the night of February 5, 1988. A 300 line/mm grating was used, which provided an effective wavelength coverage of 4806Å to 7675Å, and a spectral resolution of 9.41Å FWHM. To calibrate the wavelength scale, HeNeAr comparison-lamp observations were made at each sky position. The CCD was preflashed for 4 seconds. Radial velocities were determined using the wavelength shift of the galaxy emission lines. The results have been tabulated in Table 3.

F. 10 μm Broadband Photometry Observations

Follow-up 10 μm broadband observations of thirty galaxies were made to confirm optical identifications of IRAS sources. These measurements were obtained using the NASA 3.0m Infrared Telescope Facility (IRTF) on Mauna Kea, Hawaii, February 9 and 10, 1988, using the facility germanium bolometer at the Cassegrain focus. The beam aperture used was 6" and the chopper throw was 30" in the N-S direction. Six standard stars (α Tau, β And, β Gem, μ UMa, α Boo, and α Her) were also observed, in order to calibrate the signal and measure terrestrial absorption, and to check the alignment of the infrared and optical beams. Fluxes of these stars were obtained from Tokunaga (1986). Integration times ranged from 400 to 2800 seconds. The detected galaxies have been identified in Table 3.

Table 1. Regions Covered in Observational Survey

α Range			δ Range		
0^h	–	2^h	0°	–	30°
3^h	–	4^h	0°	–	20°
4^h	–	5^h	0°	–	5°
7^h	–	8^h	50°	–	90°
8^h	–	9^h	23.5°	–	40°
9^h	–	10^h	23.5°	–	50°
10^h	–	11^h	23.5°	–	32.5°
14^h	–	15^h	23.5°	–	32.5°
16^h	–	18^h	23.5°	–	90°
18^h	–	20^h	60°	–	90°
20^h	–	21^h	80°	–	90°
21^h	–	22^h	–10°	–	10°
22^h	–	23^h	–20°	–	20°
23^h	–	24^h	–20°	–	30°

Table 2. Galaxies in Observing Program

IRAS Name	Optical Association	IRAS Position						Classification (UGC)	Appearance on Image
		α			δ				
		h	m	s	°	′	″		
00014+2028	N7817	0	1	24.5	20	28	26	Sb/Sc	S
00047+2725	N1	0	4	42.0	27	25	50	Sb pair with N2	S
00073+2538	N23	0	7	19.3	25	38	47	SBa pair with N26	S
00119+2810	U141	0	11	57.1	28	10	12	SB0a	S
00132+1548	U148	0	13	16.2	15	48	40	S	S
00141+0647	U155	0	14	9.5	6	47	54	S	S
00151+1110	N63	0	15	9.0	11	10	12	S Peculiar	S Peculiar
00196+1012	N95	0	19	39.5	10	12	59	Sc	S
00221+2049		0	22	7.4	20	49	26		S
00276+0149	N132	0	27	37.1	1	49	6	SBb/Sc	S
00287+0811	U312 or MK 552	0	28	45.8	8	11	40	SB disturbed	pair
00366+0035	N192	0	36	40.7	0	35	33	SBa	S
00387+2513	N214	0	38	47.9	25	13	28	Sc	S
00409+1404	N234	0	40	55.3	14	4	10	Sc	S
00454+0801	M+01-03-003	0	45	26.0	8	1	31		S
00477+2414		0	47	42.5	24	14	36		S
00491+2514		0	49	11.3	25	14	32		S
00509+1225	U545	0	50	56.7	12	25	10	compact, Seyfert	compact
00521+2858	U556	0	52	7.8	28	58	27	S Peculiar	S
00537+1337	U580 or U582	0	53	45.1	13	37	42	pair in contact	2 pairs
01086+2739	ZG 108+27	1	8	38.0	27	39	53		pair S
01103+0043	N428	1	10	20.2	0	43	5	SAB(s)m	
01167+0418	ZG 116+04, MK 567	1	16	42.8	4	18	59		pair

Table 2. (Continued)

IRAS Name	Optical Association	IRAS Position						Classification (UGC)	Appearance on Image
		α			δ				
		h	m	s	°	′	″		
01171+0308	N470	1	17	9.5	3	8	51	Sb/Sc	S
01173+1431	N471	1	17	20.3	14	31	26	S0, multiple system	S with companion
01173+1405	ZG 117+14	1	17	22.8	14	5	54		S with companion
01191+1719	U903	1	19	6.6	17	19	52	S	S
01191+0459	N488	1	19	10.4	4	59	37	Sb	
01197+0044		1	19	42.9	0	44	44		pair with bridge
01217+0122		1	21	47.8	1	22	55		S with companion
01219+0331	N520, ARP 157	1	21	59.6	3	31	52	Irr II Peculiar	Peculiar
01276+2958		1	27	39.8	29	48	9		S
01324+2138		1	32	25.1	21	38	39		S
01340+1532	N628	1	34	5.5	15	32	38	Sc	
01346+0537	N632	1	34	41.2	5	37	26	S0 pair with N631	S
01403+1323	N660	1	40	21.6	13	23	41	SB[a] distorted?	S, disturbed nucleus
01410+1154	U1209	1	41	4.9	11	54	46	S-Irr Disturbed	S
01418+1651	ZW 035	1	41	48.1	16	51	7		S with companion
01450+2710	N672	1	45	4.1	27	10	53	SBc	S
01457+1116	N673	1	45	42.6	11	16	24	Sc	S
01458+1221	MK 575	1	45	52.9	12	21	56		SB
01479+0553	N693	1	47	54.2	5	53	52	S	S
01481+2144	N694, MK 363	1	48	11.3	21	44	54	Peculiar	
01484+2220	N695	1	48	28.0	22	20	8	Peculiar	S with companion
01485+2206	N697	1	48	31.1	22	6	41	Sc	S
01492+0602	N706	1	49	12.8	6	2	51	Sc	S
01503+1227	M+02-05-054	1	50	18.7	12	27	44		S

Table 2. (Continued)

IRAS Name	Optical Association	IRAS Position						Classification (UGC)	Appearance on Image
		α			δ				
		h	m	s	°	′	″		
01555+0250	U1449, ARP 126	1	55	31.0	2	50	33	pair Irr, contact, disrupted	pair
01556+2507	U1451	1	55	41.4	25	7	3	SBb? pair with U1462	S
01565+1845	N772	1	56	34.6	18	45	52	Sb pair with N770	S
01572+0009	MK 1014	1	57	16.6	0	9	8		Peculiar with tails
01587+2614	U1507	1	58	43.5	26	14	38	SBa pair with U1510	pair, contact
03017+0724		3	1	47.5	7	24	32		S
03079+0018		3	7	59.5	0	18	19		S with companion
03119+1448		3	11	58.9	14	48	52		pair with bridge
03144+0104	U2638	3	14	27.3	1	4	22	Sab	S Peculiar
03222+1617		3	22	16.2	16	17	35		Peculiar
03275+1535		3	27	35.7	15	35	52		S
03288+0108		3	28	49.0	1	8	13		pair
03312+0906		3	31	16.2	9	6	11		Peculiar, 2 nuclei?
03315+0055		3	31	32.1	0	55	41		S with companion
03359+1523		3	35	57.2	15	23	6		pair
03371+1046		3	37	11.9	10	46	51		S
03514+1546	ZG 351+15	3	51	25.9	15	46	54		Peculiar
03521+0028		3	52	8.5	0	28	21		Peculiar
04002+0149	U2936	4	0	12.3	1	49	39	Sc	S
04050+0350	U2963	4	5	1.2	3	50	15	Sc disturbed	
04149+0125	M+00-11-046	4	14	59.5	1	25	11		Pair
04151+0126	ZG 415+01	4	15	7.3	1	26	21		
04192+0355	ZG 419+03	4	19	16.7	3	55	46		S with companion
04332+0209		4	33	12.3	2	9	24		

Table 2. (Continued)

IRAS Name	Optical Association	IRAS Position α h	m	s	δ °	′	″	Classification (UGC)	Appearance on Image
04470+0314	ZG 447+03	4	47	2.0	3	14	30		S
04502+0258	U3193	4	50	16.7	2	58	32	SBb	S with companion
04513+0104	M+00-13-025	4	51	20.7	1	4	25		pair
04520+0311	U3201, MK 1088	4	52	1.5	3	11	14	SB0/SBa	S
07006+8429	N2268	7	0	36.6	84	27	47	Sc	S
07055+7155	U3697	7	5	30.3	71	55	1	disturbed	S
07067+7149	U3714	7	6	43.4	71	49	59	S? disturbed	E?
07099+5504		7	9	59.1	55	4	22		S
07101+8550	N2276	7	10	11.5	85	50	53	Sc disturbed, pair with N2300(E)	S
07112+6447	N2347	7	11	15.3	64	47	56	Sb pair with U3750	S
07184+8016	N2336	7	18	24.6	80	16	30	SBc pair with U3834	
07203+5803	U3828	7	20	22.5	58	3	54	Sb/SBb	S
07227+5934		7	22	47.6	59	34	45		S
07233+6917	N2366	7	23	23.9	69	17	30	Irr + Irr	
07236+7213	U3852, MK 8	7	23	38.8	72	13	54	double or triple	pair, contact
07271+6320	ZG 727+63	7	27	7.3	63	20	56		E or S0?
07321+6543	N2403	7	32	11.9	65	43	23	Sc (M81 group)	S
07447+7428	U4028	7	44	46.1	74	28	54	S	Peculiar
07467+7337	U4041	7	46	43.0	73	37	51	S	S Peculiar with companion
07540+5648	N2469	7	54	0.0	56	48	51	S	S
07581+5052	N2500	7	58	8.0	50	52	10	SABm	S
08001+2331	N2512, MK 384	8	0	6.0	23	31	59	SBb	SB
08070+3406	N2532	8	7	4.1	34	6	17	Sc	S
08082+2521	N2535, ARP 82	8	8	13.0	25	21	15	S pair with N2536, bridge	pair

Table 2. (Continued)

IRAS Name	Optical Association	IRAS Position α h	m	s	δ °	′	″	Classification (UGC)	Appearance on Image
08096+3624	N2543	8	9	40.5	36	24	21	SBb	S
08111+2401	ZG 811+24	8	11	6.0	24	1	10		S
08143+3536	U4306	8	14	23.2	35	36	7	S	S
08300+3714		8	30	5.2	37	14	54		S? with companion?
08322+2838	N2608	8	32	14.0	28	38	49	SBb/SBc with N2619	S
08323+3003		8	32	19.4	30	3	35		triple S
08327+2855	ZG 832+28	8	32	44.0	28	55	37		S
08354+2555	N2623, ARP 243	8	35	25.0	25	55	49	disturbed, tails	Peculiar with tails
08495+3336	N2683	8	49	35.2	33	36	48	Sb	S
08507+3520	U4653, ARP 195	8	50	47.6	35	20	18	triple, SBb, contact, plume	triple S
08572+3915		8	57	13.0	39	15	39		pair
08579+3447		8	57	59.3	34	47	14		Peculiar
09026+3759		9	2	38.3	37	59	33		S Peculiar
09028+2538	N2750	9	2	51.0	25	38	19	Sc	S
09089+4509	N2776	9	8	56.1	45	9	37	Sc	S
09108+4019	N2782, ARP 215	9	10	54.0	40	19	12	S Peculiar	S
09120+2956	N2789	9	12	0.0	29	56	19	S0a	S
09120+4107	N2785	9	12	3.0	41	7	32	Irr or Peculiar pair with U4867	S?
09126+4432	U4881, ARP 55	9	12	39.6	44	32	20	pair, contact, disturbed	pair, contact, tail
09141+4212	N2798	9	14	11.0	42	12	2	SBa disturbed + S	pair
09168+3308	U4947	9	16	53.0	33	8	42	SB	Peculiar with 2 nuclei, 2 tails
09206+4925	N2854	9	20	37.6	49	25	14	SBa pair with N2856	S
09208+4927	N2856	9	20	53.4	49	27	50	S pair with N2854	S

Table 2. (Continued)

IRAS Name	Optical Association	IRAS Position						Classification (UGC)	Appearance on Image
		α			δ				
		h	m	s	°	′	″		
09273+2945	N2893, MK 401	9	27	20.0	29	45	35	SBa	S
09333+4841	M+08-18-012	9	33	18.5	48	41	54		S with companion
09399+3204	N2964	9	39	55.0	32	4	36	Sb/Sc pair with N2968	S
09435+3508		9	43	30.3	35	8	55		S
09456+3339	N3003	9	45	40.3	33	39	3	SB?c	S
09479+3347	N3021	9	47	58.8	33	47	20	S	S
09534+2727	U5335	9	53	8.0	27	27	58	Peculiar	S Peculiar
09554+3236	N3067	9	55	26.1	32	36	32	Sab	S
09583+4714		9	58	21.7	47	14	10		triple
10078+2439	MK 717, U5488	10	7	52.0	24	39	36		S
10245+2845	N3245, U5663	10	24	30.0	28	45	44	S0	S
10282+2903	N3265	10	28	17.9	29	3	15	E	E?
10369+2659	ZG 1036+27	10	36	57.0	26	59	15		S
10394+1400	N3338	10	39	27.7	14	0	31	Sc	
10407+2511	N3344	10	40	46.4	25	11	7	Sc	S
10460+2619	MK 727	10	46	0.5	26	19	4		E?
X1051+175	N3454	10	51	48.3	17	35	17	pair with N3455	
10565+2448		10	56	35.4	24	48	43		triple
10576+2914	N3486	10	57	40.0	29	14	44	Sc	S
14008+2816	M+05-33-042	14	0	48.9	28	16	18		S
14026+3058	ZG 1402+30	14	2	36.0	30	58	45		S
14151+2705	MK 673,U9141	14	15	6.0	27	5	17	S, contact, disturbed	S with 2 nuclei, companion
14158+2741		14	15	48.9	27	41	48		S with tail, companion
14165+2510	U9165	14	16	30.0	25	10	17	S	S

Table 2. (Continued)

IRAS Name	Optical Association	IRAS Position α h	m	s	δ °	′	″	Classification (UGC)	Appearance on Image
14190+3013	U9191	14	19	0.6	30	13	17	S, 1 of 2 galaxies	
14221+2450	N5610	14	22	7.0	24	50	24	SBa	distorted SB with companion
14280+3126	N5653	14	28	0.0	31	26	17	S Peculiar	S Peculiar
14356+3041	U9425	14	35	40.0	30	41	57	pair, connected, plumes	pair, bridge, tails
14547+2448	ARP 302	14	54	47.9	24	48	57		pair S
16104+5235	N6090	16	10	24.0	52	35	4	pair, contact, long plume	pair S, bridge
16107+2824	U10273	16	10	43.6	28	24	45	strongly Peculiar	
16161+4015		16	16	7.5	40	15	49		triple
16180+3753	N6120	16	18	0.8	37	53	35	Peculiar, pair with N6119	S Peculiar
16305+4823		16	30	34.7	48	23	37		S Peculiar?
16340+5252	M+09-27-053	16	34	3.4	52	52	52		
16343+3752		16	34	23.1	37	52	31		S Peculiar with companion
16350+7818	N6217	16	35	4.7	78	18	2	Sb	S
16362+5815	M+10-24-007	16	36	15.7	58	15	55		SB
16403+2510	U10514	16	40	19.3	25	10	46	S-Irr Peculiar	Peculiar
16404+5910	M+10-24-026	16	40	25.2	59	10	39		SB
16412+3655	N6207	16	41	17.4	36	55	37	S	S
16418+6540	U10524	16	41	51.1	65	40	41	SBb	SB
16471+4847	MK 499	16	47	8.2	48	47	54		
16474+3430		16	47	24.2	34	30	18		pair, contact
16478+6303	N6247	16	47	51.4	63	3	44	Peculiar	pair, tail
16484+4249	N6239	16	48	26.9	42	49	35	SB Peculiar	S, Peculiar nucleus?
16487+5447		16	48	43.5	54	47	36		pair
16577+5900	N6286	16	57	44.8	59	00	38	Peculiar, pair with N6285	pair S

Table 2. (Continued)

IRAS Name	Optical Association	IRAS Position α h	m	s	δ °	′	″	Classification (UGC)	Appearance on Image
17012+8356	ZW 673	17	01	15.4	83	56	28		pair
17013+3131	U10675	17	01	21.9	31	31	38	Double, plume, very long bridge	pair, disturbed, with plume
17028+5817		17	02	52.8	58	17	46		pair S
17069+6047	N6306	17	06	59.2	60	47	27	S, pair with N6307	pair S
17082+6206		17	08	14.3	62	06	15		S
17132+5313		17	13	14.3	53	13	51		pair
17180+6039	N6361	17	18	03.9	60	39	25	Sb	S
17313+7544	N6412	17	31	23.6	75	44	31	Sc	S
17366+8646	U10923	17	36	38.3	86	46	42	pair, strongly disturbed	pair disturbed S
17392+3845		17	39	14.4	38	45	21		S with companion, bridge
17499+7009	N6503	17	49	57.8	70	09	25	Sc	S
17501+6825	M+11-22-006	17	50	10.5	68	25	13		S Peculiar with 2 companions
17517+6422		17	51	45.3	64	22	11		pair
17526+3253	U11035	17	52	39.1	32	53	36	Strongly Peculiar	Peculiar, tail
17530+3446	U11041	17	53	4.5	34	46	59	Sab	S
17548+2401	ZG 1754+24	17	54	52.8	24	01	20		S
17552+2757	U11060	17	55	12.3	27	57	58	Sa, pair with U11064	S
17578+4553		17	57	49.9	45	53	18		S
17583+3430	ZG 1758+34	17	58	23.5	34	30	02		S
18131+6820	N6621	18	13	10.1	68	20	53	Double, disrupted	pair
18212+7432	N6643	18	21	13.5	74	32	43	Sc	S
18308+6756	N6667	18	30	49.6	67	56	57	Peculiar	S Peculiar
18335+6705	N6679	18	33	35.3	67	05	03	double, bridge	pair
18425+6036	[illegible]701	18	42	35.1	60	36	04	SBa	SB

Table 2. (Continued)

IRAS Name	Optical Association	IRAS Position						Classification (UGC)	Appearance on Image
		α			δ				
		h	m	s	°	′	″		
18443+7433		18	44	20.6	74	33	20		S
19120+7320	U11415	19	12	03.2	73	20	27	S, pair with N6786, distorted	pair S
X1911+733	N6786	19	11	56.5	73	19	48	SB, pair with U11415, distorted	pair S
21052+0340	U11680	21	5	13.5	3	40	23	Sc+compact companion, connected	S with companion, bridge
21089-0214	U11691	21	8	55.4	−2	14	19	S Peculiar	S Peculiar
21091-0134	MK 512	21	9	10.7	−1	34	41		S
21116+0158	U11703	21	11	40.1	1	58	11	S	S
21144-0656	M-01-54-008	21	14	28.4	−6	56	13		
21171-0859	M-02-54-004	21	17	11.7	−8	59	37		S
21271+0627	ZG 2127+06	21	27	9.6	6	27	40		S Peculiar
21442+0007		21	44	17.2	0	7	21		pair S
21497-0824		21	49	47.2	−8	24	31		S
21504-0628		21	50	28.4	−6	28	56		S, Peculiar nucleus?
22032+0512		22	03	15.6	5	12	33		E?
22045+0959	N7212	22	4	33.2	9	59	20	S with companion, distorted	pair, contact, tail
22074-1654	N7218	22	7	28.7	−16	54	22		S
22204-1547	M-03-57-006	22	20	26.5	−15	47	39		
22221+1748	M+03-57-002	22	22	8.6	17	48	2		S
22243+1421		22	24	22.8	14	21	17		E?, compact
22287-1917	M-03-57-017	22	28	42.8	−19	17	31		S
22317-1036	N7309	22	31	44.3	−10	36	42		S
22329-1528	M-03-57-024	22	32	56.3	−15	28	6		E
22449+0757		22	44	57.9	7	57	49		pair S

Table 2. (Continued)

IRAS Name	Optical Association	IRAS Position α h	m	s	δ °	′	″	Classification (UGC)	Appearance on Image
22469-1932	M-03-58-007	22	46	55.6	−19	32	24		SB, with 2 companions
22471+0110		22	47	7.6	1	10	7		pair S
22491-1808		22	49	9.5	−18	8	19		Peculiar, 2 tails
22509-0041		22	50	59.1	−0	40	43		S
22575+1542	N7448	22	57	34.8	15	42	48	Sc	S
22586+0523	U12304	22	58	36.2	5	23	8	S	S
22595+1541	N7465	22	59	31.9	15	41	55	SB0	S
23011+0046	ZG 2301+00	23	1	8.4	0	46	30		S Peculiar
23024+1203	N7479	23	2	26.6	12	3	9	SBb	S
23024+1916	ZG 2302+19	23	2	28.2	19	16	55		S
23031+1856		23	3	7.9	18	56	23		S with companion
23032+0316	N7483	23	3	15.2	3	16	28	SBa	SB
23050+0359		23	5	1.3	3	59	33		pair
23065+1754	N7497	23	6	33.6	17	54	15	Sc	S
23106+0603	N7518	23	10	41.7	6	3	7	Sa	S Peculiar
X2312+062	M+01-59-015	23	12	5.9	6	17	25		S Peculiar
23121+0415	N7541	23	12	11.5	4	15	40	Sc pair with N7537(Sb)	S
23135+2516	ZG 2313+25	23	13	31.2	25	16	48		S
23157+0618	N7591	23	15	44.1	6	18	48	SBb	SB
23157-0441	N7592	23	15	47.5	−4	41	21		pair, contact, tail
23161+2457	U12490	23	16	9.3	24	57	26	SBa	SB with companion
23164-0845	N7606	23	16	29.3	−8	45	33		
23176+2356	N7620	23	17	36.9	23	57	26	Sc	S
23179+1657	N7625	23	17	59.6	16	57	4		S Peculiar

Table 2. (Continued)

IRAS Name	Optical Association	IRAS Position α h	m	s	δ °	′	″	Classification (UGC)	Appearance on Image
23179+2702	N7624	23	17	54.3	27	2	27	Sc	S
23201+0805		23	20	11.8	8	5	10		S
23204+0601	ZG 2320+06	23	20	28.4	6	1	31		disturbed, tails
23213+0923	N7648	23	21	22.7	9	23	40	S0	
23215-1208	M-02-59-015	23	21	31.7	−12	8	22		S
23252+2318	N7673	23	25	12.1	23	18	53	compact, pair with N7677	S
23254+0830	N7674, ARP 182	23	25	24.7	8	30	14	SBb disturbed pair with N7675	pair
23256+2315	N7677	23	25	36.7	23	15	22	SB?b pair with N7673	S
23259+2208	N7678	23	25	56.5	22	8	31	Sc/SBc	S
23262+0314	N7679, ARP 216	23	26	13.8	3	14	14	S0 pair with N7682(SBa)	S
23277+1529	U12633	23	27	42.1	15	29	8	SB	S
23309-0215	U12661	23	30	54.8	−2	15	29	Sab	pair S
23327+2913		23	32	42.7	29	13	25		pair
23336+0152	N7714, ARP 284	23	33	39.9	1	52	35	S pair with N7715(S), bridge	Peculiar
23362-0647	N7721	23	36	14.5	−6	47	36		S
23363-1314	N7723	23	36	21.7	−13	14	21		SB
23381+2654		23	38	11.8	26	54	4		Peculiar
23387+2516	ZG 2338+25	23	38	44.8	25	16	27		Peculiar, two nuclei?
23394-0353	M-01-60-022, ARP 295	23	39	25.3	−3	53	42		S
23410+0228		23	41	5.8	2	28	24		Peculiar
23413+2547	N7741	23	41	23.6	25	47	54	SBc	S
23414+0014	N7738	23	41	28.2	0	14	20	SBb	S
23417+1029	N7742	23	41	43.6	10	29	27	S0? pair with N7743	S

Table 2. (Continued)

IRAS Name	Optical Association	IRAS Position						Classification (UGC)	Appearance on Image
		α			δ				
		h	m	s	°	′	″		
23433+1147	U12773	23	43	23.0	11	47	6	S-Irr	S
23445+2911	N7752	23	44	30.5	29	11	44	connected with N7753	S with companion
23446+1519	ZG 2344+15	23	44	36.7	15	19	6		SB
23456+2056		23	45	41.7	20	56	25		S Peculiar
23471+2939	U12798	23	47	8.1	29	39	17	S	S
23485+1952	N7769	23	48	31.0	19	52	18	Sab	S
23488+1949	N7771	23	48	52.1	19	49	57	SBa disturbed	SB with companion
23488+2018	MK 331	23	48	52.9	20	18	20		S
23560+1026	U12872	23	56	0.2	10	26	58	S Peculiar	S with companion?
23564+1833	U12879	23	56	27.9	18	33	23	S	S
23566-0833		23	56	41.2	−8	33	15		pair S
23568+2028	N7798	23	56	51.8	20	28	17	S	S
23587+1249	N7803	23	58	46.6	12	49	57	S0a	S with companion
23591+2312	U12915	23	59	7.8	23	12	58		pair S, tails
23597+1241	N7810	23	59	45.1	12	41	34	S0	S

Table 3. Optical Data on Pairs and Possible Merger Remnants

IRAS NAME	IRAS Position[a] α h	m	s	δ °	′	″	Optical Source(s)	Optical Positions[a] α h	m	s	δ °	′	″	v_h	m_B	Notes
00047+2725	0	4	42.0	27	25	50	• N1	0	4	41.3	27	25	48	4548	13.4	4,11
							N2	0	4	42.4	27	24	0	7366	14.8	7,11,22
00073+2538	0	7	19.3	25	38	47	• N23	0	7	19.3	25	38	50	4566	13.12	2,4
							N26	0	7	51.3	25	33	16	4583	13.9	2,12
00287+0811	0	28	45.8	8	11	40	MK552	0	28	43.9	8	11	57	4366	15.0	4,11
							U312	0	28	48.9	8	11	34	4326	14.6	4,5,11
							U314	0	28	54.2	8	7	29	4235	15.4	4,5,11
00366+0035	0	36	40.7	0	35	33	• N192	0	36	39.6	0	35	15	4210	13.9	2,4
							N196	0	36	43.6	0	38	18	4238		2,4
							N197	0	36	44.6	0	36	59	4116		2,4
00537+1337	0	53	45.1	13	37	42	U582	0	53	45.4	13	36	21	24642	16.5	4,11
							U580	0	53	43.2	13	35	30	12034	16.0	4,11
							a	0	53	45.3	13	37	42			11
							b	0	53	46.4	13	37	51			11
							c	0	53	46.1	13	38	10			11
							d	0	53	44.3	13	38	0			11
01086+2739	1	8	38.0	27	39	53	ZG 108+27A	1	8	36.7	27	39	46	10006	15.5	4,11
							ZG 108+27B	1	8	35.5	27	39	29			11
01167+0418	1	16	42.8	4	18	59	MK 567	1	16	42.6	4	18	55	9928	14.9	4,11
							b stellar?	1	16	44.7	4	19	17			11
							c	1	16	35.7	4	20	13			11
01171+0308	1	17	9.5	3	8	51	• N470	1	17	10.5	3	8	53	2370	12.75	2,12
							N474	1	17	31.7	3	9	17	2333	12.51	2,12
01173+1431	1	17	20.3	14	31	26	• N471	1	17	20.2	14	31	16	4138	14.9	4,11
							U838	1	16	6.6	14	43	40	6903	14.2	4,11
01173+1405	1	17	22.8	14	5	54	• ZG 117+14A	1	17	23.4	14	5	48	9362	14.9	4,11
							ZG 117+14B	1	17	27.2	14	5	39			11
01197+0044	1	19	42.9	0	44	44	A	1	19	44.1	0	44	46	16626		4,11
							B	1	19	43.4	0	44	48	16795		4,11
01217+0122	1	21	47.8	1	22	55	A	1	21	50.0	1	22	54	5144		4,11
							B	1	21	48.6	1	22	56			11

Table 3. (Continued)

IRAS NAME	IRAS Position[a] α h	m	s	δ °	′	″	Optical Source(s)	Optical Positions[a] α h	m	s	δ °	′	″	v_h	m_B	Notes
01219+0331	1	21	59.6	3	31	52	• N520	1	21	59.4	3	32	13	2162	12.75	2,4
01346+0537	1	34	41.2	5	37	26	• N632	1	34	41.0	5	37	23	3151	13.5	4,11
							companion	1	34	42.0	5	38	53			11
							N631	1	34	10.6	5	34	51	3310	15.0	7,11,22
01403+1323	1	40	21.6	13	23	41	• N660	1	40	20.7	13	23	32	856	11.9	2,4
							U1195	1	39	46.4	13	43	30	776	13.9	2,5,22
01418+1651	1	41	48.1	16	51	7	ZW 035	1	41	47.9	16	51	7	8091	16.0	11
							companion	1	41	47.6	16	50	57			11
01450+2710	1	45	4.1	27	10	53	• N672	1	45	4.2	27	11	5	411	11.76	1
							U1249	1	44	41.6	27	4	55	362	12.2	2,7
01479+0553	1	47	54.2	5	53	52	N693	1	47	54.1	5	53	52	1593	13.5	11
							N676	1	46	20.6	5	39	35	1517	10.5	2,12
01481+2144	1	48	11.3	21	44	54	• N694	1	48	12.5	21	45	5	2966	13.7	2,4
							U1313	1	48	22.2	21	40	1	2928	14.0	2,5,22
01484+2220	1	48	28.0	22	20	8	N695	1	48	27.5	22	20	8	9705	13.7	4,11
							companion	1	48	27.3	22	20	32			11
01555+0250	1	55	31.0	2	50	33	• U1449 SW	1	55	30.0	2	50	22	5431	14.0	4,11,14
							U1449 NE	1	55	31.3	2	50	41	5551		4,11
01556+2507	1	55	41.4	25	7	3	• U1451	1	55	40.8	25	7	3	4916	14.3	4,11
							U1462	1	56	20.2	25	8	36	5059	15.6	7,11
01565+1845	1	56	34.6	18	45	52	• N772	1	56	35.3	18	45	50	2489	11.42	2,4
							N770	1	56	28.2	18	42	46	2543	14.2	2,12
01572+0009	1	57	16.6	0	9	8	• MK1014	1	57	15.8	0	9	10	48902	15.2	4,9,24
01587+2614	1	58	43.5	26	14	38	• U1507	1	58	40.3	26	14	28	5102	13.9	2,4
							U1510	1	58	56.0	26	18	15	5009	14.4	2,7,8
03119+1448	3	11	58.9	14	48	52	a	3	11	59.7	14	48	52	23006	16.0	4,11
							b	3	11	59.0	14	48	59			11
03144+0104	3	14	27.3	1	4	22	• U2638	3	14	27.4	1	4	19	7098	16.0	4,11,15
							B	3	14	29.7	1	5	20			11
03222+1617	3	22	16.2	16	17	35	A	3	22	16.1	16	17	36	12089		4,11
							B	3	22	16.1	16	17	25			11

Table 3. (Continued)

IRAS NAME	IRAS Position[a] α h	m	s	δ °	′	″	Optical Source(s)	Optical Positions[a] α h	m	s	δ °	′	″	v_h	m_B	Notes
03288+0108	3	28	49.0	1	8	13	* a	3	28	49.2	1	8	13	9295		4,11
							b	3	28	47.9	1	7	2			11
							c	3	28	52.6	1	7	31			11
03312+0906	3	31	16.2	9	6	11	A	3	31	14.0	9	5	59	5553		4,11
							B	3	31	13.9	9	6	5			11
03315+0055	3	31	32.1	0	55	41	A	3	31	31.3	0	55	40	14372		4,11,16
							B	3	31	31.3	0	56	13			11
							C	3	31	35.9	0	56	10			11
03359+1523	3	35	57.2	15	23	6	a	3	35	58.3	15	23	8	10600		4,11
							b	3	35	57.6	15	23	10			11
03521+0028	3	52	8.5	0	28	21		3	52	8.03	0	28	16.5			9,10,11
04050+0350	4	5	1.2	3	50	15	* U2963							5296	15.3	4,5
04149+0125	4	14	59.5	1	25	11	M+00-11-046 companion	4	14	59.6	1	25	9	4922	14.9	4,11,15
04192+0355	4	19	16.7	3	55	46	a	4	19	17.9	3	55	52	7346	15.2	4,11,16
							b	4	19	17.9	3	55	38			11
							c	4	19	18.8	3	55	41			11
04470+0314	4	47	2.0	3	14	30	* ZG 447+03	4	47	0.6	3	14	21	8383		11
							companion	4	47	7.1	3	14	53			11
04502+0258	4	50	16.7	2	58	32	U3193	4	50	15.5	2	58	29	4436	14.7	4,11
							b	4	50	18.8	2	58	42			11
04513+0104	4	51	20.7	1	4	25	a	4	51	20.7	1	4	25	9922		4,11
							b	4	51	19.9	1	4	29			11
07055+7155	7	5	30.3	71	55	1	* U3697	7	5	32.5	71	55	1	3157	13.1	2,3,4
							U3714	7	6	46.3	71	49	56	2889	12.7	2,3,4
07067+7149	7	6	43.4	71	49	59	* U3714	7	6	46.3	71	49	56	2889	12.7	2,3,4
							U3697	7	5	32.5	71	55	1	3157	13.1	2,3,4
07099+5504	7	9	59.1	55	4	22	* a	7	10	0.3	55	4	23	9782		4,11
							b	7	10	2.4	55	7	16			11
							c	7	9	58.4	55	7	50			11

Table 3. (Continued)

IRAS NAME	IRAS Position[a] α h	m	s	δ °	′	″	Optical Source(s)	Optical Positions[a] α h	m	s	δ °	′	″	v_h	m_B	Notes
07101+8550	7	10	11.5	85	50	53	• N2276	7	10	22.0	85	50	58	2391	12.3	2,4
							N2300	7	15	45.1	85	48	31	1986	12.2	2,7
07112+6447	7	11	15.3	64	47	56	• N2347	7	11	16.2	64	47	53	4424	13.21	2,4
							U3750	7	10	43.1	65	00	46	4451		2,4
07184+8016	7	18	24.6	80	16	30	• N2336	7	18	28.0	80	16	35	2252	11.3	2,7
							U3834	7	21	56.3	79	58	30		12.7	2,7
07233+6917	7	23	23.9	69	17	30	B	7	23	13.5	69	17	39	70	15.5	4,11,25
							N2366	7	23	34.2	69	18	42	145	11.6	2,7,25
							N2363	7	23	26.4	69	17	29			11,25
07236+7213	7	23	38.8	72	13	54	• U3852	7	23	36.8	72	13	58	3534	13.8	2,4,17
07447+7428	7	44	46.1	74	28	54	• U4028	7	44	42.8	74	29	7	3943	12.7	4,11
07467+7337	7	46	43.0	73	37	51	• U4041	7	46	44.1	73	37	51	3449	13.9	2,4,16
08082+2521	8	08	13.0	25	21	15	• N2535,ARP 82	8	8	13.1	25	21	22	4104	13.49	1,4
							N2536,ARP82B	8	8	15.7	25	19	43	4139	14.8	1,4
08300+3714	8	30	5.2	37	14	54		8	30	5.5	37	14	54	12750	17.0	4,11
08322+2838	8	32	14.0	28	38	49	• N2608	8	32	14.9	28	38	48	2126	12.9	1,4
							N2619	8	34	30.3	28	52	53	3586		2,4
08323+3003	8	32	19.4	30	3	35	B	8	32	19.4	30	03	38	17631	18.5	1,4
							A	8	32	19.4	30	03	22	17885	18.0	1,4
							C	8	32	18.7	30	03	16			1
08354+2555	8	35	25.0	25	55	49	N2623	8	35	24.9	25	55	51	5508	14.4	1,4,9
08507+3520	8	50	47.6	35	20	18	A	8	50	46.5	35	20	8	16706	15.8	4,11
							B	8	50	46.3	35	20	27	16748	16.0	4,11
							C	8	50	46.2	35	20	38			11
08572+3915	8	57	13.0	39	15	39	• A	8	57	13.0	39	15	38	17480		6,11,14
							B	8	57	13.3	39	15	34			11
08579+3447	8	57	59.3	34	47	14	a	8	57	59.2	34	47	11	19645		4,11
							b,star?	8	57	57.3	34	47	41			11
09026+3759	9	2	38.3	37	59	33	a	9	2	37.6	37	59	38	14293		11
							b	9	2	37.1	37	59	35			11
09028+2538	9	2	51.0	25	38	19	• N2750	9	2	51.9	25	38	17	2638	13.9	11

Table 3. (Continued)

IRAS NAME	IRAS Position[a] α h	m	s	δ °	′	″	Optical Source(s)	Optical Positions[a] α h	m	s	δ °	′	″	v_h	m_B	Notes
09108+4019	9	10	54.0	40	19	12	• N2782	9	10	54.0	40	19	18	2551	12.2	2,4,9
09120+4107	9	12	3.0	41	7	32	• N2785	9	12	3.2	41	7	32	2737	14.9	4,11
							U4867	9	11	30.7	41	5	18	2880	15.2	7,11,24
09126+4432	9	12	39.6	44	32	20	U4881A	9	12	38.2	44	32	29	11773	14.9	4,11
							U4881B	9	12	37.4	44	32	22			11
09141+4212	9	14	11.0	42	12	2	• N2798	9	14	9.5	42	12	37	1755	12.9	4,5,11,14
							N2799	9	14	17.7	42	12	15	1882	14.4	4,5,11
09168+3308	9	16	53.0	33	8	42	U4947A	9	16	52.6	33	8	40	14970	15.3	4,11
							U4947B	9	16	52.0	33	8	46			11
09206+4925	9	20	37.6	49	25	14	• N2854	9	20	39.8	49	25	8	2732	13.8	2,3
							N2856	9	20	53.6	49	27	48	2638	13.9	2,3
09208+4927	9	20	53.4	49	27	50	• N2856	9	20	53.6	49	27	48	2638	13.9	2,3
							N2854	9	20	39.8	49	25	8	2732	13.8	2,3
09333+4841	9	33	18.5	48	41	54	• A	9	33	18.6	48	41	55	7777		4,11,14
							B	9	33	20.9	48	41	34	7510		4,11
							C	9	33	22.4	48	42	17			11
							D	9	33	12.3	48	41	37			11
09399+3204	9	39	55.0	32	4	36	• N2964	9	39	59.4	32	4	35	1353	12.4	2,4
							N2968	9	40	14.5	32	9	26	1345	13.25	2,12
09583+4714	9	58	21.7	47	14	10	C	9	58	21.6	47	14	15	26100		11,20
							A	9	58	19.8	47	14	3	25717		4
							B	9	58	20.8	47	14	19	26400		11,20
X1051+175	10	51	48.3	17	35	17	• N3454	10	51	49.2	17	36	42	1167	14.1	2,7
							N3455	10	51	51.6	17	33	8	1113	13.1	2,7
10565+2448	10	56	35.4	24	48	43	A (SW)	10	56	36.1	24	48	40	12926	16.0	1,4,18
							B (NE)							12937	17.5	4
14151+2705	14	15	06.0	27	05	17	MK 673 NW							10987	15.0	1,4,21
							MK 673 SE							10949		1,14,21
							• MK 673	14	15	06.1	27	05	14			13
							companion	14	15	04.0	27	05	25			13

Table 3. (Continued)

IRAS NAME	IRAS Position[a] α h	m	s	δ °	′	″	Optical Source(s)	Optical Positions[a] α h	m	s	δ °	′	″	v_h	m_B	Notes
14158+2741	14	15	48.9	27	41	48	• A	14	15	49.1	27	41	49	20902	16.0	1,4
							B	14	15	52.9	27	41	28			11
14165+2510	14	16	30.0	25	10	17.0	• U9165	14	16	31.5	25	10	9	5278	15.3	4,11
							B	14	16	26.3	25	9	8	5362		4,11
14190+3013	14	19	0.6	30	13	17	U9191							9168	15.0	4
14221+2450	14	22	7.0	24	50	24	• N5610	14	22	6.6	24	50	25	5087	14.5	4,11
							companion	14	22	12.4	24	50	6	5200		20
14356+3041	14	35	40.0	30	41	57	U9425A (N)	14	35	41.6	30	41	56	10408	15.0	1,4
							U9425B (S)	14	35	42.3	30	41	43	10349		1
14547+2448	14	54	47.9	24	48	57	• ARP 302B (N)	14	54	48.3	24	49	03	10166	14.6	1,4,19
							ARP 302A (S)	14	54	47.9	24	48	24	9837	14.8	1,4
							stellar	14	54	47.8	24	48	42			1
16104+5235	16	10	24.0	52	35	4	N6090a	16	10	24.3	52	35	1	8730	14.0	2,4,5
							N6090b	16	10	24.5	52	35	8			2
16107+2824	16	10	43.6	28	24	45	U10273							7381	15.3	4
16161+4015	16	16	7.5	40	15	49	A	16	16	8.4	40	15	40	23288		4,11
							B	16	16	7.7	40	15	29			11
							C	16	16	7.8	40	15	36			11
16180+3753	16	18	0.8	37	53	35	• N6120	16	18	1.3	37	53	36	9203	14.3	11,12
							N6119	16	17	55.1	37	55	31	9181	15.4	11
16343+3752	16	34	23.1	37	52	31	A	16	34	22.6	37	52	31			11
							AII	16	34	21.9	37	52	31			11
							B	16	34	25.7	37	52	36			11
							C	16	34	27.6	37	52	34			11
16471+4847	16	47	8.2	48	47	54	MK 499	16	47	3.0	48	47	34	7680	15.0	8,22,23
							MK 500	16	47	14.0	48	48	0	7710	16.5	8,22
16474+3430	16	47	24.2	34	30	18	A							3348		4,11
							B									11
16478+6303	16	47	51.4	63	3	44	N6247	16	47	50.5	63	3	45	5424	13.5	2,4
							B ?	16	47	53.8	63	3	56			11

Table 3. (Continued)

IRAS NAME	IRAS Position[a] α h	m	s	δ °	′	″	Optical Source(s)	Optical Positions[a] α h	m	s	δ °	′	″	v_h	m_B	Notes
16487+5447	16	48	43.5	54	47	36	• A	16	48	43.4	54	47	39	31293		11,17,23
							B	16	48	48.1	54	47	49			11
							C	16	48	49.5	54	48	28			11
16577+5900	16	57	44.8	59	0	39	• N6286	16	57	45.0	59	0	41	5600	14.2	4,11
							N6285	16	57	37.4	59	1	50		14.6	5,11
17012+8356	17	1	15.4	83	56	28	ZW 673 A	17	1	16.5	83	56	19	13764	17.5	11
							ZW 673 B	17	1	10.9	83	56	20			11
17013+3131	17	1	21.9	31	31	38	• U10675	17	1	21.5	31	31	38	10143	15.4	4,11
							companion	17	1	24.2	31	33	23			11
17028+5817	17	2	52.8	58	17	46	A	17	2	53.1	58	17	50	31779		11
							B	17	2	54.7	58	17	48			11
17069+6047	17	6	59.2	60	47	27	• N6306	17	7	00.0	60	47	37	2973	14.3	2,4
							N6307	17	7	3.2	60	48	55	3283	14.0	2,7
17132+5313	17	13	14.3	53	13	51	A	17	13	14.2	53	13	51	15270		11
							B stellar?	17	13	13.4	53	13	49			11
							C	17	13	17.3	53	13	7			11
17366+8546	17	36	38.3	86	46	42	U10923 A	17	36	22.3	86	46	38	7900	14.3	2,4
							U10923 B	17	36	28.4	86	46	51			2
17392+3845	17	39	14.4	38	45	21	• A	17	39	14.4	38	45	21	12300	15.0	11
							B	17	39	13.9	38	44	5			11
							C	17	39	18.4	38	46	12			11
							D	17	39	19.6	38	46	37			11
17501+6825	17	50	10.5	68	25	13	• M+11-22-006	17	50	9.4	68	25	10	15357	15.2	11
							B	17	50	2.6	68	24	46			11
							C	17	50	19.8	68	25	33			11
17517+6422	17	51	45.3	64	22	11	A	17	51	45.4	64	22	18	26151	16.0	4,11
							B	17	51	45.1	64	22	13			11
							C	17	51	43.1	64	22	23			11

Table 3. (Continued)

IRAS NAME	IRAS Position[a] α h	m	s	δ °	′	″	Optical Source(s)	Optical Positions[a] α h	m	s	δ °	′	″	v_h	m_B	Notes
17526+3253	17	52	39.1	32	53	36	U11035 A	17	52	38.9	32	53	36	7429	14.3	4,11
							U11035 B	17	52	40.0	32	53	29			11
17552+2757	17	55	12.3	27	57	58	* U11060	17	55	12.7	27	57	54	4621	14.9	11
							U11064	17	55	42.6	27	50	19	7030	14.5	7,11
18131+6820	18	13	10.1	68	20	53	* N6621	18	13	10.2	68	20	50	6230	13.6	2,7
							N6622	18	13	14.4	68	20	15	5941		2,22
18335+6705	18	33	35.3	67	5	3	* N6679	18	33	33.7	67	5	50	6696	13.6	2,5
							N6677	18	33	35.1	67	6	25	6696		2
							U11290	18	33	39.4	67	4	13	5334	13.9	2,4
19120+7320	19	12	3.2	73	20	27	* U11415	19	12	4.1	73	20	28	7500	15.1	3,4,11
							N6786	19	11	53.1	73	19	28	7997	13.7	3,11,22
X1911+733	19	11	56.5	73	19	48	* N6786	19	11	53.1	73	19	28	7997	13.7	3,11,22
							U11415	19	12	4.1	73	20	28	7500	15.1	3,4
21052+0340	21	5	13.5	3	40	23	U11680a	21	5	10.7	3	40	15	7840	14.5	2,4
							U11680b	21	5	15.1	3	40	37			2
21144-0656	21	14	28.4	-6	56	13	M-01-54-008							877		4
21271+0627	21	27	9.6	6	27	40	ZG 2127+06 a	21	27	9.8	6	27	47	3476	15.0	4,11
							b	21	27	9.2	6	27	51			11
							c	21	27	10.5	6	27	42			11
							d	21	27	14.7	6	27	8			11
21442+0007	21	44	17.2	0	7	21	A	21	44	17.7	0	7	20	22187		4,11
							B	21	44	18.2	0	7	28			11
22045+0959	22	4	33.2	9	59	20	N7212 A	22	4	33.8	9	59	19	7800	15.10	4,11
							N7212 B	22	4	34.4	9	59	32			11
							companion	22	4	32.1	9	58	46			11
22449+0757	22	44	57.9	7	57	49	A	22	44	57.4	7	57	48	11140		4,11
							companion	22	44	56.7	7	58	4			11
22469-1932	22	46	55.6	-19	32	24	M-03-58-007A	22	46	56.1	-19	32	21	9549		4,11
							B	22	46	54.7	-19	32	0			11
							C	22	46	55.1	-19	31	49			11

Table 3. (Continued)

IRAS NAME	IRAS Position[a] α h	m	s	δ °	′	″	Optical Source(s)	Optical Positions[a] α h	m	s	δ °	′	″	v_h	m_B	Notes
22471+0110	22	47	7.6	1	10	7	A	22	47	6.0	1	9	58	17288		4,11
							B	22	47	6.4	1	9	57			11
22491-1808	22	49	9.5	−18	8	19		22	49	9.0	−18	8	19	23312		4,11
22595+1541	22	59	31.9	15	41	55	• N7465	22	59	31.8	15	41	50	1959	13.3	2,12
							N7463	22	59	22.7	15	42	48	2445	13.5	2,12
							N7464	22	59	24.7	15	42	17	1877	14.5	2,12
							N7448	22	57	34.9	15	42	50	212	12.23	2,12
23031+1856	23	3	7.9	18	56	23	• A	23	3	7.5	18	56	20	7815		11
							B	23	3	6.3	18	58	16			4,11
23050+0359	23	5	1.3	3	59	33	A	23	5	3.1	3	59	46	14271		11
							B	23	5	3.8	3	59	44			11
23106+0603	23	10	41.7	6	3	7	• N7518	23	10	40.5	6	2	58	3531	14.5	4,11
							companion									
X2312+062	23	12	5.9	6	17	25	M+01-59-015	23	12	2.0	6	17	1	6387	15.7	4,11
							condensation	23	12	1.6	6	16	49			11
23121+0415	23	12	11.5	4	15	40	• N7541	23	12	10.3	4	15	43	2607	12.8	2,12
							N7537	23	12	1.9	4	13	33	2648	14.13	2,12
23157-0441	23	15	47.5	−4	41	21	N7592A	23	15	46.8	−4	41	20	7328	14.0	4,11
							N7592B	23	15	47.9	−4	41	22			11
23161+2457	23	16	9.3	24	57	26	• U12490	23	16	10.3	24	57	34	8081	14.0	4,11
							B	23	16	12.4	24	59	30			11
23204+0601	23	20	28.4	6	1	31		23	20	29.1	6	1	37	16480	16.0	4,9,11
23252+2318	23	25	12.1	23	18	53	• N7673	23	25	11.8	23	18	51	3402	12.7	2,3,4
							N7677	23	25	36.2	23	15	18	3543	13.9	2,3,4
23254+0830	23	25	24.7	8	30	14	N7674	23	25	24.4	8	30	12	8698	13.6	4,11
							N7675	23	25	26.4	8	30	26	8662		11,22
23256+2315	23	25	36.7	23	15	22	• N7677	23	25	36.2	23	15	18	3543	13.9	2,3,4
							N7673	23	25	11.8	23	18	51	3402	12.7	2,3,4
23262+0314	23	26	13.8	3	14	14	• N7679	23	26	12.8	3	14	11	5120	13.47	2,12
							N7682	23	26	30.2	3	15	28	5109	14.30	2,12

Table 3. (Continued)

IRAS NAME	IRAS Position[a] α h	m	s	δ °	′	″	Optical Source(s)	Optical Positions[a] α h	m	s	δ °	′	″	v_h	m_B	Notes
23309-0215	23	30	54.8	−2	15	29	• U12661							5203	15.0	4
							companion									
23327+2913	23	32	42.7	29	13	25	A	23	32	42.4	29	13	24	31981		4,11
							B	23	32	42.4	29	13	37			11
23336+0152	23	33	39.9	1	52	35	• N7714	23	33	41.0	1	52	41	2804	13.10	11,12
							N7715	23	33	48.3	1	52	48	2795	14.9	7,11
23387+2516	23	38	44.8	25	16	27	ZG 2338+25A	23	38	47.7	25	16	31	9310	14.7	4,11
							B	23	38	44.6	25	16	19			11
							C	23	38	45.2	25	17	5			11
23394-0353	23	39	25.3	−3	53	42	• M 01-60-022	23	39	26.7	−3	53	32	5707		4,11
							companion	23	39	30.2	−3	51	31			11
23406+0415	23	40	38.9	4	15	56	ZG 2340+04A							11367	15.4	4
							B									
							C									
23417+1029	23	41	43.6	10	29	27	• N7742	23	41	42.9	10	29	24	1655	12.37	4,11
							N7743	23	41	48.6	9	39	25	1658	12.5	2,12
23445+2911	23	44	30.5	29	11	44	N7752	23	44	27.1	29	10	54	5142	14.3	4,11
							N7753	23	44	33.3	29	12	24	5180	13.2	11,12
23456+2056	23	45	41.7	20	56	25		23	45	41.5	20	56	22	7326	16.0	4,11,15
23485+1952	23	48	31.0	19	52	18	• N7769	23	48	31.5	19	52	21	4197	13.04	4,11
							N7771	23	48	51.8	19	50	3	4364	13.39	11,12
23488+1949	23	48	52.1	19	49	57	• N7771	23	48	51.8	19	50	3	4364	13.39	11,12
							N7770	23	48	49.8	19	49	8	4161	14.52	4,11
23560+1026	23	56	0.2	10	26	58	U12872	23	56	0.6	10	27	0	5264	13.8	4,11
							B	23	56	0.3	10	27	30			11
							C	23	56	1.5	10	27	10			11
							D	23	55	59.5	10	26	43			11
23566-0833	23	56	41.2	−8	33	15	A	23	56	37.9	−8	33	30	14779		4,11
							B	23	56	37.3	−8	33	28			11

Table 3. (Continued)

IRAS NAME	IRAS Position[a] α h	m	s	δ °	′	″	Optical Source(s)	Optical Positions[a] α h	m	s	δ °	′	″	v_h	m_B	Notes
23587+1249	23	58	46.6	12	49	57	* N7803	23	58	46.1	12	49	59	5300	13.8	4,11
							B	23	58	52.4	12	50	3			11
							C	23	58	41.4	12	50	5			11
23591+2312	23	59	7.8	23	12	58	* U12915	23	59	8.6	23	12	59	4436	13.9	2,7,22
							U12914	23	59	4.0	23	12	23	4383	13.2	2,4

Notes for Table 3:

[a]All positions 1950.0 coordinates.

[1]Optical positions from SKHL.

[2]Optical positions from Dressel and Condon (1976).

[3]The two galaxies in this pair are each listed in the PSC separately, and are thus listed twice in this Table.

[4]Velocities and m_B from SKHL or from J.P.Huchra.

[5]m_B from UGC.

[6]Redshift from Sanders *et al.* (1987), also, they found that most of the 10 μm flux comes from A.

[7]z, m_B from UGC.

[8]$m_B = m_{pg}$ from Markaryn and Lipovetskii (1971).

[9]Only one nucleus.

[10]ID confirmed by E. Becklin at 10 μm.

[11]Optical positions measured on 2-axis Grant at KPNO ($\sigma < 1''$).

[12]Velocities and m_B from Huchra *et al.* (1983).

[13]Positions are of MK 673 and companion. MK 673 is not resolvable on the POSS plates.

[14]Detected at 10μm at the IRTF, Feb 8–10, 1988; other source was not detected, so this is the assumed optical ID.

[15]A may have faint condensation in envelope--too faint to see on POSS to get optical position.

[16]A has faint companion (AII) which is not visible on POSS and thus we have no position for it.

[17]Image shows galaxy is a pair, but too close and faint to resolve on POSS to get optical positions.

[18]S. Willner confirmed (10 μm) that A is the IRAS source. A also may have a faint companion AII.

[19]S. Willner found $B_{10\,\mu m} = 32$ mJy; $A_{10\,\mu m} < 30$ mJy.

[20]Redshift obtained February 6, 1988, at the 2.1^m Kitt Peak telescope, using the Gold Camera.

[22]Redshift from Palumbo *et al.* (1983).

[23]Optical position from Peterson (1973).

[24]Optical position from Kojoian, Elliot, and Tovmassian (1981).

[25]NGC 2363 is a giant HII region in the southern tip of NGC 2366. There is also a small companion, B, to the west of the NGC 2366/2366 system.

Table 4. Galaxy Parameters

IRAS Name	Optical Association	Corrected IRAS Fluxes[a,b] 12 µm	25 µm	60 µm	100 µm	v_h	σ_v	m_B	Notes
00014+2028	N7817	0.65(1)	0.53(−7)	5.88(9)	15.30(3)	1051	18	11.71	3,13
00047+2725	N1	<0.26(4)	<0.23(−6)	2.43(10)	6.66(3)	4548	10	13.4	1
00073+2538	N23	0.75(18)	1.26(3)	10.62(7)	14.80(−1)	4566	15	13.12	3,13
00119+2810	U141	<0.27(9)	0.30(−4)	2.75(8)	4.77(0)	6814	30	15.7	1
00132+1548	U148	0.18(19)	0.33(4)	2.46(8)	4.98(1)	4156		14.0	10
00141+0647	U155	0.26(18)	0.45(2)	2.53(7)	5.43(2)	3968		14.6	10,22
00151+1110	N63	0.35(12)	0.46(0)	3.07(6)	4.13(0)	1179		12.6	10,21
00196+1012	N95	0.27(−3)	0.20(−10)	2.44(9)	5.15(2)	4891		13.4	10,21,22
00221+2049		<0.26(4)	<0.23(9)	2.28(9)	4.22(1)	5355	36	15.5	1
00276+0149	N132	0.31(7)	0.32(−4)	3.12(10)	7.46(2)	5316		13.8	10,22
00287+0811	MK 552	0.21(26)	0.74(10)	4.99(5)	5.64(−2)	4366	34	15.0	10,22,23
00366+0035	N192	0.34(9)	0.38(−3)	3.69(8)	6.21(0)	4210		13.9	10,21
00387+2513	N214	<0.40(−5)	0.27(−12)	2.28(9)	6.70(3)	4484	20	13.17	1
00409+1404	N234	0.37(15)	0.52(0)	3.63(9)	9.24(2)	4449		13.5	10,23
00454+0801	N257	0.29(−1)	0.22(−9)	2.26(10)	6.33(3)	5278		13.7	10
00477+2414		<0.28(13)	<0.36(−2)	2.60(7)	4.44(−1)	10200			1,8
00491+2514		<0.20(−71)	<0.36(44)	2.24(6)	2.62(−4)	9962	37		1
00509+1225	U545	0.65(25)	1.11(3)	1.93(−5)	2.46(−8)	18116		14.0	10
00521+2858	U556	0.43(6)	0.43(−4)	6.31(9)	10.22(0)	4564	33	15.3	1
00537+1337	U580, U582	<0.17(3)	<0.16(−8)	2.25(10)	4.05(−1)	24642	35	16.5	10,24
01086+2739	ZG 108+27	<0.27(8)	0.28(−5)	2.38(7)	3.71(−2)	10006	38	15.5	1,8
01103+0043	N428	0.69(2)	0.58(−7)	2.83(6)	4.78(1)	1078		11.9	10,11,22,23
01167+0418	ZG 116+04; MK 567	0.36(19)	0.57(1)	3.43(5)	4.80(−3)	9928		14.9	10,21,22
01171+0308	N470	0.55(22)	1.49(7)	7.69(6)	12.29(1)	2370		12.75	10,22

Table 4. (Continued).

IRAS Name	Optical Association	Corrected IRAS Fluxes[a,b] 12 μm	25 μm	60 μm	100 μm	v_h	σ_v	m_B	Notes
01173+1405	ZG 117+14	<0.48(31)	1.63(11)	11.35(2)	9.58(−7)	9362	36	14.9	1,8,18
01173+1431	N471	<0.31(11)	0.37(−2)	3.03(6)	3.84(−2)	4138	25	14.0	1,8
01191+1719	U903	0.40(15)	0.60(2)	8.68(9)	14.77(1)	2518	7	14.7	1,8,18
01191+0459	N488	0.07(−83)	0.19(24)	2.07(10)	10.89(4)	2180		11.6	10,11,21,23,24
01197+0044		0.19(38)	0.61(10)	2.41(1)	2.95(−7)	16626	38		10,22
01217+0122		0.18(28)	0.82(10)	2.21(1)	2.51(−3)	5144			10,21,22
01219+0331	N520; ARP 157	1.07(23)	3.29(10)	32.99(8)	45.68(0)	2162		12.75	13
01276+2958		<0.26(6)	0.26(−7)	2.27(4)	2.32(−6)	11009	57		1,8
01324+2138		<0.28(10)	<0.31(−5)	2.39(7)	3.69(−3)	14116	39	15.3	1
01340+1532	N628	2.11(2)	1.79(−6)	22.88(10)	67.68(3)	656	2	10.07	9
01346+0537	N632	<0.39(22)	0.90(6)	5.21(5)	6.49(−1)	3151	20	13.5	1
01403+1323	N660	2.80(21)	7.64(8)	72.39(8)	105.35(0)	856	80	11.9	9
01410+1154	U1209	<0.34(25)	<0.94(5)	2.33(3)	4.04(0)	5124	01	15.0	1
01418+1651	ZW 035	<0.33(30)	1.22(14)	14.00(5)	13.11(−5)	8091	100	16.0	1
01450+2710	N672	<0.28(12)	0.37(−2)	3.67(9)	8.55(2)	411	60	11.76	1
01457+1116	N673	<0.32(10)	0.37(−2)	3.48(10)	8.49(2)	5173	151	13.3	1
01458+1221	MK575	<0.31(23)	<0.71(5)	2.96(6)	6.21(1)	5474	90	14.0	1,3
01479+0553	N693	<0.40(17)	0.70(4)	8.05(8)	11.30(0)	1593	24	13.5	1,2
01481+2144	N694	<0.50(11)	<0.58(−3)	2.57(5)	3.81(0)	2966	81	13.7	1
01484+2220	N695	0.56(16)	0.83(1)	8.81(8)	13.22(−2)	9705	37	13.7	1,3
01485+2206	N697	0.47(8)	0.50(−3)	5.51(10)	18.20(4)	3109	20	12.7	1
01492+0602	N706	<0.47(15)	<0.69(0)	3.57(8)	9.01(2)	4993	18	13.2	1,3
01503+1227	M+02-05-054	<0.82(1)	0.66(−8)	6.84(9)	12.63(1)	4560	6	14.0	1
01555+0250	U1449; ARP 126	0.37(15)	0.55(1)	5.23(8)	8.57(0)	5431	35	14.0	10
01556+2507	U1451	<0.31(23)	0.75(8)	7.36(9)	13.14(1)	4916	29	14.3	1
01565+1845	N772	0.34(16)	0.54(3)	5.47(10)	22.54(4)	2489	23	11.42	1

Table 4. (Continued).

IRAS Name	Optical Association	Corrected IRAS Fluxes[a,b] 12 μm	25 μm	60 μm	100 μm	v_h	σ_v	m_B	Notes
01572+0009	MK 1014	0.28(73)	0.79(10)	2.03(−13)	1.83(−24)	48902		15.2	10,22
01587+2614	U1507	<0.26(4)	<0.23(−6)	2.25(9)	4.91(2)	5102	35	13.9	1
03017+0724		0.38(−2)	0.29(−11)	2.59(8)	<4.83(0)	7798	31		10,21
03079+0018		<0.16(14)	0.21(−1)	3.00(6)	3.04(−7)	14180	30		10
03119+1448		<0.08(39)	0.22(11)	2.32(7)	2.87(−8)	23006	57	16.0	
03144+0104	U2638	0.14(26)	0.37(9)	3.26(9)	4.96(−1)	7098	32	16.0	10
03222+1617		<0.17(24)	0.35(6)	4.09(10)	6.85(−2)	12089	56		10
03275+1535		0.15(25)	0.35(7)	2.21(6)	3.37(−1)	7454	56		10,22
03288+0108		<0.16(14)	0.21(−1)	2.61(4)	2.19(−7)	9295	51		10
03312+0906		0.19(21)	0.40(5)	2.62(9)	6.75(2)	5553	30		10,21,23,24
03315+0055		0.15(10)	0.17(−5)	2.13(10)	3.70(−2)	14372	58		10
03359+1523		0.15(10)	0.17(−4)	2.12(9)	3.73(−1)	10600	300		10
03371+1046		0.12(33)	0.43(12)	3.22(11)	13.57(6)	10706	31		10,23,24
03514+1546	ZG 351+15	0.33(23)	0.73(6)	6.01(9)	12.89(1)	6675			10,24
03521+0028		<0.21(90)	0.69(15)	2.34(−12)	2.18(−26)			20	10,22
04002+0149	U2936	0.36(13)	0.48(0)	5.88(10)	13.05(2)	3828	8	15.7	10,23,24
04050+0350	U2963	0.25(4)	0.22(−9)	2.31(9)	4.43(1)	5296	25	15.3	2,8,10,21,23
04149+0125	M+00-11-046	0.17(21)	0.35(5)	2.67(9)	5.86(2)	4922		14.9	10,21,22,23,24
04151+0126	ZG 415+01	0.22(20)	0.42(5)	3.78(9)	7.16(1)	4922		14.9	10,21,22,23,24
04192+0355	ZG 419+03	0.17(18)	0.28(2)	2.26(9)	4.94(1)	7346		15.2	10
04332+0209		0.28(26)	1.21(10)	4.14(3)	5.02(−2)	3580	55		10,22,23,24
04470+0314	ZG 447+03	0.17(31)	0.64(12)	3.69(6)	5.31(−2)	8383			10,22,23
04502+0258	U3193	0.21(8)	0.22(−3)	3.11(9)	5.72(1)	4436		14.7	10
04513+0104	M+00-13-025	0.12(34)	0.58(15)	3.22(8)	6.90(1)	9922	31		10,22,23,24
04520+0311	N1691, MK 1088	0.48(24)	1.25(7)	7.35(6)	9.91(−1)	4585		13.2	10,21,22

Table 4. (Continued).

IRAS Name	Optical Association	Corrected IRAS Fluxes[a,b] 12 μm	25 μm	60 μm	100 μm	v_h	σ_v	m_B	Notes
07006+8429	N2268	0.49(12)	0.63(−1)	5.53(9)	14.47(3)	2268		12.48	10,21
07055+7155	U3697	0.14(24)	0.41(8)	2.26(8)	5.48(2)	3157		13.1	10,22
07067+7149	U3714	0.31(14)	0.44(1)	4.11(9)	8.86(2)	2889		12.7	10
07099+5504		<0.11(24)	0.24(7)	3.31(10)	5.33(−1)	9782			10
07101+8550	N2276	1.36(9)	1.52(−2)	15.33(9)	29.06(1)	2391		12.3	13
07112+6447	N2347	0.20(−2)	0.15(−9)	2.72(10)	6.15(2)	4424		13.21	10,21,23
07184+8016	N2336	<0.26(4)	<0.24(−5)	3.10(11)	14.61(4)	2252		11.3	11,14
07203+5803	U3828	0.46(9)	0.52(−3)	4.44(8)	8.63(1)	3217		12.7	10,21
07227+5934		0.26(0)	0.22(−10)	2.80(9)	4.44(−2)	12231			10,21
07233+6917	N2366	0.22(22)	0.77(10)	4.89(5)	5.51(−1)	70	34	11.6	10,21,23,24
07236+7213	U3852; MK 8	0.15(24)	0.41(8)	2.53(6)	3.38(−1)	3534		13.8	10,21
07271+6320	ZG 727+63	<0.31(24)	0.78(6)	3.80(2)	3.39(−4)	4420		14.9	1,10
07321+6543	N2403	3.86(16)	6.46(3)	56.18(9)	152.89(3)	131		9.07	9
07447+7428	U4028	0.36(13)	0.49(−1)	3.45(7)	6.16(1)	3943		12.7	10,22
07467+7337	U4041	<0.26(9)	0.30(−2)	2.82(8)	4.87(1)	3449		13.6	10
07540+5648	N2469	<0.28(11)	0.34(−1)	3.62(8)	5.37(0)	3493		13.2	10
07581+5052	N2500	0.27(14)	0.39(1)	3.22(8)	6.25(2)	516		12.3	10,21,22,23
08001+2331	N2512, MK384	0.30(21)	0.61(4)	4.07(7)	7.37(1)	4647	53	14.2	7
08070+3406	N2532	0.59(16)	0.89(1)	4.78(8)	11.47(2)	5251		13.1	10,21,22
08082+2521	N2535, ARP 82	0.14(21)	0.30(6)	4.05(10)	7.63(1)	4104	37	13.5	7
08096+3624	N2543	0.24(16)	0.38(2)	3.08(8)	6.31(2)	2415		12.7	10,21
08111+2401	ZG 811+24	0.23(22)	0.48(5)	3.03(7)	5.85(1)	6052	27	15.3	7
08143+3536	U4306	0.34(12)	0.43(−1)	3.80(8)	6.54(1)	2448		15.1	10
08300+3714		0.12(30)	0.29(8)	2.27(3)	2.09(−8)	12785		17.0	10
08322+2838	N2608	0.27(13)	0.36(0)	2.49(9)	6.02(3)	2126	32	12.9	7
08323+3003		<0.11(18)	0.15(1)	3.24(10)	4.18(−6)	17885	38	18.0	7

Table 4. (Continued).

IRAS Name	Optical Association	Corrected IRAS Fluxes[a,b] 12 μm	25 μm	60 μm	100 μm	v_h	σ_v	m_B	Notes
08327+2855	ZG 832+28	0.18(21)	0.34(4)	2.41(6)	3.25(−2)	7621	29	15.3	7
08354+2555	N2623, ARP 243	0.39(29)	2.11(17)	25.7(6)	24.8(−4)	5508	27	14.4	7
08495+3336	N2683	0.84(−10)	0.45(−13)	9.15(10)	35.23(4)	415		10.74	9
08507+3520	U4653	0.11(27)	0.22(6)	2.67(10)	4.82(−2)	16748		15.0	10,23
08572+3915		0.14(9)	1.73	7.53	4.59	17480	20		5
08579+3447		0.13(9)	0.14(−5)	3.03(11)	4.79(−4)	19645	33		10
09026+3759		0.13(32)	0.35(8)	2.07(1)	1.83(−9)	14293	46		10
09028+2538	N2750	<0.20(23)	0.59(9)	4.27(8)	7.67(1)	2670	31	12.7	7
09089+4509	N2776	0.34(7)	0.36(−3)	3.93(10)	9.82(3)	2624		12.2	10,21,22,23
09108+4019	N2782	0.84(19)	1.61(4)	9.80(6)	14.19(0)	2551		12.2	10,21
09120+2956	N2789	0.28(16)	0.42(0)	2.24(7)	5.28(2)	6313	29	13.8	7
09120+4107	N2785	0.67(17)	1.10(3)	9.46(8)	16.36(1)	2737		14.9	10,21
09126+4432	U4881, ARP 55	0.24(32)	0.70(11)	6.73(8)	9.24(−4)	11773		14.9	10
09141+4212	N2798	0.98(24)	3.41(10)	21.50(6)	30.08(0)	1741		13.0	10
09168+3308	U4947	0.15(38)	0.55(12)	2.86(4)	4.06(−4)	14970		15.3	10
09206+4925	N2854	0.13(23)	0.36(10)	7.35(10)	15.64(2)	2732		13.8	10,22,23,24
09208+4927	N2856	0.42(22)	1.02(8)	8.71(8)	16.11(1)	2638		13.9	10,23,24
09273+2945	N2893, MK 401	0.26(21)	0.63(6)	2.65(5)	3.55(0)	1678	31	13.6	7
09333+4841	M+08-18-012	0.26(29)	0.85(11)	6.25(7)	8.46(−2)	7790		15.0	10,21
09399+3204	N2964	0.79(19)	1.58(5)	12.9(8)	24.6(2)	1353	31	12.4	7
09435+3508		0.18(14)	0.24(−2)	2.36(5)	2.50(−6)	12453		16.5	10,21
09456+3339	N3003	0.40(16)	0.65(2)	3.63(8)	8.19(2)	1546		12.52	10,21,22,23
09479+3347	N3021	0.40(8)	0.42(−3)	4.46(9)	10.76(3)	1540		13.23	10
09534+2727	U5335	0.29(16)	0.46(2)	3.82(8)	7.06(1)	1236	32	14.3	7
09554+3236	N3067	0.68(15)	1.07(2)	9.60(8)	18.03(1)	1456		12.7	10
09583+4714		<0.16(49)	0.54(13)	2.72(−1)	2.67(−13)	25717	26		10
10078+2439	MK 717, U5488	0.28(27)	0.82(8)	3.79(2)	3.67(−5)	6365	30	14.6	7

Table 4. (Continued).

IRAS Name	Optical Association	Corrected IRAS Fluxes[a,b] 12 µm	25 µm	60 µm	100 µm	v_h	σ_v	m_B	Notes
10245+2845	N3245	<0.16(9)	0.19(−2)	2.35(8)	3.76(1)	1370	19	12.0	7
10282+2903	N3265	0.15(22)	0.40(8)	2.60(6)	3.66(0)	1429	28	14.1	7
10369+2659	ZG 1036+27	0.30(13)	0.40(−1)	3.45(8)	5.94(0)	5844	32	15.1	7
10394+1400	N3338	<0.28(9)	<0.31(−2)	4.94(10)	12.41(3)	1330		12.1	11,14
10407+2511	N3344	0.47(13)	0.67(1)	8.80(10)	26.9(3)	582	27	11.1	7
10460+2619	MK 727	0.14(31)	0.65(12)	2.32(1)	2.19(−6)	7687	34	15.7	7
X1051+175	N3454	0.18(13)	0.25(0)	2.06(9)	5.21(3)	1167		14.1	11,16
10565+2448		0.24(40)	1.44(20)	12.75(6)	14.47(−6)	12926	36	16.0	7
10576+2914	N3486	0.33(−6)	0.21(−10)	6.14(10)	16.12(3)	679	10	11.1	7
14008+2816	M+05-33-042	0.20(16)	0.29(1)	2.29(8)	4.27(1)	4560	27	14.7	7
14026+3058	ZG 1402+30	0.13(28)	0.36(10)	3.00(8)	5.19(0)	7578	35	15.5	7
14151+2705	MK673,U9141	0.18(23)	0.34(4)	3.03(9)	5.35(−1)	10987	40	15.0	7
14158+2741		<0.09(16)	0.13(−1)	2.60(11)	3.83(−5)	20902	39	16.0	7
14165+2510	U9165	0.24(19)	0.40(3)	3.60(9)	7.25(1)	5278	36	15.3	7
14190+3013	U9191	0.16(18)	0.25(1)	2.31(9)	5.25(1)	9168	34	15.0	2,8,10,23
14221+2450	N5610	0.34(25)	0.88(8)	5.43(6)	7.99(−1)	5087	26	14.5	7
14280+3126	N5653	0.80(19)	1.50(4)	12.05(8)	22.37(1)	3582	29	13.4	7
14356+3041	U9425	0.18(31)	0.53(9)	2.53(3)	3.06(−4)	10408	33	15.0	7
14547+2448	ARP 302	0.31(20)	0.53(3)	7.08(11)	14.71(1)	10166	31	14.6	7
16104+5235	N6090	0.39(31)	1.30(10)	6.81(5)	9.72(−3)	8730		14.0	1,11
16107+2824	U10273	0.13(18)	0.22(3)	2.34(10)	5.73(2)	7381	38	15.3	7
16161+4015		<0.25(1)	<0.22(−12)	2.50(7)	3.44(−7)	23288	43		1
16180+3753	N6120	0.29(22)	0.54(4)	4.35(8)	8.26(0)	9203	28	14.3	1,3
16305+4823		<0.22(−12)	0.14(−20)	2.07(2)	1.88(−14)	26329	44		1
16340+5252	M+09-27-053	<0.26(3)	<0.23(−8)	2.43(9)	5.14(1)	8684	38		1
16343+3752		<0.25(2)	<0.23(−10)	2.23(8)	3.97(−2)	15269	66	17.0	1

Table 4. (Continued).

IRAS Name	Optical Association	Corrected IRAS Fluxes[a,b] 12 μm	25 μm	60 μm	100 μm	v_h	σ_v	m_B	Notes
16350+7818	N6217	0.59(22)	1.67(8)	11.33(8)	21.44(1)	1385		12.1	1,11
16362+5815	M+10-24-007	<0.24(−2)	0.19(−12)	2.19(8)	3.61(−3)	15687	41		1
16403+2510	U10514	<0.26(10)	0.30(−3)	2.86(7)	3.92(−2)	6783	35	15.4	7
16404+5910	M+10-24-026	<0.27(7)	0.27(−6)	2.60(7)	3.70(−2)	9085	36		1
16412+3655	N6207	0.32(19)	0.66(5)	5.42(9)	11.64(2)	852	100	12.26	13
16418+6540	U10524	<0.26(4)	0.24(−6)	3.81(10)	7.41(1)	7598	28	14.5	1,8
16471+4847	MK 499	<0.26(3)	<0.23(−7)	3.10(3)	2.55(−6)	7680	100		14,20
16474+3430		<0.25(−1)	0.21(−16)	2.32(2)	2.47(−14)	33418	47		1
16478+6303	U10572	0.30(18)	0.51(3)	4.78(9)	8.67(1)	4524	23	13.5	1,2,8
16484+4249	N6239	<0.28(13)	0.38(0)	3.75(8)	6.27(1)	938	12	12.9	1
16487+5447		<0.22(−13)	0.14(−21)	3.01(5)	2.81(−15)	31293	41		1
16577+5900	N6286	0.57(8)	0.60(−3)	11.45(11)	21.99(1)	5600	300	14.2	2,8,13
17012+8356	ZW 673	<0.25(−2)	0.20(−11)	2.43(6)	2.79(−6)	13764	40	17.5	1
17013+3131	U10675	<0.27(10)	<0.31(−4)	2.29(4)	2.55(−5)	10143	38	15.4	1,2,8
17028+5817		<0.37(49)	0.17(114)	2.84(14)	3.67(−9)	31779	59		1
17069+6047	N6306,N6307	<0.29(17)	0.48(2)	3.39(7)	5.11(0)	2973	28	14.3	1
17082+6206		<0.27(9)	0.30(−4)	3.24(8)	5.24(−1)	7774	33	15.6	1
17132+5313		<0.31(24)	0.55(4)	6.67(6)	7.42(−7)	15270	41		1
17180+6039	N6361	0.37(11)	0.45(−1)	4.90(10)	14.50(3)	3862	56	13.9	1,2,8
17313+7544	N6412	0.22(9)	<0.24(−2)	2.28(10)	7.66(3)	1328	70	12.62	1
17366+8646	U10923	0.36(17)	0.55(1)	5.08(9)	10.26(1)	7900	22	14.3	1,2,8
17392+3845		<0.24(−6)	0.16(−13)	2.40(10)	4.39(−1)	12300		15.0	1
17499+7009	N6503	1.33(−1)	0.98(−8)	12.15(9)	30.84(3)	60	71	10.9	13
17501+6825	M+11-22-006	<0.26(3)	0.24(−9)	2.98(9)	5.08(−2)	15357	13	15.2	1
17517+6422		<0.19(−24)	0.18(101)	2.24(11)	2.79(−9)	26151	23	16.0	1,8
17526+3253	U11035	<0.28(11)	0.33(−2)	3.76(9)	7.09(0)	7429	36	14.3	
17530+3446	U11041	0.41(19)	0.74(4)	6.45(9)	13.70(2)	4800		13.9	1,2,8

Table 4. (Continued).

IRAS Name	Optical Association	Corrected IRAS Fluxes[a,b] 12 μm	25 μm	60 μm	100 μm	v_h	σ_v	m_B	Notes
16350+7818	N6217	0.59(22)	1.67(8)	11.33(8)	21.44(1)	1385		12.1	1,11
17548+2401	ZG 1754+24	<0.30(21)	0.60(5)	6.81(8)	9.69(−1)	5944	34	15.7	1
17552+2757	U11060	<0.28(9)	0.32(−3)	3.26(9)	6.95(2)	4621	29	14.9	1
17578+4553		0.24(15)	0.34(1)	3.86(9)	7.54(1)	5763	55		1,8
17583+3430	ZG 1758+34	<0.24(−6)	0.16(−12)	2.46(9)	4.09(−1)	7458	47	15.6	1
18131+6820	N6621	0.32(27)	0.98(10)	7.04(8)	12.56(0)	6230		13.6	1,11
18212+7432	N6643	1.39(3)	1.19(−6)	13.22(9)	33.62(3)	1538		11.8	11,13
18308+6756	N6667	<0.30(7)	0.31(−4)	2.96(9)	6.43(2)	2582	30	13.7	1
18335+6705	N6679	0.23(3)	0.21(−7)	2.94(10)	5.97(1)	6696	150	13.6	1,2,8
18425+6036	N6701	0.79(17)	1.30(3)	11.72(8)	20.09(0)	3983	33	12.9	2,8,13
18443+7433		<0.20(−18)	0.13(−26)	2.15(0)	1.80(−20)	40395	93		1
19120+7320	U11415	<0.52(3)	0.46(−7)	4.94(6)	<5.75(−4)	7500	13	15.1	
X1911+733	N6786	<0.33(32)	3.08(19)	11.07(1)	10.30(−6)	7997	13.7		1,19,20
21052+0340	U11680	<0.38(13)	0.49(−2)	3.31(6)	4.72(−2)	7840	27	14.5	1
21089-0214	U11691	0.30(4)	0.29(−7)	3.53(10)	7.97(1)	9217	35	14.5	1
21091-0134	MK 512	<0.37(−7)	0.24(−14)	2.96(7)	3.97(−3)	9675	22		1,8
21116+0158	U11703	<0.30(21)	0.63(5)	4.14(7)	6.81(0)	4009	31	14.3	1,3
21144-0656	M-01-54-008	<0.26(3)	<0.23(−7)	3.43(11)	7.06(1)	8777	581		1,4,15
21171-0859	M-02-54-004	0.31(15)	<0.47(1)	3.98(9)	7.94(2)	2540	30		1,8
21271+0627	ZG 2127+06	<0.27(9)	0.31(−2)	3.47(8)	5.80(0)	3476	35	15.0	1
21442+0007		<0.26(3)	<0.24(−11)	2.25(7)	3.68(−5)	22187	24		1,8
21497-0824		<0.32(26)	0.72(5)	3.33(3)	3.76(−5)	10330	41		1,8
21504-0628		<0.31(25)	<0.52(1)	3.56(−4)	2.57(−15)	23263	22		1,8
22032+0512		<0.28(10)	<0.31(−5)	2.43(4)	2.69(−6)	12529	60		1
22045+0959	N7212	<0.41(21)	0.74(2)	3.12(5)	5.11(−1)	7800		15.10	1
22074-1654	N7218	0.38(13)	0.53(1)	5.60(9)	10.54(1)	1662	15	12.89	12

Table 4. (Continued).

IRAS Name	Optical Association	Corrected IRAS Fluxes[a,b] 12 μm	25 μm	60 μm	100 μm	v_h	σ_v	m_B	Notes
22204-1547	M-03-57-006	<0.28(13)	<0.36(−1)	2.24(7)	4.23(1)	5045	55		1,8
22221+1748	M+03-57-002	<0.29(−81)	<0.57(35)	3.34(7)	4.67(−1)	6142	42		1,8
22243+1421		<0.24(−3)	0.19(−13)	3.32(4)	2.96(−11)	19389	51		1,8
22287-1917	M-03-57-017	0.35(24)	0.80(7)	6.30(8)	10.46(0)	7263	125		1,8
22317-1036	N7309	<0.44(0)	<0.35(−9)	2.82(9)	7.22(2)	4013	15	13.1	1
22329-1528	M-03-57-024	<0.30(21)	<0.57(2)	2.34(4)	3.62(−1)	6512	55		1,8
22449+0757		<0.27(10)	<0.31(−4)	2.91(8)	4.36(−2)	11140	37		1,8
22469-1932	M-03-58-007	<0.48(22)	0.89(1)	2.48(1)	3.55(−3)	9549	55		1,8
22471+0110		<1.13(−38)	<0.62(60)	2.95(5)	3.91(−6)	17288	34		1,4
22491-1808		<0.32(28)	<0.59(4)	5.42(−2)	3.93(−15)	23312	22		1,8
22509-0041		<0.33(33)	0.81(8)	5.12(1)	4.80(−10)	17478	55		1,8
22575+1542	N7448	0.46(13)	0.61(1)	8.35(10)	17.93(2)	2192	20	12.23	3,12
22586+0523	U12304	<0.42(20)	<0.80(2)	2.16(4)	4.65(2)	3461	20	15.4	1
22595+1541	N7465	<0.35(8)	0.38(−3)	2.96(8)	6.98(3)	195	23	13.3	1,3
23011+0046	ZG 2301+00	<0.18(29)	0.44(7)	2.54(1)	2.27(−8)	12605	48	15.7	10,18,22
23024+1203	N7479	1.79(20)	3.75(4)	15.87(5)	24.32(0)	2399	32	11.3	3,13
23024+1916	ZG 2302+19	<0.34(19)	0.59(4)	8.21(8)	10.78(−2)	7373	300	15.2	1,8
23031+1856		<0.29(17)	0.44(0)	2.19(1)	2.02(−6)	7815	22		1,8
23032+0316	N7483; U12353	0.26(22)	0.55(4)	2.54(5)	4.05(0)	5000		14.3	2,10,21,22,23
23050+0359		0.31(29)	0.69(6)	3.78(4)	4.74(−5)	14271	24		10,21,22
23065+1754	N7497	0.33(4)	0.30(−5)	4.88(10)	13.50(3)	1710	15	13.3	3,12
23106+0603	N7518	<0.13(22)	0.34(9)	5.28(9)	7.49(0)	3531		14.5	10
23121+0415	N7541	1.71(9)	1.95(−2)	22.99(9)	39.70(1)	2607		12.8	13
X2312+0615	M+01-59-015	0.19(13)	0.26(0)	3.14(4)	2.70(−5)	6387	40	15.7	4,14,21,22,24
23135+2516	ZG 2313+25	0.41(32)	1.96(14)	10.02(4)	11.60(−4)	8215	300		8
23157+0618	N7591; U12486	0.37(27)	1.36(11)	8.15(7)	13.77(0)	4964		13.8	10,22
23157-0441	N7592	<0.45(26)	1.19(8)	8.53(6)	10.40(−3)	7328	34	14.0	1

Table 4. (Continued).

IRAS Name	Optical Association	Corrected IRAS Fluxes[a,b] 12 μm	25 μm	60 μm	100 μm	v_h	σ_v	m_B	Notes
23161+2457	U12490	<0.36(18)	0.57(1)	4.58(7)	7.21(−1)	8081	32	14.0	1
23164-0845	N7606	<0.44(13)	<0.61(0)	3.78(8)	9.64(3)	2341	75		14,20
23176+2356	N7620	<0.29(4)	0.27(−7)	2.93(9)	6.18(1)	9565	29	13.5	1
23179+1657	N7625	0.72(16)	1.16(2)	10.28(8)	17.66(1)	1620	10	13.45	13
23179+2702	N7624	0.88(22)	1.88(3)	5.30(3)	7.57(−1)	4500		13.7	1,11
23201+0805		0.18(30)	0.48(8)	2.44(9)	7.81(4)	11393			10,24
23204+0601	ZG 2320+06	0.25(34)	0.67(9)	4.47(5)	5.97(−5)	16480	100	16.0	10,24
23213+0923	N7648	0.32(22)	0.77(7)	5.18(6)	7.20(−1)	3593		13.5	10,22
23215-1208	M-02-59-015	<0.39(11)	0.46(−3)	2.69(7)	4.91(0)	6800	39		1,8
23252+2318	N7673	<0.29(18)	0.52(4)	5.62(7)	6.88(−1)	3402	12	12.7	1
23254+0830	N7674; ARP 182	0.89(24)	1.87(2)	5.26(2)	7.47(−2)	8698	25	13.6	13
23256+2315	N7677	0.34(22)	0.79(6)	4.13(6)	6.11(0)	3543	15	13.9	1
23259+2208	N7678	0.50(18)	0.91(4)	7.78(9)	15.16(1)	3489	10	12.68	1
23262+0314	N7679; ARP 216	0.64(21)	1.26(4)	7.98(6)	12.20(−1)	5120		13.2	13
23277+1529	U12633	<0.30(15)	0.44(1)	3.40(7)	5.37(0)	4236	36	15.4	1,8
23309-0215	U12661	<0.30(22)	<0.62(3)	2.15(5)	4.36(1)	5203	22	15.0	1,8
23327+2913		<0.28(13)	<0.32(−8)	2.08(0)	2.24(−14)	31981	22		8
23336+0152	N7714; ARP 284	0.57(25)	3.14(12)	11.62(2)	11.20(−3)	2804		13.1	10
23362-0647	N7721	0.32(15)	0.50(2)	4.31(9)	11.50(3)	2015	20	12.34	12
23363-1314	N7723	0.50(17)	0.86(2)	4.85(8)	11.08(2)	1913	20	12.07	12
23381+2654		<0.24(−12)	0.13(−17)	2.27(10)	3.85(−1)	10198	22		1,8
23387+2516	ZG 2338+25	<0.30(6)	0.30(−6)	3.46(10)	7.46(1)	9310	33	14.7	1
23394-0353	M-01-60-022	<0.45(21)	<0.84(4)	5.12(6)	7.69(−1)	5707	35		1,8
23410+0228		0.25(32)	0.48(2)	2.31(−1)	2.53(−12)	27335			10,21,24
23413+2547	N7741	0.40(−6)	0.25(−11)	3.11(9)	6.91(2)	750	10	12.26	3,13

Table 4. (Continued).

IRAS Name	Optical Association	Corrected IRAS Fluxes[a,b] 12 μm	25 μm	60 μm	100 μm	v_h	σ_v	m_B	Notes
23414+0014	N7738	0.49(17)	0.76(1)	4.71(6)	7.55(−1)	6711		14.4	10,21,22
23417+1029	N7742	<0.29(15)	<0.45(2)	3.27(8)	6.57(2)	1655	19	12.37	1
23433+1147	U12773	<0.34(10)	0.39(−3)	3.44(8)	6.01(0)	4261	20	14.6	1
23445+2911	N7752	<0.33(14)	0.46(1)	5.28(9)	10.42(1)	5142	20	14.3	1
23446+1519	ZG 2344+15	<0.33(31)	1.35(10)	4.12(−2)	3.30(−7)	7772	39	15.5	1,8
23456+2056		<0.37(8)	<0.39(−5)	2.44(9)	7.61(3)	7326	62	16.0	1
23471+2939	U12798	<0.38(0)	0.30(−9)	2.64(9)	5.72(2)	5326	32	15.5	1
23485+1952	N7769	<0.46(12)	0.58(−1)	5.20(9)	11.81(2)	4197	25	13.04	1
23488+1949	N7771	1.12(20)	2.22(5)	23.38(8)	36.79(0)	4364	32	13.39	13
23488+2018	MK 331	0.67(28)	2.74(13)	17.89(5)	20.44(−3)	5363		14.9	1
23560+1026	U12872	<0.37(17)	0.59(1)	3.37(8)	7.22(2)	5264	31	13.8	1
23564+1833	U12879	<0.37(−2)	0.27(−10)	2.88(8)	4.16(−1)	5361	31	15.0	1,2,8
23566-0833		<0.26(6)	<0.26(−7)	2.63(6)	3.17(−6)	14779	60		1,8
23568+2028	N7798	0.38(17)	0.66(3)	5.48(8)	10.16(1)	2403	15	12.7	1
23587+1249	U12906	<0.28(12)	<0.35(−2)	2.26(8)	4.37(1)	5300	27	13.8	1
23591+2312		<0.44(16)	<0.68(2)	5.99(9)	14.64(2)	4383	26	13.2	1
23597+1241	N7810	<0.29(16)	<0.45(1)	3.57(9)	7.22(1)	5532	29	14.3	1

Notes for Table 4:

[a] All fluxes have been color and K-corrected, as in SKHL.

[b] The percentage correction p follows the corrected flux density c, in parenthesis. The uncorrected flux density = c / (p/100 + 1).

[1] Fluxes from PSC.

[2] m_h from UGC.

[3] v_h, m_B from Huchra *et al.* (1983).

[4] F(60) from the SSS; the rest are from the PSC.

[5] Fluxes and v_h from Sanders *et al.* (1987).

[7] All values from SKHL.

[8] v_h from JPH.

[9] Fluxes from Rice *et al.* (1988).

[10] Fluxes are from Add-Scan data.

[11] v_h, m_B from UGC.

[12] Fluxes from Devereux (1987).

[13] Fluxes from Young *et al.* (1988).

[14] F(60) from the SSSC; the other infrared fluxes from PSC.

[15] F(60) and F(100) from the SSSC; the other infrared fluxes from the PSC.

[16] $M_B = m_{pg}$ from Markaryn and Liporetskii (1971).

[18] m_B from JPH.

[19] v_h from UGC.

[20] Redshift from Palumbo *et al.* (1983).

[21] Extended at 12 μm.

[22] Extended at 25 μm.

[23] Extended at 60 μm.

[24] Extended at 100 μm.

IRAS Name	Other Names	Date	Integration Time (sec)	Airmass	Notes
00014+2028	N7817	9/12/87	300	1.02	
00047+2725	N1	9/12/87	90	1.01	
00073+2538	N23	9/12/87	45	1.01	
00119+2810	U141	9/12/87	300	1.01	
00132+1548	U148	11/18/86	300	1.05	
00141+0647	U155	11/17/86	130	1.16	
00151+1110	N63	11/18/86	130	1.07	
00196+1012	N95	11/18/86	110	1.08	
00221+2049		9/12/87	300	1.01	
00276+0149	N132	11/18/86	350	1.33	
00287+0811	U312; MK 552	11/18/86	300	1.15	
00366+0035	N192	11/18/86	200	1.33	
00387+2513	N214	9/12/87	120	1.02	
00409+1404	U463	11/18/86	600	1.06	
00454+0801	M+01-03-003	11/18/86	200	1.14	
00477+2414		9/12/87	600	1.02	
00491+2514		9/12/87	330	1.03	
00509+1225	U545	11/18/86	180	1.06	
00521+2858	U556	9/12/87	300	1.06	
00537+1337	U580; U582	11/18/86	300	1.05	
00537+1337	cluster	9/12/87	300	1.16	
01086+2739	ZG 108+27	9/14/87	150	1.03	
01167+0418	ZG 116+04; MK 567	11/18/86	175	1.13	
01171+0308	N470	11/18/86	130	1.14	
01173+1405	N471	9/14/87	30	1.06	
01173+1431	ZG 117+14	9/14/87	120	1.08	a
01191+1719	U903	9/14/87	450	1.04	
01195+0041	N493	11/18/86	800	1.18	
01197+0044		11/18/86	875	1.17	
01217+0122		11/18/86	470	1.22	
01219+0331	N520; ARP 157	11/18/86	300	1.21	
01276+2958		9/14/87	450	1.00	
01324+2138		9/14/87	240	1.02	
01346+0537	N632	9/14/87	90	1.11	
01403+1323	N660	9/14/87	180	1.06	
01410+1154	U1209	9/14/87	180	1.07	
01418+1651	ZW 035	9/14/87	450	1.04	
01450+2710	N672	9/14/87	450	1.04	
01457+1116	N673	9/14/87	360	1.14	
01484+2220	N695	9/15/87	300	1.03	

Table 5. Observation Log

Table 5. (Continued)

IRAS Name	Other Names	Date	Integration Time (sec)	Airmass	Notes
01485+2206	N697	9/15/87	450	1.02	
01492+0602	N706	9/15/87	360	1.11	
01503+1227	M+02-05-054	9/15/87	150	1.06	
01555+0250	U1449; ARP 126	11/18/86	420	1.20	
01556+2507	U1451	9/15/87	200	1.01	
01565+1845	N772	9/15/87	120	1.03	
01572+0009	MK 1014	11/18/86	140	1.26	
01572+0009	MK 1014	11/18/86	140	1.26	
01572+0009	MK 1014	11/18/86	140	1.26	
01572+0009	MK 1014	11/18/86	140	1.26	
01587+2614	U1507	9/15/87	380	1.01	
03017+0724		11/13/86	150	1.32	
03079+0018		11/13/86	420	1.21	
03119+1448		11/18/86	700	1.05	
03119+1448		11/18/86	700	1.07	
03144+0104	U2638	11/13/86	400	1.19	
03222+1617		11/18/86	420	1.06	
03275+1535		11/18/86	300	1.08	
03288+0108		11/13/86	400	1.19	
03315+0055		11/13/86	400	1.22	
03315+0055		11/13/86	400	1.22	
03359+1523		11/18/86	300	1.08	
03371+1046		11/18/86	300	1.08	
03514+1546	ZG 351+15	11/18/86	350	1.09	
03521+0028		11/13/86	450	1.22	
04002+0149	U2936	11/13/86	200	1.28	
04149+0125	M+00-11-046	11/13/86	400	1.33	
04151+0126	ZG 415+01	11/13/86	30	1.35	b
04192+0355	ZG 419+03	11/13/86	150	1.33	
04332+0209		11/13/86	200	1.33	
04332+0209		11/13/86	350	1.33	
04470+0314	ZG 447+03	11/13/86	400	1.32	
04502+0258	U3193	11/13/86	170	1.36	
04513+0104	M+00-13-025	11/13/86	275	1.42	
04520+0311	U3201; MK1088	11/13/86	75	1.41	
07006+8429	N2268	11/17/86	140	1.66	
07055+7155	U3697	11/17/86	600	1.36	
07067+7149	U3714	11/17/86	200	1.37	
07099+5504		11/17/86	350	1.19	
07101+8550	N2276	11/18/86	260	1.70	

Table 5. (Continued)

IRAS Name	Other Names	Date	Integration Time (sec)	Airmass	Notes
07112+6447	N2347	11/18/86	230	1.20	
07203+5803	U3828	11/18/86	200	1.12	
07227+5934		11/18/86	300	1.17	
07233+6917	N2366 or N2363	11/18/86	300	1.30	
07236+7213	U3852	11/18/86	350	1.31	
07271+6320	ZG 727+63	11/18/86	110	1.17	
07315+6543		11/18/86	230	1.20	
07321+6543	N2403	11/18/86	30	1.20	
07321+6543	N2403	11/18/86	30	1.20	
07321+6543	N2403	11/18/86	30	1.20	
07321+6543	N2403	11/18/86	30	1.20	
07321+6543	N2403	11/18/86	30	1.20	
07321+6543	N2403	11/18/86	30	1.20	
07321+6543	N2403	11/18/86	30	1.20	
07321+6543	N2403	11/18/86	30	1.20	
07321+6543	N2403	11/18/86	30	1.20	
07321+6543	N2403	11/18/86	30	1.20	
07321+6543	N2403	11/18/86	30	1.20	
07321+6543	N2403	11/18/86	30	1.20	
07321+6543	N2403	11/18/86	30	1.20	
07321+6543	N2403	11/18/86	30	1.20	
07447+7428	U4028	11/18/86	300	1.35	
07467+7337	U4041	11/18/86	420	1.34	
07540+5648	N2469	11/18/86	300	1.11	
08001+2331	N2512, MK384	2/6/87	100	1.06	c
08001+2331	N2512, MK384	2/6/87	100	1.07	c
08070+3406	N2532, U4256	2/7/87	210	1.13	
08082+2521	ARP 82B	2/6/87	240	1.05	c
08082+2521	N2535, ARP 82	2/6/87	240	1.06	c
08096+3624	N2543	2/7/87	180	1.12	
08096+3624	N2543	2/9/87	300	1.03	d
08096+3624	N2543	2/9/87	300	1.04	d
08096+3624	N2543	2/9/87	300	1.04	d
08096+3624	N2543	2/9/87	300	1.04	d
08096+3624	N2543	2/9/87	300	1.04	d
08111+2401	ZG 811+24	2/6/87	100	1.04	c
08143+3536	U4306	2/7/87	210	1.08	

Table 5. (Continued)

IRAS Name	Other Names	Date	Integration Time (sec)	Airmass	Notes
08300+3714		2/7/87	60	1.12	
08300+3714		2/7/87	60	1.12	
08300+3714		2/7/87	60	1.12	
08300+3714		2/7/87	60	1.12	
08300+3714		2/7/87	60	1.12	
08300+3714		2/7/87	60	1.12	
08300+3714		2/7/87	60	1.13	
08322+2838	N2608	2/6/87	240	1.05	b, c
08323+3003		2/6/87	300	1.00	c
08323+3003		2/6/87	300	1.00	c
08323+3003		2/6/87	300	1.00	c
08323+3003		2/6/87	300	1.00	c
08323+3003		2/6/87	300	1.00	c
08323+3003		2/6/87	300	1.03	c
08323+3003		2/6/87	600	1.02	c
08323+3003		2/6/87	600	1.03	c
08323+3003		2/6/87	600	1.03	c
08323+3003		2/7/87	300	1.05	
08323+3003		2/7/87	300	1.05	
08323+3003		2/7/87	300	1.06	
08327+2855	ZG 832+28	2/6/87	210	1.01	c
08354+2555	N2623, ARP 243	2/6/87	210	1.01	c
08354+2555	N2623, ARP 243	2/6/87	210	1.01	c
08354+2555	N2623, ARP 243	2/7/87	210	1.05	
08495+3336	N2683, U4641	2/7/87	180	1.12	
08507+3520	U4653	2/7/87	250	1.10	
08507+3520	U4653	2/7/87	250	1.11	
09026+3759		2/6/87	300	1.01	c
09026+3759		2/6/87	300	1.01	c
09026+3759		2/7/87	300	1.05	
09028+2538	N2750, U4769	2/5/87	250	1.02	c
09089+4509	N2776,U4838	2/7/87	210	1.07	
09108+4019	N2782, U4862	2/7/87	120	1.05	
09120+2956	N2789	2/5/87	110	1.01	c
09120+4107	U4876	2/7/87	120	1.05	
09126+4432	U4881	2/7/87	300	1.04	
09126+4432	U4881	2/7/87	300	1.04	
09141+4212	N2798,N2799	2/7/87	150	1.03	

Table 5. (Continued)

IRAS Name	Other Names	Date	Integration Time (sec)	Airmass	Notes
09168+3308	U4947	2/6/87	400	1.00	c
09168+3308	U4947	2/6/87	800	1.01	c
09168+3308	U4947	2/7/87	240	1.08	
09206+4925	N2854	2/7/87	270	1.06	
09208+4927	U2856	2/7/87	240	1.05	
09273+2945	N2893, MK 401	2/5/87	120	1.01	c
09333+4841	M+08-18-012	2/7/87	240	1.05	
09399+3204	N2964	2/5/87	120	1.01	c
09435+3508		2/6/87	500	1.01	c
09456+3339	N3003, U5251	2/6/87	400	1.01	c
09479+3347	N3021, U5280	2/6/87	250	1.01	c
09534+2727	U5335	2/5/87	220	1.02	c
09554+3236	N3067	2/6/87	300	1.02	c
09583+4714		2/7/87	300	1.04	
09583+4714		2/7/87	300	1.04	
09583+4714		2/7/87	300	1.04	
09583+4714		2/7/87	300	1.04	
09583+4714		2/7/87	300	1.05	
09583+4714		2/7/87	300	1.05	
10078+2439	MK 717, U5488	2/5/87	180	1.03	c
10078+2439	MK 717, U5488	2/5/87	180	1.03	c
10078+2439	MK 717, U5488	2/5/87	180	1.03	c
10078+2439	MK 717, U5488	2/5/87	180	1.03	c
10245+2845	N3245	2/5/87	40	1.02	c
10282+2903	N3265	2/5/87	150	1.01	c
10369+2659	ZG 1036+27	2/5/87	300	1.02	c
10407+2511	N3344	2/5/87	30	1.02	c
10460+2619	MK 727	2/5/87	220	1.01	c
10460+2619	MK 727	2/5/87	220	1.01	c
10460+2619	MK 727	2/5/87	220	1.01	c
10565+2448		2/5/87	240	1.01	c
10565+2448		2/5/87	240	1.01	c
10565+2448		2/5/87	240	1.01	c
10565+2448		2/5/87	240	1.01	c
10576+2914	N3486	2/5/87	100	1.00	c
14008+2816	M+05-33-042	2/7/87	240	1.09	d
14008+2816	M+05-33-042	2/9/87	300	1.02	d
14008+2816	M+05-33-042	2/9/87	300	1.02	d
14026+3058	ZG 1402+30	2/7/87	300	1.07	d

Table 5. (Continued)					
IRAS Name	Other Names	Date	Integration Time (sec)	Airmass	Notes
14151+2705	MK673,U9141	2/7/87	210	1.08	d
14151+2705	MK673,U9141	2/7/87	210	1.08	d
14158+2741		2/7/87	300	1.06	d
14158+2741		2/7/87	300	1.06	d
14165+2510	U9165 companion	2/7/87	300	1.04	d
14165+2510	U9165	2/7/87	300	1.05	d
14221+2450	N5610	2/7/87	210	1.0	d
14280+3126	N5653,U9318	2/7/87	150	1.02	d
14356+3041	U9425	2/7/87	300	1.03	d
14547+2448	ARP 302	2/7/87	300	1.05	d
16104+5235	N6090	9/15/87	250	1.46	
16161+4015		9/14/87	120	1.15	
16305+4823		9/14/87	600	1.25	
16340+5252	M+09-27-053	9/15/87	450	1.44	
16343+3752		9/15/87	450	1.14	
16350+7818	N6217	9/17/87	60	1.51	a, e
16362+5815	M+10-24-007	9/17/87	360	1.25	e
16403+2510	U10514	9/15/87	130	1.18	
16404+5910	M+10-24-026	9/17/87	450	1.27	e
16412+3655	N6207	9/15/87	225	1.19	
16418+6540	U10524	9/17/87	30	1.36	e
16478+6303	N6247	9/17/87	180	1.34	e
16484+4249	N6239	9/15/87	120	1.26	
16487+5447		9/17/87	600	1.37	e
17012+8356	ZW 673	9/13/87	450	1.64	d
17013+3131	U10675	9/12/87	60	1.12	
17028+5817		9/13/87	300	1.20	d
17069+6047	N6306,N6307	9/13/87	450	1.28	d
17082+6206		9/13/87	450	1.31	d
17132+5313		9/13/87	450	1.28	d
17180+6039	N6361	9/13/87	300	1.35	d
17313+7544	N6412	9/13/87	450	1.53	d
17366+8646	U10923	9/13/87	300	1.79	d
17392+3845		9/12/87	200	1.10	
17499+7009	N6503	9/13/87	300	1.47	d
17501+6825	M+11-22-006	9/13/87	350	1.48	d
17517+6422		9/13/87	600	1.49	d
17526+3253	U11035	9/12/87	600	1.10	
17530+3446	U11041	9/12/87	60	1.13	

Table 5. (Continued)

IRAS Name	Other Names	Date	Integration Time (sec)	Airmass	Notes
17548+2401	ZG 1754+24	9/12/87	150	1.06	
17552+2757	U11060	9/11/87	330	1.06	
17578+4553		9/12/87	72	1.17	
17583+3430	ZG 1758+34	9/12/87	700	1.13	
18131+6820	N6621	9/12/87	300	1.59	
18212+7432	N6643	9/14/87	300	1.41	
18308+6756	N6667	9/14/87	600	1.29	
19120+7320	U11415	9/12/87	10		
21052+0340	U11680	9/14/87	240	1.19	
21089-0124	U11691	9/15/87	60	1.21	
21091-0134	MK 512	9/15/87	60	1.20	
21116+0158	U11703	9/14/87	330	1.23	
21171-0859	M-02-54-004	9/15/87	100	1.32	
21497-0824		9/15/87	200	1.32	
21504-0628		9/15/87	300	1.28	
22032+0512		9/12/87	300	1.15	
22045+0959	N7212	9/12/87	300		
22074-1654	N7218	9/17/87	450	1.60	e
22221+1748	M+03-57-002	9/15/87	450	1.04	
22243+1421		9/15/87	450	1.05	
22287-1917	M-03-57-017	9/17/87	200	1.66	e
22317-1036	N7309	9/17/87	450	1.38	e
22329-1528	M-03-57-024	9/17/87	150	1.49	e
22449+0757		9/12/87	150	1.13	
22469-1932	M-03-58-007	9/17/87	200	1.63	e
22471+0110		9/12/87	600	1.19	
22491-1808		9/17/87	450	1.58	e
22509-0041		9/15/87	300	1.19	
22575+1542	N7448	9/15/87	200	1.04	
22586+0523	U12304	9/12/87	900	1.14	
22595+1541	N7465	9/15/87	45	1.04	
23011+0046	ZG 2301+00	11/13/86	400	1.14	
23024+1203	N7479	9/13/87	180	1.03	d
23024+1916	ZG 2302+19	9/13/87	400	1.03	d
23031+1856		9/13/87	600	1.05	d
23032+0316	U12353	11/13/86	400	1.14	
23050+0359		11/13/86	400	1.14	

Table 5. (Continued)

IRAS Name	Other Names	Date	Integration Time (sec)	Airmass	Notes
23065+1754	N7497	9/13/87	450	1.06	d
23106+0603	N7518	11/13/86	150	1.14	
23121+0415	N7541	11/13/86	600	1.13	
X2312+062	M+01-59-01	11/13/86	600	1.14	
23135+2516	ZG 2313+25	9/17/87	120	1.01	e
23157+0618	U12486	11/13/86	225	1.29	
23157-0441	N7592	9/15/87	250	1.24	
23161+2457	U12490	9/17/87	200	1.01	e
23176+2356	N7620	9/17/87	600	1.01	e
23179+1657	N7625	9/13/87	250	1.07	d
23179+2702	N7624	9/17/87	450	1.00	e
23201+0805		11/13/86	225	1.29	
23201+0805		11/13/86	450	1.29	
23204+0601	ZG 2320+06	11/13/86	450	1.38	
23204+0601	ZG 2320+06	11/18/86	420	1.10	
23213+0923	N7648	11/13/86	450	1.39	
23215-1208	M-02-59-015	9/17/87	30	1.43	
23252+2318	N7673	9/17/87	300	1.01	e
23254+0830	N7674; ARP 182	11/13/86	200	1.44	
23256+2315	N7677	9/17/87	60	1.04	e
23259+2208	N7678	9/17/87	30	1.05	e
23262+0314	N7679; ARP 216	11/13/86	112	1.14	
23277+1529	U12633	9/13/87	225	1.08	d
23309-0215	U12661	9/15/87	360	1.21	
23327+2913		9/17/87	900	1.05	e
23336+0152	N7714; ARP 284	11/13/86	45	1.15	
23362-0647	N7721	9/15/87	360	1.28	
23363-1314	N7723	9/17/87	100	1.47	
23381+2654		9/17/87	90	1.35	e
23387+2516	ZG 2338+25	9/17/87	600	1.07	e
23394-0350	M-01-60-022	9/15/87	260	1.24	
23410+0228		11/13/86	450	1.15	
23414+0014	N7738	11/13/86	150	1.18	
STANDARD	N2264	11/13/86	200	1.18	d
STANDARD	N2264	11/17/86	400	1.21	
STANDARD	N2264	11/17/86	60	1.46	
STANDARD	N2264	11/17/86	60	1.47	
STANDARD	N2264	11/18/86	130	1.40	

Table 5. (Continued)

IRAS Name	Other Names	Date	Integration Time (sec)	Airmass	Notes
STANDARD	N2264	2/7/87	120	1.18	d
STANDARD	N2264	2/7/87	60	1.15	
STANDARD	N2419	2/5/87	300	1.01	c
STANDARD	N2419	2/6/87	100	1.04	c
STANDARD	N4147	2/5/87	150	1.22	c
STANDARD	N4147	2/5/87	40	1.05	c
STANDARD	N4147	2/6/87	90	1.09	c
STANDARD	N4147	2/7/87	80	1.05	
STANDARD	N4147	2/7/87	90	1.21	d
STANDARD	N7006	11/13/86	10	1.07	
STANDARD	N7006	11/13/86	10	1.88	
STANDARD	N7006	11/13/86	200	1.07	
STANDARD	N7006	11/13/86	200	1.92	
STANDARD	N7006	11/18/86	10	1.10	
STANDARD	N7006	11/18/86	30	1.10	
STANDARD	N7790	11/18/86	100	1.26	
STANDARD	N7790	11/18/86	8	1.27	

Notes for Table 5:

[a]Out of focus.

[b]Bright foreground star.

[c]No preflash.

[d]Cloudy, not photometric.

[e]Wispy clouds.

CHAPTER III

CLASSIFICATION AS INTERACTING OR NON-INTERACTING

A. Working Definition of Interacting Galaxies

The goal in this project is to distinguish galaxies whose far-infrared emission is mainly due to an interaction with another galaxy, from galaxies with a relatively stable rate of far-infrared emission. In this Chapter, a review of various theoretical results on interactions is given, and limiting interaction parameters are chosen to define a strong interaction for this study. In the next Chapter, these theoretical results are checked empirically, by comparing 60 μm luminosities for galaxies with different interaction parameters.

There are five parameters which influence the strength of an induced far-infrared burst. The first two are the relative mass of the companion and its separation, which determine the tidal strength. The third factor is the velocity of passage of the companion, in that a rapid passage is less likely to induce tidal distortions and star formation than a slow passage (Toomre and Toomre 1972; Farouki and Shapiro 1982; Noguchi and Ishibashi 1986). Limits on each of these three criteria will be considered separately in this Chapter.

The fourth important parameter is the morphological type of the progenitor galaxies. Previous studies show that the total far-infrared luminosity depends on the amount of molecular hydrogen present in galaxies (Young *et al.* 1984; Young *et al.* 1986). Further, the Noguchi (1987) models of galaxy encounters suggest that the initial stellar and gas distributions in a galaxy affect the amount of induced activity.

The fifth factor is the direction of passage of the companion. Numerical modeling of galaxy encounters show that tidal distortions and mergers are more likely to occur if the spin and orbital angular momentum are aligned, that is, when the encounter is direct (Wright 1972; Toomre and Toomre 1972; White 1979). Furthermore, the models of Noguchi and Ishibashi (1986) show that the orbits of gas clouds are much less disturbed in a retrograde collision than in a direct collision, and the star formation rate is not significantly enhanced (less than a factor of 1.2) in a retrograde encounter. Further, companions which orbit out of the plane of the disk cause less disturbance than planar orbits.

These last two parameters cannot be properly addressed with the available data for the galaxies in this sample, and are thus ignored in this study. This introduces some scatter into the results.

1. Pair Separation

The behavior of gas clouds during close encounters of galaxies has been modeled by Noguchi and Ishibashi (1986), and star formation rates estimated. They find that the rate of cloud-cloud collisions, which they equate with the star formation rate, are enhanced by a factor of ~7 in an encounter between galaxies of equal mass with a pericentric separation $D_p = 2 \times$ the radius R. In their study, the model galaxy is a disk with an exponential radial distribution of gas, and the disk is truncated at a radius R which is 4 times the exponential scalelength. In contrast, the cloud-cloud collision rate (star formation rate) is only enhanced a factor of ~2 times for $D_p = 3R$. They find that this enhancement diminishes rapidly between $D_p = 2.5R$ and 3R. However, they also find that there is a time delay between closest encounter and maximum induced cloud collision rate, implying that the maximum separation for this study should be set somewhat larger than 2R. In this study, therefore, the maximum separation is set to 3 times the radius. Note, however, that the observed separation used in this study is a projected separation, which introduces uncertainty into the results, in the sense that some widely separated pairs may be inadvertently included in the interacting sample.

The next question is, how to measure the radius? A commonly used measure of galaxy size is the diameter of the *blue* image corresponding to a surface brightness of 25 mag arcsec^{-2}. Since I-band ($\lambda_{eff} \sim 0.9$ μm) rather than blue images are available for most of the galaxies in this study, an analogous I-band measurement is preferable. For a typical spiral, B–I ~ 1.5 (Pierce and Tully 1988), so D_{25} corresponds to the diameter at $\mu_I = 23.5$ mag arcsec^{-2}. A higher surface brightness, corresponding to ~10% of the typical full moon sky brightness encountered in this study, was selected for this study. This brightness, ~22 mag/arcsec^2, was recorded with a S/N ~ 4–5 in the 5–10 minute integrations obtained for this study.

2. Mass Ratio

The second criterion is the mass ratio. If the change in the star formation rate is proportional to the tidal force, then, since the tidal force is proportional to $m_1 m_2/D^3$, a change in pericentric separation from $D_p = 2R$ to $D_p = 3R$ should be approximately equivalent to a decrease in mass of the companion from $m_1/m_2 = 1$ to $m_1/m_2 = 1/4$, where m_1 = the mass of the companion and m_2 = the mass of the infrared source. For this study, the I-band luminosity ratio is set to a slightly lower level of 1/4, as it is assumed in this work that the I-band luminosity is proportional to the stellar mass. For the 42 galaxy pairs which were larger than the field covered by the I-band images, or whose separation is larger than the field of view covered by the I-band image, the blue luminosity ratio was used instead of the I-band ratio. In only four of these 42 cases (NGC 192, NGC 2798, NGC 7541, and NGC 7714), did this lead to an uncertainty in classification; the rest are either "non-interacting", or have blue luminosity ratios much less than 1/4 or else very close to unity.

3. Velocity Difference

Finally, the maximum velocity difference allowable between two galaxies for a strong far-infrared enhancement to occur must be estimated. A slow passage of two galaxies is more likely to cause tidal disruptions and eventual merger than rapid passage; numerical modeling results show that encounters between galaxies in bound and parabolic orbits lead to mergers more often than hyperbolic passage (Toomre 1977; Miller and Smith 1980; Farouki and Shapiro 1982). Further, the models of Noguchi and Ishibashi (1986) of the behavior of gas clouds in disks undergoing gravitational encounters show that a parabolic passage has a much greater effect on cloud-cloud collisions and star formation rate than a hyperbolic passage. Farouki and Shapiro (1982) find that for a merger to occur between disk galaxies, the maximum velocity difference at pericenter must be less than 2–3 times the circular velocity. A typical massive spiral has a rotational velocity of ~250 km/s (Krumm and Shapiro 1977), leading to a maximum velocity difference of ~500–750 km/s for mergers. A conservative limit of 500 km/s is chosen for this study. This criterion is also important in eliminating foreground and background galaxies. Previous studies of interacting pairs have used limits of 1000 km/s (Solomon and Sage 1988) and 600 km/s (Keel *et al.* 1985) to define their samples. Since none of the pairs in this sample have velocity differences in the range 500–1000 km/s, the same results would be obtained with any of these three definitions.

In addition to pairs which fulfill these three criteria, galaxies which have a single nucleus with two strong tails are labeled interacting, since numerical modeling results of colliding galaxies (Toomre and Toomre 1972) show that two tails can result from the collision of two spiral galaxies of approximately equal mass.

In the next Chapter, these theoretical results and selection criteria are tested empirically by comparing the 60 μm luminosity with mass ratio and separation, and determining statistically the enhancement in far-infrared luminosity as a function of these interaction parameters.

B. Interacting Galaxies

Out of the 275 galaxies in the sample, 140 have possible companions or are possible merger remnants. For these galaxies, I-band luminosity ratios (assumed equal to the stellar mass ratio), separations, and velocity differences were determined. The working definition of "interacting", $m_1/m_2 \geq 1/4$, $D \leq 3R$, and $\Delta v \leq 500$ km/s, was then applied to the galaxies in the pair sample. It was found that 56 of the 140 galaxies fit the "interacting" criteria, 198 are non-interacting, and 21 have an uncertain classification for various reasons (see Section D).

There are three different types of galaxies that fall in the interacting class. These are, first, those with completely merged nuclei and two tidal tails (6 galaxies), second, those in which the two galaxies have connecting material, either a bridge or a common envelope, but still have two distinct nuclei (14 galaxies), and third, close pairs which are in or nearly in contact (36 galaxies).

The galaxy Arp 243 (IRAS 08354+2555) is the prototype of a merger remnant with a single body and two pronounced tidal tails (*c.f.*, Joy 1986). Two other galaxies of this type are IRAS 22491−1808, shown in Figure 2, and ZG 2320+06 (IRAS 23204+0601). In addition, the tail-like structures observed in Markarian 1014 by MacKenty and Stockton (1984), are confirmed in the new I-band image; thus, it is also classified as a merger remnant. The well-known galaxy NGC 520 (Arp 157; IRAS 09168+3308) is another galaxy with tidal tails which is thought to be a merger remnant (Stockton and Bertola 1980; Joseph and Wright 1985). Figure 3 shows UGC 11035 (IRAS 17526+3253), which is also classified here as a merger remnant, due to the tail-like structures.

Figures 4 through 7 show examples of galaxies whose bodies have merged, but which still have two distinct nuclei. Two nuclei are resolved in UGC 4947 (IRAS 09168+3308) (Figure 7), which is classified as SB in the UGC. The greater dynamical range available with the CCD compared to the plates, or the greater dust penetrating power of the I–band over the B and R bands, made it possible to distinguish the two intensity peaks. Two examples of galaxies which appear to have connecting bridges are IRAS 01197+0044 and IRAS 03119+1448, shown in Figures 8 and 9.

IRAS 09583+4714 (Figure 10) is an example of the third type of interacting galaxy: close pairs with no bridge. The leftmost galaxy in the Figure, designated here as object C, is the closest optical source to the IRAS position.

C. Non-Interacting Galaxies

There are 198 galaxies which do not fit the interaction criteria, and are classified as non-interacting in this study. These range from symmetrical, isolated spirals, to post-encounter galaxies which have moved apart more than three radii, to galaxies with very low-mass companions. Several of these galaxies show obvious tidal distortions due to a companion. To estimate how morphological structure relates to the far-infrared luminosity, two extreme subsets of this set of 198 galaxies were obtained. These are, first, the set of galaxies which fail the interaction criteria, yet are clearly gravitationally distorted by a companion. There are 20 galaxies in this group. The other extreme group consists of those galaxies which are clearly isolated symmetrical spirals. There are 65 galaxies in the non-interacting sample which fit in this subset. Clearly, there will be biases in choosing these subsets, as the visibility of morphological structural characteristics such as bridges and tails is a function of distance, as is the subjective selection of symmetrical spirals. Thus, these two subsets consist only of nearby, optically bright galaxies. Less than half of the 198 galaxies are included in the sum of these two subsets. However, a comparison of the far-infrared properties of these two sets is useful in determining the range in far-infrared luminosity as a function of morphological structure, for the galaxies which are not classified as interacting in this study. This comparison is done in Chapter IV.

Examples of the disturbed galaxies which are included in the "non-interacting" sample, are, first, NGC 7679 (IRAS 23262+0314), part of Arp 216. This is not classified as interacting, because it is separated from its partner NGC 7682 by ~5 × times its radius (Figure 11). One arm may be distorted; this may be due to NGC 7682.

Another widely separated pair not classified as interacting is Arp 295 (IRAS 23394-0353), which is connected by a bridge. The IRAS source is identified with the optical galaxy in the southwest, which itself has a long tail and is also connected by a long bridge to another galaxy 2′ to the northeast. Another of this type is UGC 10675 (IRAS 17013+3131). This is a pair of galaxies; the fainter has only ~6% of the I-band luminosity of the brighter, and is at a distance of ~ 10 × the radius of UGC 10675. No redshift of the companion is available at present, however, the POSS plates show a faint bridge which appears to connect the two galaxies and an opposing plume on the brighter galaxy (component A in Table 3; the IRAS source). Another similar galaxy pair is IRAS 17392+3945 (Figure 13). The bridge is ~4 × the radius of the brighter galaxy (component A in Table 3; the IRAS source), and the fainter galaxy (component C in Table 3) has an I-band luminosity of only ~15% that of component A.

There are other examples of disturbed galaxies whose companions are faint—if they are detected at all—which are thus classified as non-interacting. NGC 5610 (IRAS 14221+2450) has a distorted outer ring-like structure (Figure 14). The distortion is presumably due to the small companion to the southeast, which is at the same redshift, but has an I-band luminosity of only 4% that of NGC 5610.

D. Ambiguous Galaxies

The 21 galaxies which have not been classified fall into several different categories. Some have uncertain optical identifications, some are barely resolved, and others have peculiar structures which are not clearly induced by an interaction or merger. These are put into a separate class of "ambiguous galaxies." This class includes some of the most unusual and interesting galaxies in this sample. In this section, they are discussed in some detail.

1. IRAS 03521+0028

The source IRAS 03521+0028 has the faintest optical counterpart in this sample. Galaxies which are bright at 60 μm but optically faint are of interest because several such sources have been found to be distant, very luminous galaxies (Houck *et al.* 1985). IRAS 03521+0028 does not appear on the Palomar O (blue-sensitive) plate, and appears only very faintly on the Palomar E (red-sensitive) plate. A high-contrast reproduction of the POSS red plate in the vicinity of the IRAS source is shown in Figure 15, and the CCD I-band image is shown in Figure 16. The marked nebula lies very near the IRAS position (see Table 3 for the optical position determined from the Grant Machine).

IRAS 03521+0028 was observed on November 13, 1986, September 15, 1987, and September 16, 1987. The first two nights were photometric; some haze was present the last night. The I band magnitude was found to be 17.4 ± 0.5, 17.4 ± 0.5, and 17.3 ± 0.2 respectively, so the haze was negligible in that region of sky the last night. That last night, IRAS 03521+0028 was also observed with R and V broad band filters, and values of m_V = 19.0 ± 0.5 and m_R = 18.4 ± 0.5 were determined. The V–I is redder than that of normal spirals (Pierce and Tully 1988).

A redshift is not yet available for this object to confirm that it is extragalactic; however, the image shows that it is clearly nonstellar. The nebulosity is extended in the east-west direction, with a size of ~8" × 4". The similarity of the IRAS colors with other IRAS galaxies suggests that the source is extragalactic. It has the highest ratio of L(60 μm)/ L(B) in this sample, > 250, comparable to the "blank field" 60 μm sources discovered by Houck *et al.* (1984). All of these sources except one were later determined to be very distant, luminous galaxies by subsequent CCD imaging and optical spectroscopy (Houck *et al.* 1985); the exception was assumed to be galactic cirrus.

Assuming B–V = 0.6, typical for late-type spirals (de Vaucouleurs 1977), B = 19.6 ± 0.5. A redshift may be estimated using the result that there is a narrow range of absolute blue magnitudes in IRAS-selected galaxies (SKHL). Using B = 19.6 ± 0.5 for IRAS 03521+0028 and the mean value of absolute blue magnitude from SKHL, $\langle M_B \rangle = -19.2 \pm 0.8$, IRAS 03521+0028 lies at 580 ± 250 Mpc, or, using $H_o = 100$ km/s/Mpc, 58,000 ± 25,000 km/s. This gives an estimated 60 μm luminosity of log L(60) = 12.1 ± 0.3.

For this discussion, IRAS 03521+0028 is ambiguous both because its redshift is only estimated, and because its classification as interacting is uncertain. The asymmetry seen in Figure 16 suggests that it may be a merger remnant.

2. Other Peculiar Galaxies

The galaxy NGC 660 (IRAS 01403+1323) is another galaxy classified as ambiguous in this study. It is classified as a "SB[a] distorted?" galaxy in the UGC, and Solomon and Sage (1987) call it a merger remnant, citing the 1415 MHz and 2695 MHz radio continuum maps by Condon *et al.* (1982) which show two peaks in the nucleus. The I-band image obtained for this study, however, shows only one nuclear peak; the same result is seen for the near-infrared SIII emission line (Young, Kleinmann, and Allen 1988).

Two galaxies, IRAS 09108+4019 and IRAS 14158+2741 are ambiguous because they exhibit, besides a single nucleus, a single tail. These cannot be assumed to be merger remnants as readily as the two-tailed systems such as Arp 243. NGC 2782 (Arp 215; IRAS 09108+4019) has a broad faint tail extending toward the east, whose optical extent is twice the optical radius (Figure 17). It also may have ripple-like structures similar to those seen by Schweizer and Seitzer (1988) in spirals, suggesting that it may be a merger remnant. An I-band image of the center, however, shows only one nucleus (Figure 18). Numerical modeling could test whether this peculiarity can be reproduced successfully by a merger simulation. IRAS 14158+2741 is another galaxy with a single tail-like structure (Figure 19). A possible low-mass companion exists at ~4R which may have caused the distortion, however, a redshift is not available for this companion galaxy to confirm that it is at the same distance. Alternately, IRAS 14158+2741 may be a merger remnant, with only one tail visible.

There are several other peculiar IRAS galaxies that cannot be identified conclusively as interacting or non-interacting, because their radii are less than 10 arcseconds on the I-band images. These are IRAS 08579+3447 (z = 0.065), IRAS 16305+4823 (z = 0.088), IRAS 23381+2654 (z = 0.034), and IRAS 23410+0228 (z = 0.091), which appear in Figures 20–23. IRAS 08579+3447 has a peculiar nucleus which may be double. IRAS 23381+2654 also has a peculiar nucleus. IRAS 23410+0228 has a short extension towards the north, which may be a tidal structure.

Three galaxies are classified as ambiguous because I-band images were not obtained for them, and their structure cannot be determined from the POSS plates. These are UGC 2963 (IRAS 04050+0350), classified Sc disturbed in the UGC, UGC 9191 (IRAS 14190+3013), classified S with companion in the UGC, and UGC 10273 (IRAS 16107+2824), classified as strongly peculiar.

3. Galaxies With Uncertain Optical Identification

Two IRAS sources are ambiguous because the optical identification is uncertain, and different identifications would give different results. The first is IRAS 00537+1337, associated with the pair UGC 580 and UGC 582 in the PSC. However, there is a faint pair of galaxies just to the north of UGC 580/582 (see Figure 24), and measurements of positions using the Grant machine show that galaxy A from this pair is closer to the IRAS position (see Table 3) than either UGC 580 or UGC 582. Figure 25 shows the I-band image of the pair of galaxies labelled A and B; C and D appear to be stellar. None of the possible optical counterparts have ground-based 10 μm measurements at present; also, there is no redshift available for galaxy A. UGC 580 and 582 are called "in contact" by the UGC, however, the velocity of UGC 582 is 24,600 km/s, 12,600 km/s greater than that for UGC 580. Further, an I-band image of UGC 580/582 (Figure 26) shows that UGC 580 is disturbed, while UGC 582 appears undisturbed. This suggests that these two galaxies are unassociated, and the material seen between them in the POSS photo reproduction is part of UGC 580. Galaxy A has an apparent blue magnitude of ~18, suggesting that its distance is ~28,000/H_o Mpc.

The source IRAS 07233+6917 is associated with NGC 2366 or NGC 2363 by the PSC. This system is shown in Figure 27. NGC 2363 is the giant HII region at the southern tip of NGC 2366 (Kennicutt, Balick, and Heckman 1980). There is also a small companion, B, to the west of NGC 2363. The position listed in Table 3 for NGC 2366 is the central position from Dressel and Condon (1976); the positions for NGC 2363 and the companion were measured using the Grant machine. The IRAS position falls between NGC 2363 and the companion. If the IRAS source were NGC 2363, IRAS 07233+6917 would be "non-interacting." Conversely, if the IRAS source were the companion, the source would be "interacting." This IRAS source is thus classified as ambiguous.

E. Conclusions

The galaxies in the sample were classified as interacting or non-interacting according to the definition: $m_1/m_2 \geq 1/4$, $D \leq 3R$, and $\Delta v \leq 500$ km/s. It was found that 20 ± 3% fit the interaction criteria, 72 ± 5% were non-interacting, and 8

± 2% were unclassifiable. The percentage of interacting galaxies is somewhat smaller than the 37% found by Lonsdale *et al.* (1984) for another 60 μm flux-limited sample, because this study used more stringent criteria to define interaction. Twenty of the galaxies classified as non-interacting show clear evidence for gravitational distortion from a companion, however, the companion was either too distant or of too low a mass for the pair to be classified as interacting in this study.

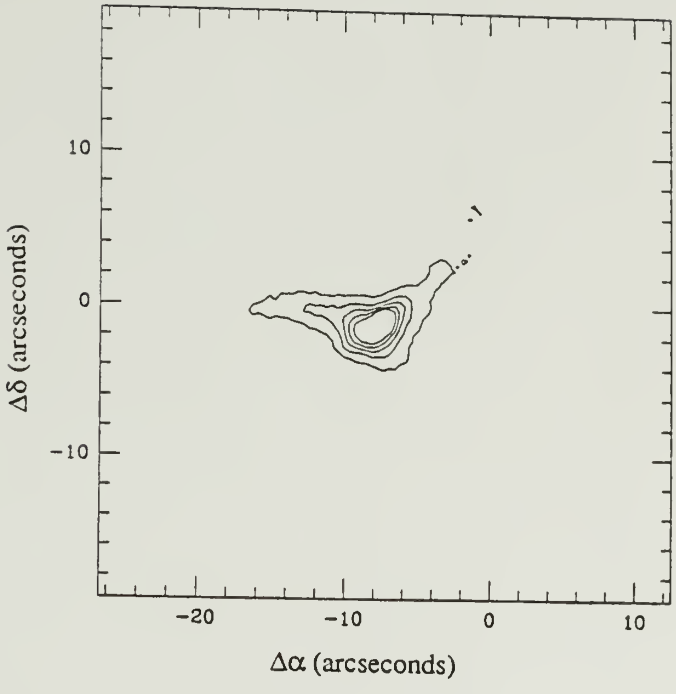

Figure 2. IRAS 22491−1808. This appears to be a two-tailed merger remnant, similar to Arp 243. For all Figures, north is up and east is to the left, unless otherwise stated. Also, all Figures of galaxies are contour plots made from the I-band images obtained for this study, and (0,0) is the IRAS position.

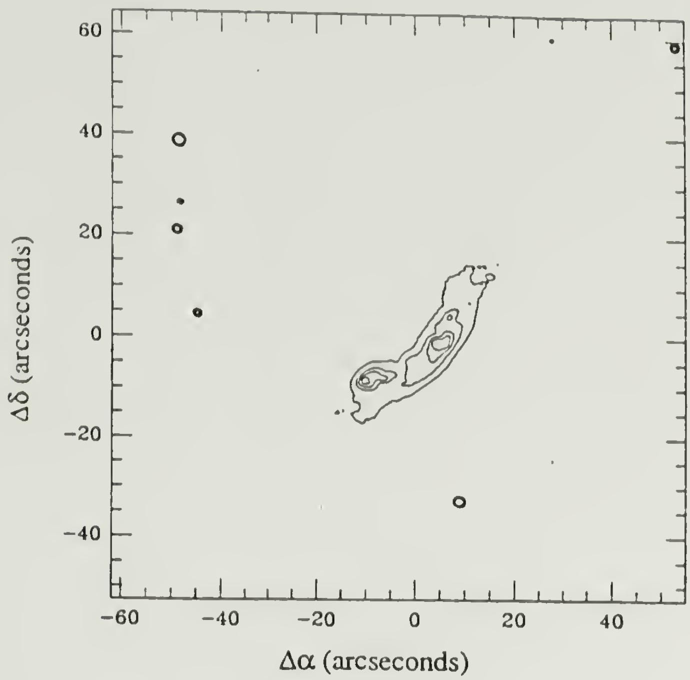

Figure 3. UGC 11035 (IRAS 17526+3253). This is classified as a merger remnant in this study.

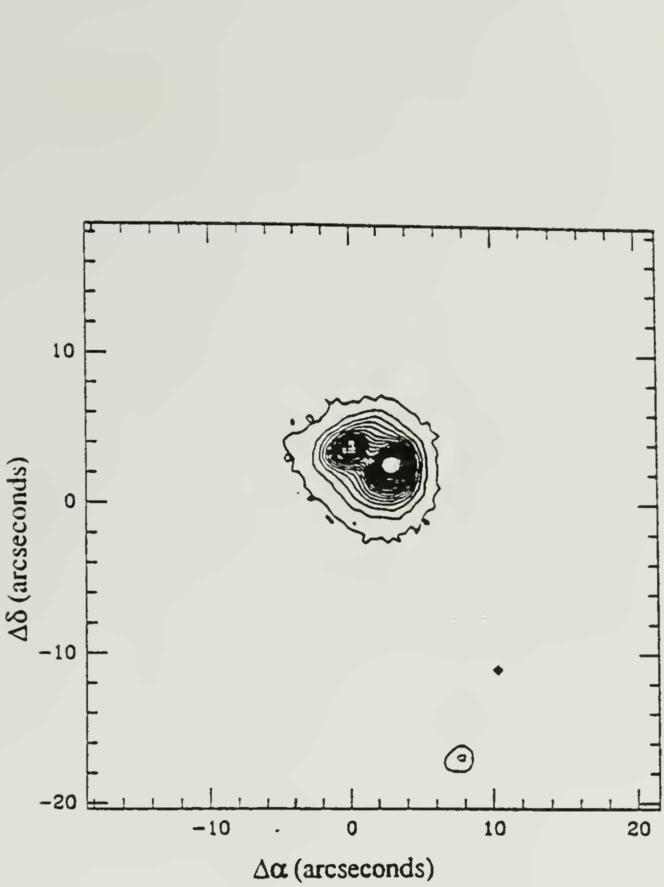

Figure 4. IRAS 16487+5447.

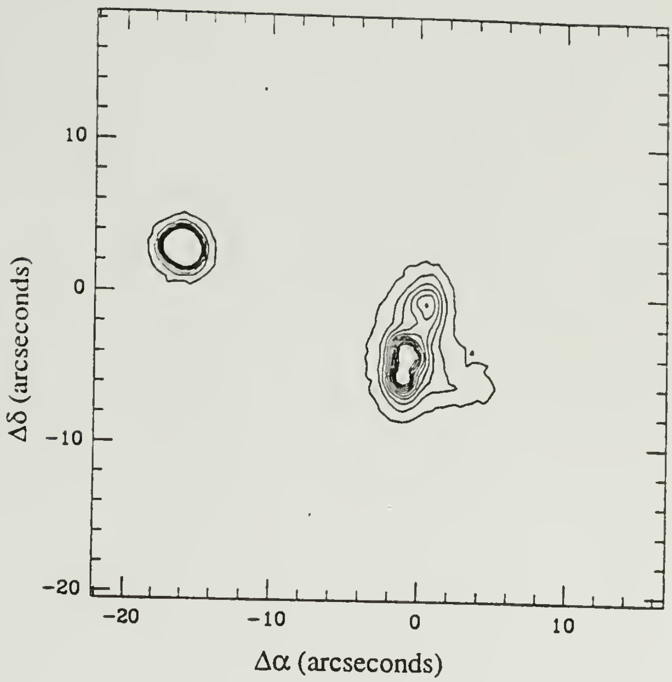

Figure 5. IRAS 16474+3430.

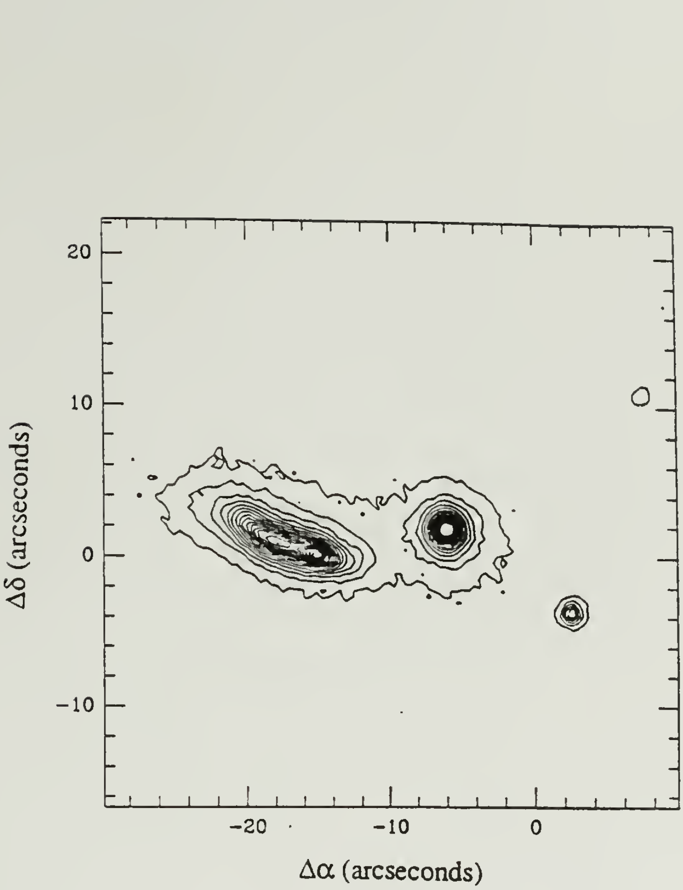

Figure 6. IRAS 03359+1523.

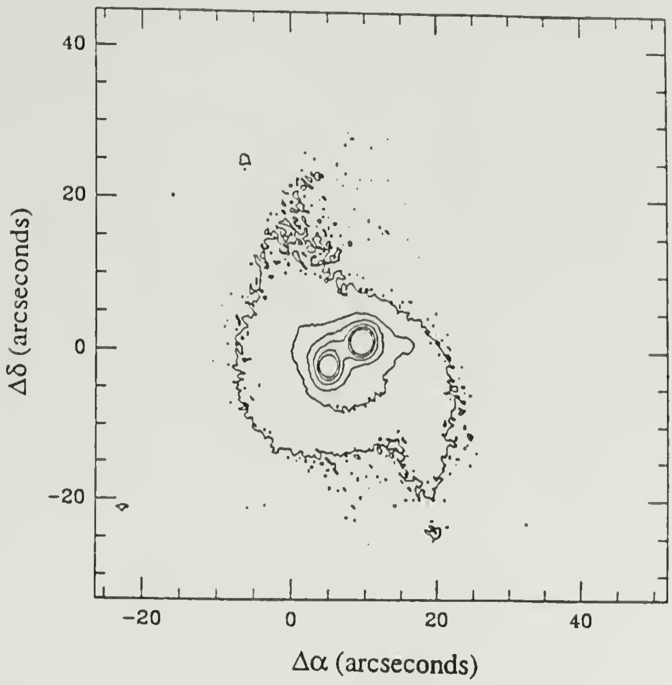

Figure 7. UGC 4947 (IRAS 09168+3308).

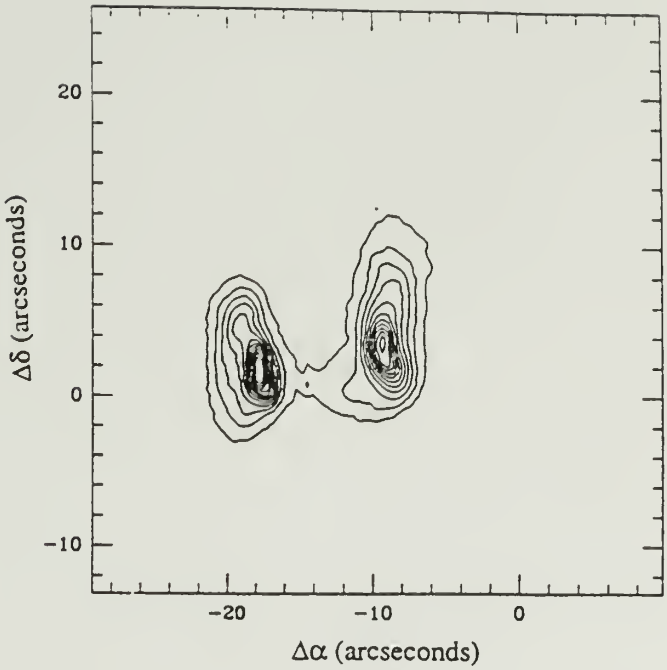

Figure 8. IRAS 01197+0044.

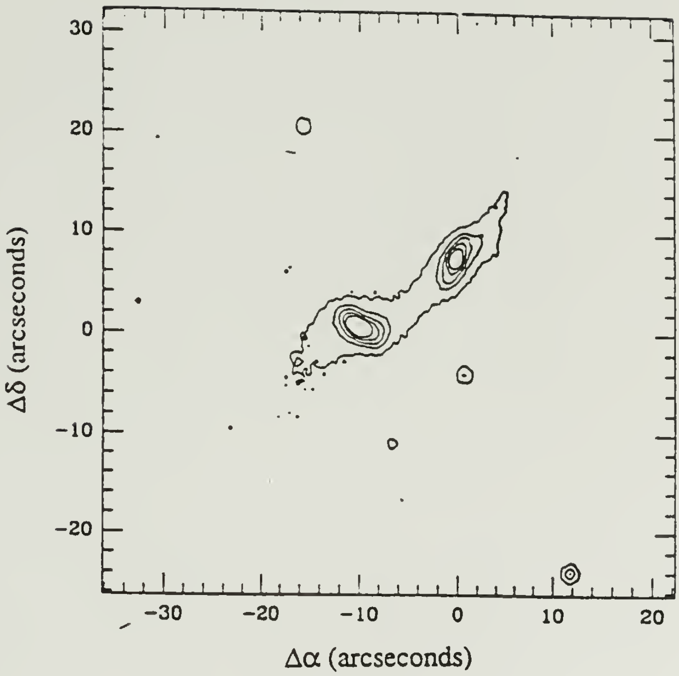

Figure 9. IRAS 03119+1448.

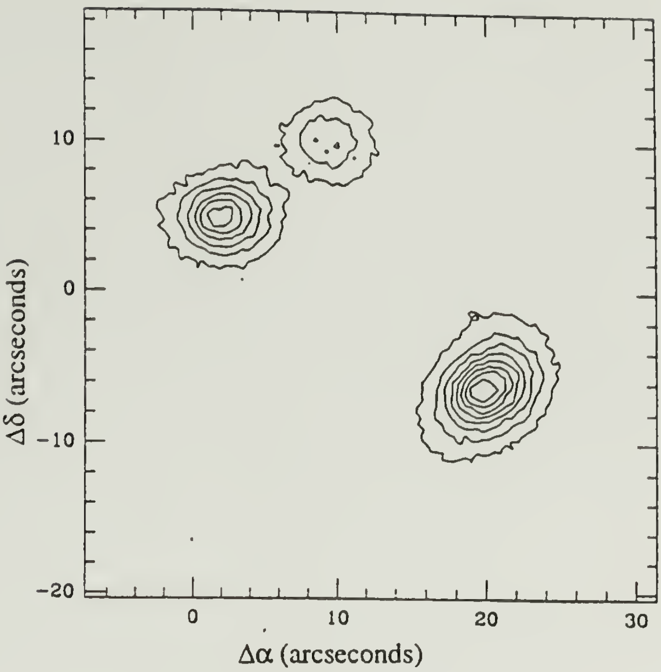

Figure 10. IRAS 09583+4714.

Figure 11. Arp 216 (NGC 7679 + NGC 7682; IRAS 23262+0314). This photo is reproduced from the Arp Atlas (1966). North is to the right and east is up. The western galaxy is NGC 7679, the IRAS source, while the other is NGC 7682. Because these two galaxies are widely separated, NGC 7679 is not classified as interacting in the study, in spite of the gravitational distortion of the eastern arm, which may have been caused by the passage of NGC 7682.

Figure 12. Arp 295 (IRAS 23394–0353). This is a reproduction of the Arp Atlas (1966) photo of Arp 295. North is up and east is to the left in this photo. The galaxy in the southwest is the IRAS source. This galaxy is not classified as interacting in this study, in spite of the bridge connecting it to the other half of Arp 295, because the separation is greater than 3R.

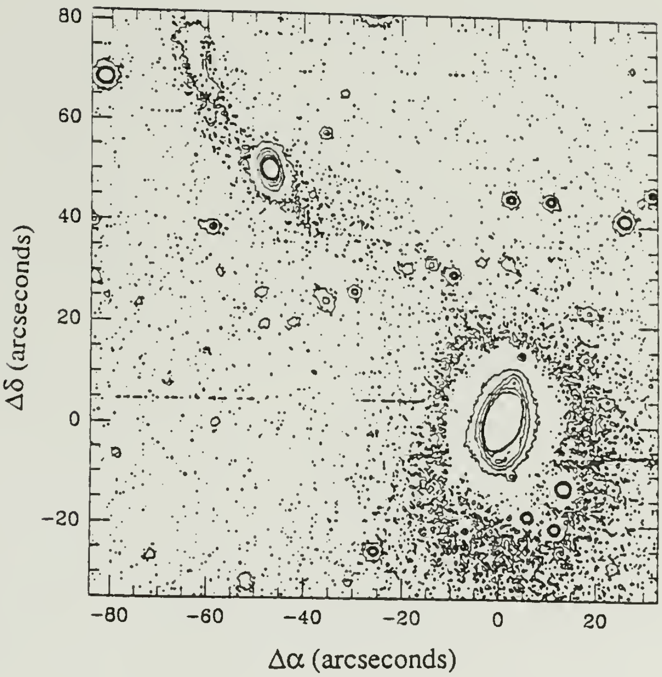

Figure 13. IRAS 17392+3845. The brighter galaxy is the IRAS source.

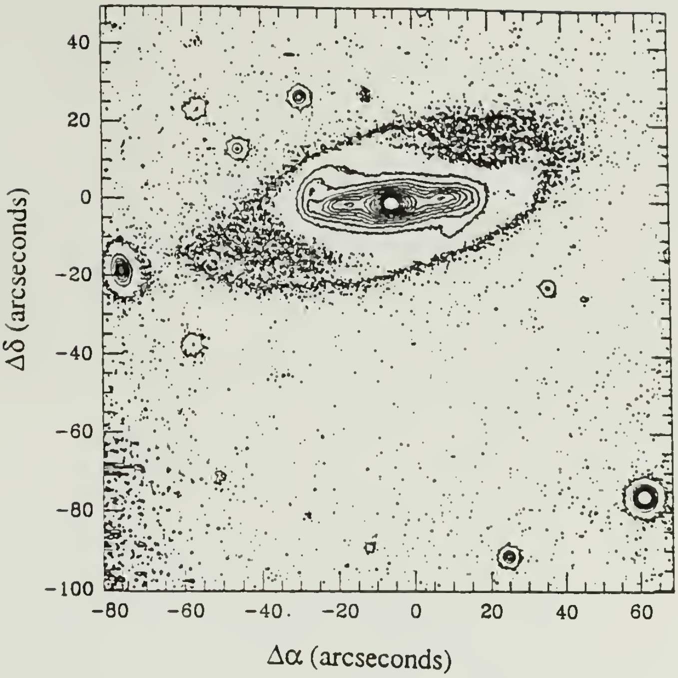

Figure 14. NGC 5610 (IRAS 14221+2450). This is not classified as interacting in this study, in spite of the gravitational distortion due to the small companion, because the companion has an I-band luminosity of only 4% that of NGC 5610.

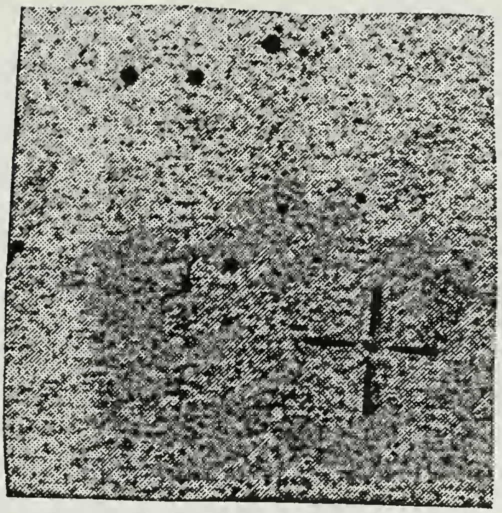

Figure 15. Finding chart for IRAS 03521+0028. This is a reproduction of the E POSS plate.

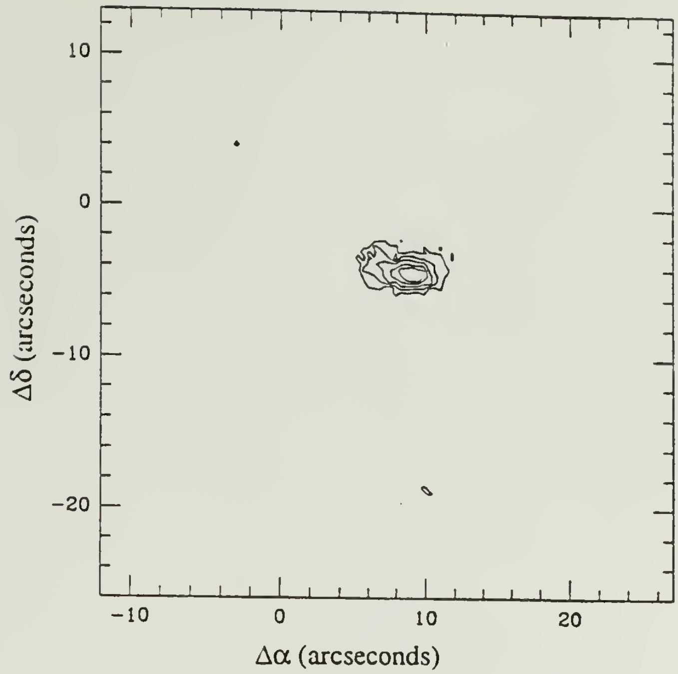

Figure 16. IRAS 03521+0028.

Figure 17. Arp 215 (NGC 2782; IRAS 09108+4019). This is a reproduction of the Arp Atlas (1966) photo. North is to the right and east is up in this photo.

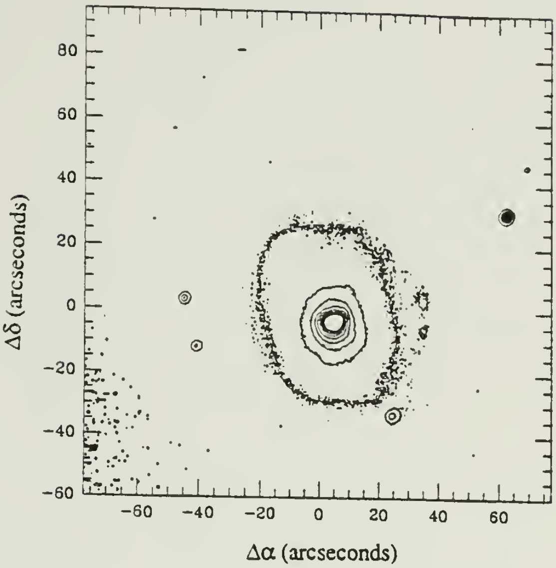

Figure 18. The center 2.5′ × 2.5′ of Arp 215 (NGC 2782; IRAS 09108+4019), in I-band.

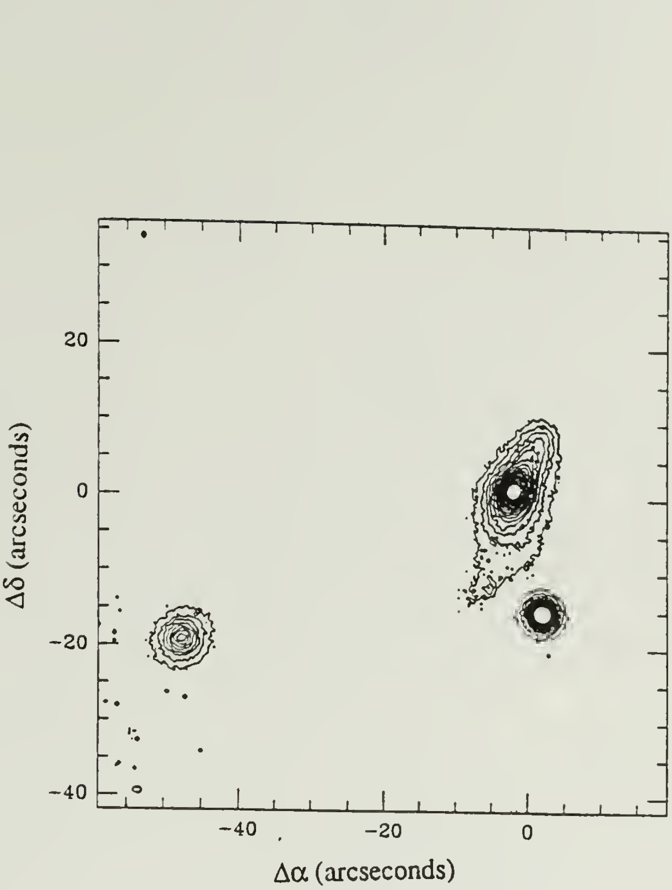

Figure 19. IRAS 14158+2741. The IRAS source is the brightest galaxy. The source in the southwest is a star; the source to the east is a galaxy.

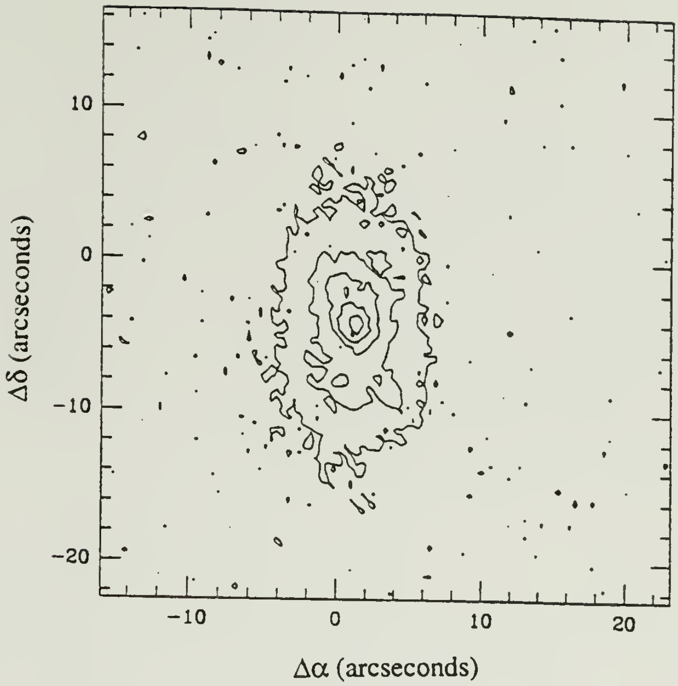

Figure 20. IRAS 08579+3447.

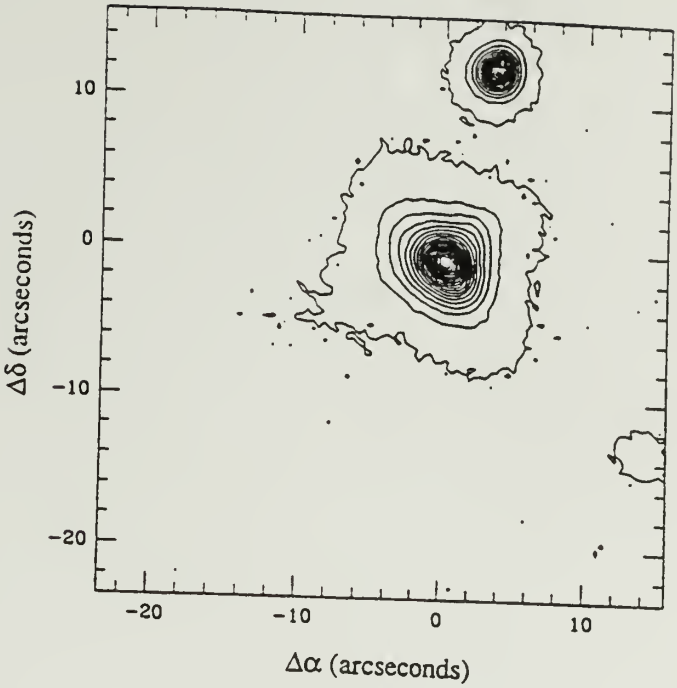

Figure 21. IRAS 16305+4823. The source to the north is a star.

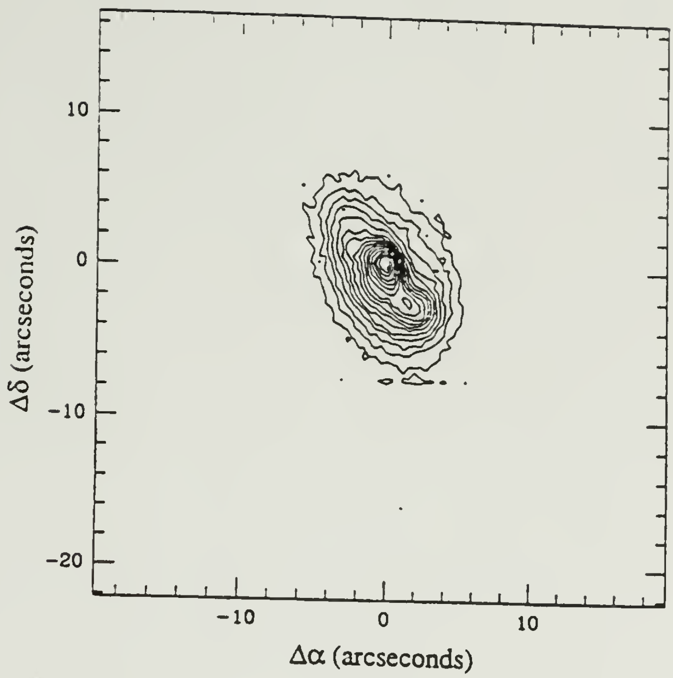

Figure 22. IRAS 23381+2654.

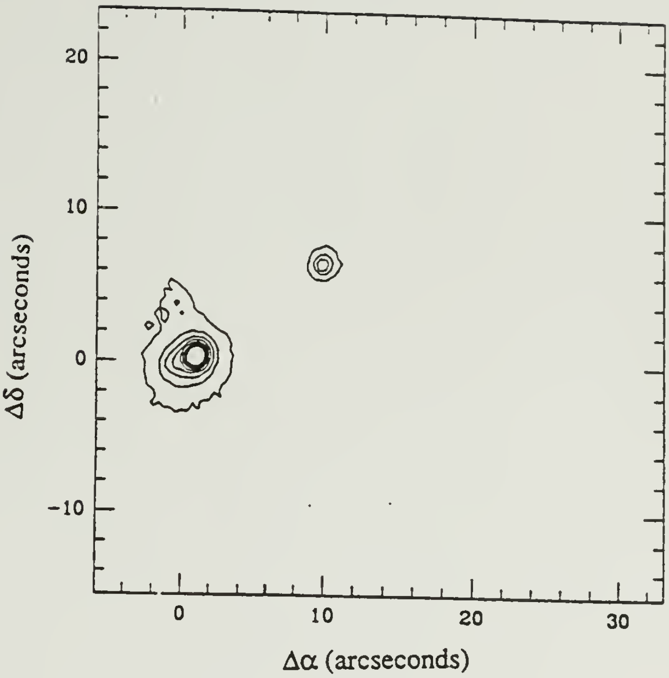

Figure 23. IRAS 23410+0228.

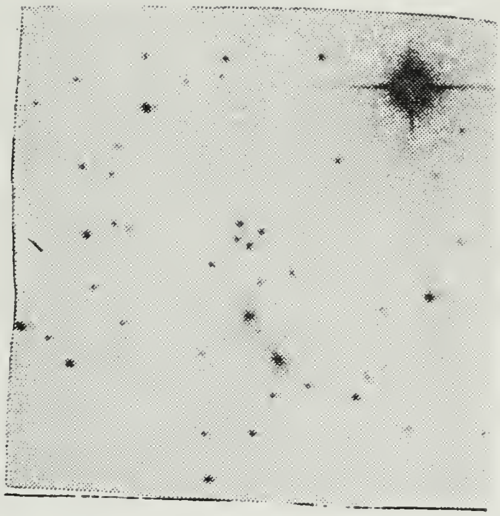

Figure 24. A reproduction of the E POSS photo near IRAS 00537+1337. The galaxy directly below the diamond-shaped group near the center of this Figure is UGC 582; the galaxy to its southwest is UGC 580. The southern-most source in the diamond-shaped group to the north of UGC 582 is galaxy A. Sources B, C, and D are named clockwise from A on this photo. B is a galaxy and C and D are stars.

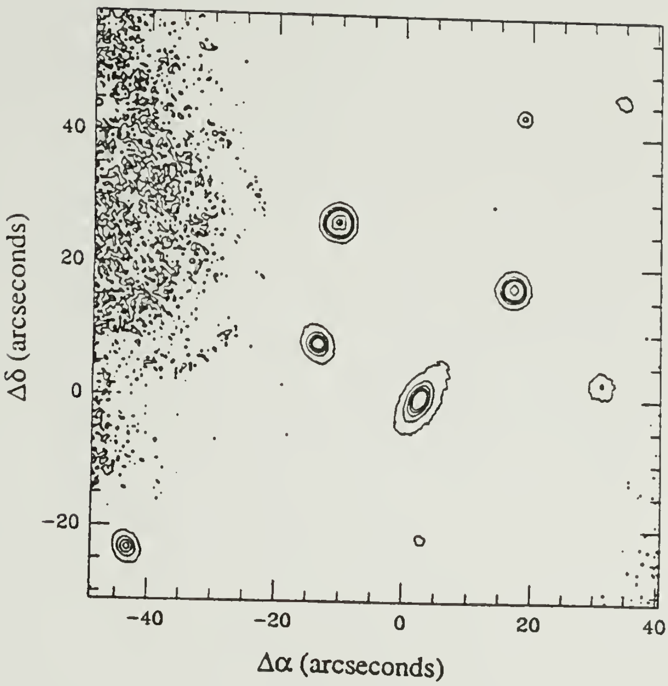

Figure 25. The I-band image of the pair of galaxies near IRAS 00537+1337. The southern-most source in the diamond-shaped group is galaxy A. Sources B, C, and D are named clockwise from A on this photo. B is a galaxy and C and D are stars. The extended structure to the east in this image is due to moonlight.

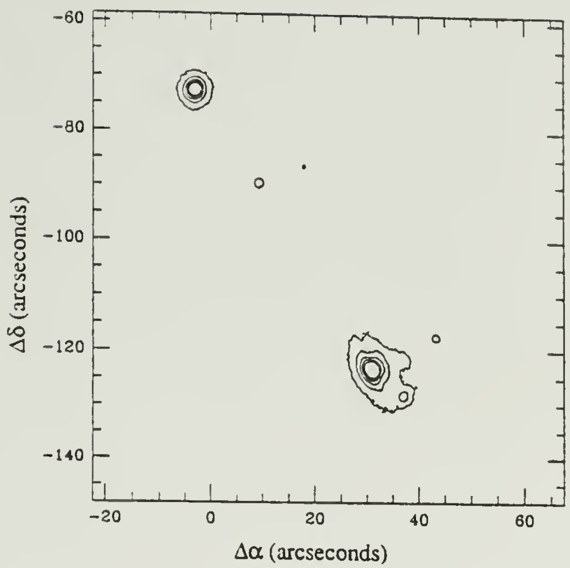

Figure 26. The I-band image of UGC 580 and UGC 582. UGC 582 is the NE galaxy. UGC 580 is the SW galaxy.

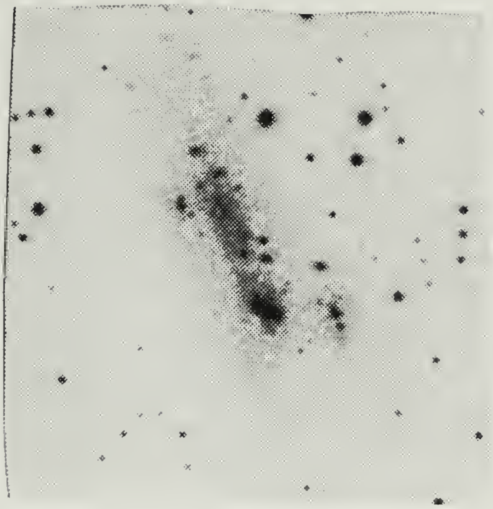

Figure 27. A reproduction of the E POSS photo near IRAS 07233+6917. The galaxy to the east is NGC 2366; the HII region in the south of NGC 2366 is NGC 2363. The companion to the west is labeled B.

CHAPTER IV

THE 60 μm LUMINOSITY FUNCTIONS OF INTERACTING AND NON-INTERACTING GALAXIES

A. The Dependence of Far-Infrared Luminosity on Interaction Parameters

The definition of 60 μm luminosity used in this study is the same as that used by

$$L = 4\pi r^2 F_\nu \Delta\nu$$

where F_ν is the corrected IRAS flux density and $\Delta\nu$ is the bandwidth (=3.75 × 10^{12} Hz; Neugebauer *et al.* 1984). The distance r is calculated by assuming H_o = 100 km/s/Mpc and correcting for 300 km/s galactic rotation and deviation from the Hubble flow due to infall of 300 km/s towards the Virgo cluster, as in Huchra and Geller (1982). For the single source without an available redshift, IRAS 03521+0028, the distance was estimated from the blue magnitude, as described in Chapter III.

To investigate the dependence of far-infrared luminosity on mass ratio, 60 μm luminosity is plotted in Figure 28a as a function of mass ratio (I-band luminosity ratio) for the galaxies with bound companions. The mass ratio is defined as m_1/m_2, where m_1 is the mass of the companion, and m_2 is the mass of the infrared galaxy. The four galaxy pairs with radial velocity differences greater than 500 km/s are excluded from this Figure, as these probably are not bound systems. Also, the 21 galaxies classified as ambiguous in Chapter III are not included. Galaxies with a separation of greater than triple the radius are plotted as filled triangles; those with separation $D \leq 3R$ are plotted as circles. The open circles represent galaxies which are defined as interacting in this study, as they lie on or above the dashed line at m_1/m_2. The filled circles and the filled triangles represent galaxies which are designated as non-interacting in this study. For comparison, the total far-infrared luminosity L(FIR), calculated using the relation defined in Lonsdale *et al.* (1985), is compared with mass ratio in Figure 28b.

The complementary plots are shown in Figure 29, where luminosity is plotted as a function of separation. Figure 29a compares 60 μm luminosity with separation, while Figure 29b compares L(FIR) with separation. Different symbols are used to distinguish those galaxies with $m_1/m_2 \geq 1/4$ (open and filled circles), and those with $m_1/m_2 < 1/4$ (filled triangles). In this Figure, open circles represent galaxies which are defined as interacting in this study, because they lie on or below the dashed line at $D = 3R$. Filled circles and filled triangles represent non-interacting galaxies. Again, galaxies with radial velocity differences greater than 500 km/s are excluded from this Figure, as are ambiguous galaxies. Merger remnants with a single nucleus are assigned a separation of zero. Projection effects are present in this plot; a pair with a close projected separation may actually be widely separated.

Inspection of these two plots gives several immediate results. First, Figure 28 shows that there is a deficiency of low mass ratio ($m_1/m_2 < 1/4$) galaxies at high 60 μm luminosities, indicating that near-equal mass companions are needed to induce very high 60 μm luminosities. Second, Figure 29 shows that there is a deficiency of widely separated pairs at high luminosities, suggesting that close companions are also needed for the highest luminosities. Further, Figure 28 shows that at high mass ratios, there is a difference in the luminosity distribution of close pairs (open circles) and wide pairs (filled triangles), in that close pairs tend to be of higher luminosity. The corresponding effect is seen in Figure 29, which shows that, for close pairs ($D \leq 3R$), those with high mass ratios tend to be of higher luminosity than low mass pairs.

The information in these Figures can also be used to obtain quantitative estimates of the amount of far-infrared enhancement as a function of mass ratio and separation. In Table 6, the mean value of $\log L(60)/L_o$ is tabulated for various ranges of these parameters. For comparison, $\langle \log L(60)/L_o \rangle$ for the galaxies without bound companions in this study is 10.0 ± 0.8. The mean 60 μm luminosity for the galaxies which fit the interaction criterion, $\langle \log L(60)/L_o \rangle = 10.8 \pm 0.5$, is a factor of ~6 higher than that for the galaxies without bound companions. This is consistent with the results of Noguchi and Ishibashi (1986) discussed in Chapter III, which predict an enhancement of ~7 in the star formation rate for an equal mass encounter at a distance of 2R.

The corresponding mean total FIR luminosities are also given in Table 6. The amount of enhancement in the total far-infrared luminosity is found to be less than that of the 60 μm luminosity. This is consistent with the results of SKHL, which show that $L(60)/L(100)$ increases with $L(60)$. That is, for the lower luminosity galaxies, a higher proportion of the total flux is in the 100 μm IRAS band, due to cooler dust in the galaxy.

Table 6 shows that, for close pairs, as the mass ratio limits are increased, the mean 60 μm luminosity increases. Similarly, for high mass pairs, as the separation decreases, the mean 60 μm luminosity increases. The mean 60 μm luminosity for high mass pairs with $D > 3R$ is equal to that of galaxies without bound companions. This suggests that companions beyond 3R do not have much effect on the star formation rate, consistent with the Noguchi and Ishibashi (1986) results. However, the galaxies in the range 2R – 3R show an enhancement, supporting the choice of $D \leq 3R$ as a selection criterion for interacting galaxies. For the galaxies which fall just short of the criterion in mass, in the range $1/10 \leq m_1/m_2 < 1/4$, with $D \leq 3R$, the enhancement is only a factor of ~2. This supports the choice of $m_1/m_2 \geq 1/4$ for the mass ratio criterion. This Table also suggests a more rapid drop-off in enhancement with increased separation, compared to the drop-off with decreasing mass ratio, consistent with the mD^{-3} proportionality of tidal force.

To investigate the question raised in the last Chapter, how do morphologically distorted galaxies differ from undisturbed galaxies, the far-infrared luminosities of the two extreme subsets of the non-interacting sample, which were selected in Chapter III, are compared in Figure 30. The two samples are, first, the subset of pairs which fail the interaction criteria, yet show obvious tidal distortion from a companion, and, second, the set of obviously symmetrical spirals. There are 20 pairs in the distorted sample, and 65 symmetrical spirals. The values of $\langle \log L(60)/L_0 \rangle$ are also tabulated in Table 6. The distorted sample shows an enhancement of ~3 above that of the galaxies without bound companions, ~1/2 that of the interacting sample. The symmetric sample, on the other hand, shows a lower value of $\langle \log L(60)/L_0 \rangle$ compared to the galaxies without bound companions. Thus, the galaxies which are gravitationally distorted show a higher 60 μm luminosity than those which are undistorted. However, as noted previously, there is a selection criterion in chosing these sets, as the galaxies must be bright enough optically and of large enough angular size (therefore nearby) for these morphological characteristics to be noted. This biases the sample towards lower luminosity galaxies.

B. The Total 60 μm Luminosity Function

In this section, the 60 μm luminosity function for the total sample of 275 galaxies is derived, and compared with previous determinations. In addition, a related function, the "visibility function", or "normalized luminosity function" $\Psi(L)$ is also derived.

The 60 μm luminosity function is defined as:

$$\Phi(L) = \frac{4\pi}{\Omega}\frac{1}{\Delta mag}\sum_j \frac{1}{V_j},$$

where $\Omega/4\pi$ is the fraction of the sky covered by this survey, Δmag (= 1 magnitude) is the bin width, and V_j is the volume of the Universe out to which a galaxy of luminosity L_i is observed at the flux limit of this survey.

The visibility function describes the distribution of luminosities in a flux-limited $\Psi(L) = 1.086\, L^{3/2} \phi(L)$.

The total luminosity function is shown in Figure 31, and tabulated in Table 7. Uncertainties were calculated assuming Poisson distribution errors, proportional to $\sqrt{N}$; errors in the luminosities due to uncertainties in the infrared fluxes and deviations from Hubble flow which are not completely eliminated by the corrections for Virgocentric motion are ignored. The point at log L/L_o = 12.0 is due solely to the unusual source IRAS 03521+0028 being placed at an estimated redshift of 0.19. Figure 31 also shows the luminosity functions derived by SKHL and Soifer *et al.* (1987). The Soifer *et al.* (1987) luminosity function was determined using a sample of 324 galaxies with a 60 flux limit of 5.4 Jy. For this Figure, the data from Soifer *et al.* (1987) were converted to H_o = 100 km/s/Mpc and this definition of L(60).

The 60 μm luminosity function cannot be described adequately by a single power law for the entire range of luminosities. Thus, only the upper end was fit. The best fit parameters to a power law of form $\phi(L) = \gamma L^b$, for $L \geq 10^{10} L_o$, are given in Table 8. These are consistent with the best fit obtained by SKHL.

The total visibility function is shown in Figure 32, and is fit to a hyperbola, as in Condon (1984) and HCH, of form: $\log\left\{\Psi\right\} = Y - \left\{B^2 + \left\{\frac{\log L - X}{W}\right\}^2\right\}^{1/2}$. The best fit parameters are given in Table 9.

Figure 32 also shows the visibility function derived by HCH from the Soifer *et al.* (1987) data. The evolutionary models of HCH make use of the Soifer *et al.* (1987) luminosity function, so it is important to compare these two results. Figures 31 and 32 show that the data from this study are slightly below those of Soifer *et al.* (1987) at low luminosities, and the space density of galaxies at low luminosities,

$$\rho = \int_{1.6X10^8 L_o}^{10^{10} L_o} \phi(L)dL,$$ is a factor of ~2.5 lower.

These Figures show that below Log L/L_o = 10, the difference between the visibility functions widens, and reaches a factor of ~3 at L(60) = 10 .

Differences between these local luminosity functions may be due to inhomogeneities in the galaxy distribution or deviations from the Hubble flow, which may cause inaccuracies in the luminosities, especially at the low luminosity end. For 12% of the galaxies in their sample, Soifer *et al.* (1987) obtained distances using the Fisher-Tully relationship, thus decreasing problems with Hubble flow deviations. These were mainly low luminosity galaxies. However, this cannot be the only explanation for the difference, since the surface density of galaxies in the Soifer *et al.* (1987) sample is 0.022 ± 0.001 deg^{-2}, which extrapolates to 0.098 ± 0.004 deg^{-2} at 2 Jy, assuming that the surface density of galaxies for a sample with flux limit F is proportional to $F^{3/2}$. This derived surface density is 1.8 times that of the present 2 Jy survey. This difference may be due to the Soifer *et al.* (1987) sample being biased by inclusion of local supercluster galaxies.

C. The Two Components of the 60 μm Luminosity Function

Using the strict definition of interaction ($m_1/m_2 \geq 1/4$, $D \leq 3R$, and $\Delta v \leq 500$ km/s), 56 of the sample of 275 belong in the interacting class, 198 are non-interacting, and 21 are ambiguous (see Chapter III for more details). The luminosity functions of the three types are show in Figure 33, and tabulated in Table 7. Again, the uncertainties assume a Poisson distribution.

This Figure shows that non-interacting galaxies dominate at low luminosities, while interacting and ambiguous galaxies dominate at high luminosities. At L ~ $10^{11}L_o$, the interacting and non-interacting galaxy luminosity functions are approximately equal. At log L(60) = 11.2, $\phi(L)_{INTERACTING} \sim 2 \times \phi(L)_{ISOLATED}$. The value of the ambiguous galaxy luminosity function at log L(60) = 12 is due solely to IRAS 03521+0028, at its estimated redshift. The value of the ambiguous galaxy luminosity function at log L(60) = 11.6 is due solely to IRAS 18443+7433, a compact distant galaxy only a few arcseconds across on the image. The luminosity function of non-interacting galaxies drops off at $L > 10^{11}\ L_o$, while the luminosity function of interacting galaxies flattens at $L < 10^{11}L_o$, and does not extend to luminosities less than $4 \times 10^9 L_o$.

To determine the difference in space densities of the two types of galaxies, the two luminosity functions were integrated over luminosity. For $L > L(60)_{MILKY\ WAY}$ ($\sim 6 \times 10^9 L_o$, the lower edge of the bin log L(60) = 10.0), the integral of the luminosity function gives a space density $\rho_{INTERACTING} = \int_{L}^{\infty} \phi(L)dL = 1.1 \pm 0.3 \times 10^{-4}$ galaxies/Mpc^3, and $\rho_{ISOLATED} = 5.9 \pm 0.7 \times 10^{-4}$ galaxies/Mpc^3. For $L > 1.6 \times 10^8 L_o$, $\rho_{INTERACTING} = 1.6 \pm 0.5 \times 10^{-4}$ galaxies/Mpc^3, and $\rho_{ISOLATED} = 1.8 \pm 0.5 \times 10^{-2}$ galaxies/Mpc^3. Therefore, there are ~5 times as many non-interacting galaxies as interacting ones with L(60) greater than $L_{MILKY\ WAY}$, and ~100 times more with L(60) $> 2 \times 10^8 L_o$.

The presence of ambiguous galaxies in this sample introduces some uncertainty into the luminosity functions and derived space densities; however, an upper limit to the interacting galaxy luminosity function can be determined by combining the ambiguous and interacting galaxies, and calculating the luminosity function. The lower limit is simply the original interacting galaxy luminosity function. These two functions are plotted in Figure 34.

An upper limit to the luminosity function of non-interacting galaxies can be constructed in the same manner. Figure 35 shows the original non-interacting galaxy luminosity function and the luminosity function of the combined non-interacting plus ambiguous galaxy sample.

These plots show that the ambiguous galaxies have little effect on the luminosity functions. The exception is the high luminosity end of the luminosity function for non-interacting galaxies. When IRAS 03521+0028 is added to the non-interacting galaxy sample, it causes an unusual turn-up of the upper limit curve to the non-interacting galaxy luminosity at log L(60) = 12.0. On the other hand, this point fits smoothly at the high luminosity end of the interacting galaxy luminosity function.

For ease in modeling the deep source counts, these functions were parameterized. First, the luminosity functions were fit directly to a power law function. Then the data were converted to visibility functions, and were also parameterized to the hyperbolic functional form. Figure 36 shows the separated visibility functions, along with the best fit curves. The visibility function of interacting galaxies peaks at log $L(60)/L_o = 11$ while that of non-interacting galaxies peaks at log $L(60)/L_o = 10$. To include the effects of the ambiguous galaxies, the functions were each fit twice, with and without the ambiguous galaxies.

As there is no pronounced turnover of the luminosity function of interacting galaxies, it was fit to a single power law of form $\phi(L) = \gamma L^{\beta}$, in the range $4 \times 10^9 L_o \leq L(60) \leq 10^{12} L_o$. The luminosity function of non-interacting galaxies is fit to two separate power laws for $L \geq 10^{10} L_o$ and $L < 10^{10} L_o$. The visibility functions were each fit to a single hyperbola. The best fit parameters are tabulated in Tables 8 and 9.

D. The Luminosity Function of Interacting Galaxies as a Function of the Limiting Parameters of the Interaction

To investigate the dependence of the luminosity functions on the definition of interaction, the luminosity function of interacting galaxies is compared in Figure 37 to the luminosity function that would have been derived if the mass ratio criterion was more and less strict, that is, equal to 2/3 and equal to 1/10. For this experiment, the maximum separation remains at 3R and the maximum velocity difference remains at 500 km/s. Galaxies classified as ambiguous are ignored. As the limiting mass ratio is lowered from 2/3 to 1/4 to 1/10, the density of galaxies brighter than $L(60)_{MILKY\ WAY}$ increases from $0.32 \pm 0.14 \times 10^{-4}$ galaxies/Mpc^3 to $1.1 \pm 0.3 \times 10^{-4}$ galaxies/Mpc^3 to $1.8 \pm 0.4 \times 10^{-4}$ galaxies/Mpc^3. The density of interacting galaxies is then found to be increased by factors of 3.4 ± 1.8 and 1.6 ± 0.6 respectively. Also, as the limiting mass ratio is decreased, the luminosity function appears steeper, indicating, again, that pairs with low mass ratios and high luminosities are rare.

As the limiting mass ratio is decreased, the corresponding density of non-interacting galaxies is also decreased, as is the ratio of galaxy densities, $\rho_{ISOLATED}/\rho_{INTERACTING}$. A mass ratio cutoff of 2/3 gives $\rho_{ISOLATED}/\rho_{INTERACTING}(L > L_{MW}) = 21 \pm 9$, and $m_1/m_2 \geq 1/10$ gives $\rho_{ISOLATED}/\rho_{INTERACTING}(L > L_{MW}) = 2.9 \pm 0.8$.

Figure 38 shows how the luminosity function would change if the separation criterion were varied to 2R and to 10R. The minimum mass ratio is set at 1/4 and $\Delta v < 500$ km/s, and again, ambiguous galaxies are ignored. As the limiting distance separation is varied from 2R to 3R to 10R, $\rho_{INTERACTING}(L > L_{MW})$ changes from 9.1 ± 2.5 × 10^{-5} to 1.1 ± 0.3 × 10^{-4} to 1.7 ± 0.3 × 10^{-4} galaxies/Mpc^3, implying density increases of 1.2 ± 0.5 and 1.5 ± 0.6 respectively. For D ≤ 2R, the ratio $\rho_{ISOLATED}/\rho_{INTERACTING}(L > L_{MW})$ = 6.7 ± 1.8, and for D ≤ 10R, 3.1 ± 0.8.

E. Infrared Color-Luminosity Relations

For use in modeling the deep infrared source counts, and also in determining whether there are different emission mechanisms present in the two classes, the relationships between infrared color and 60 μm luminosity of interacting and of non-interacting galaxies were determined. Assuming $F \propto \nu^{-\alpha}$, the spectral index α(25/60) is plotted against 60 μm luminosity in Figure 39. Non-interacting galaxies are filled triangles, interacting galaxies are open circles. Linear fits to this plots show that there is no correlation for α(25/60) vs. L(60) for both non-interacting and interacting galaxies (r = 0.04 and –0.11, respectively). The mean values for all luminosities are <α(25/60)> = 2.4 ± 0.5 and 2.5 ± 0.6, respectively. The lack of correlation between F(25)/F(60) and L(60) for a total 60 μm flux-limited sample has already been shown in SKHL; this study shows that there is no correlation for each class individually.

The spectral index α(60/100) is plotted vs. luminosity in Figure 40. A correlation is seen for the entire sample, as in SKHL. Also, for each class there is a correlation, and the two slopes and intercepts are consistent with each other. For interacting galaxies, α(60,100) = –0.6 ± 0.1 log $(L(60)/L_o)$ + 7 ± 2 (r = –0.61), while for non-interacting galaxies, α(60,100) = –0.5 ± 0.1 log $(L(60)/L_o)$ + 6 ± 1 (r = –0.48). The difference in the mean value of $\alpha(60/100)$ seen in this Figure is a consequence of the difference in mean luminosities.

These infrared color-60 μm luminosity relationships, along with the 60 μm luminosity functions, are used in Chapter V to derive deep 60 μm source counts.

Table 6. Sensitivity of 60 μm Luminosity to Mass Ratio and Separation

	Count	$\langle \log L(60)/L_{\odot} \rangle$		$\langle \log L(FIR)/L_{\odot} \rangle^{a,c}$	
No Bound Companions	155	10.0 ± 0.8		10.5 ± 0.6	
Pairs with $m_1/m_2 \geq 1/4$					
Separation Range	Count	$\langle \log L(60)/L_{\odot} \rangle^{a}$	Enhancement[b]	$\langle \log L(FIR)/L_{\odot} \rangle^{a,c}$	Enhancement[a]
$D \leq 3R$	56	10.8 ± 0.5	~6	11.0 ± 0.5	~3
$D > 3R$	31	10.0 ± 0.8	~1	10.5 ± 0.4	~1
$2R < D \leq 3R$	10	10.8 ± 0.5	~6	11.0 ± 0.5	~3
$3R < D \leq 5R$	16	9.8 ± 1.1	~0.6	10.6 ± 0.5	~1.25
Pairs with $D \leq 3R$					
Mass Ratio Range	Count	$\langle \log L(60)/L_{\odot} \rangle^{a}$	Enhancement[b]	$\langle \log L(FIR)/L_{\odot} \rangle^{a,c}$	Enhancement[b]
$m_1/m_2 \geq 1/4$	56	10.8 ± 0.5	~6	11.0 ± 0.5	~3
$1/4 \leq m_1/m_2 < 1/2$	19	10.6 ± 0.5	~4	10.9 ± 0.5	~2.5
$1/10 \leq m_1/m_2 < 1/4$	10	10.3 ± 0.4	~2	10.6 ± 0.4	~1.25
Galaxies from Non-interacting Sample, Selected on Morphological Criteria					
Subset	Count	$\langle \log L(60)/L_{\odot} \rangle^{a}$	Enhancement[b]	$\langle \log L(FIR)/L_{\odot} \rangle^{a,c}$	Enhancement[b]
Distorted Sample	20	10.4 ± 0.4	~3	10.7 ± 0.3	~1.5
Symmetric Spirals	65	9.6 ± 0.6	~0.5	10.0 ± 0.6	~0.3

Notes to Table 6:

[a]Quoted uncertainty is rms dispersion.
[b]Enhancement of the mean, calculated compared to the galaxies without bound companions.
[c]Calculated using the relationship given in Lonsdale *et al.* (1985).

Table 7. 60 μm Luminosity Functions

	Total Sample		Interacting		Non-Interacting		Ambiguous	
Log $(L/L_{\odot})$	$\phi(L)$ $(Mpc^{-3}mag^{-1})$	N	$\phi(L)$ $(Mpc^{-3}mag^{-1})$	N	$\phi(L)$ $(Mpc^{-3}mag^{-1})$	N		$\phi(L)$ $(Mpc^{-3}mag^{-1})$
7.6	2.1×10^{-1}	3	—	—	1.9×10^{-1}	2	1.6×10^{-2}	1
8.0	—	—	—	—	—	—	—	—
8.4	9.7×10^{-3}	5	—	—	9.7×10^{-3}	5	—	—
8.8	4.9×10^{-3}	13	—	—	4.3×10^{-3}	11	6.4×10^{-4}	2
9.2	1.7×10^{-3}	14	—	—	1.7×10^{-3}	14	—	—
9.6	1.0×10^{-3}	37	5.0×10^{-3}	2	9.0×10^{-4}	33	8.1×10^{-5}	2
10.0	5.8×10^{-4}	68	7.5×10^{-4}	10	4.9×10^{-4}	56	3.2×10^{-5}	3
10.4	1.4×10^{-4}	66	2.2×10^{-5}	11	1.1×10^{-4}	49	1.4×10^{-5}	6
10.8	2.4×10^{-5}	39	8.2×10^{-6}	15	1.5×10^{-5}	23	6.6×10^{-7}	1
11.2	3.2×10^{-6}	20	1.8×10^{-6}	11	7.8×10^{-7}	5	5.7×10^{-6}	4
11.6	4.2×10^{-7}	9	3.5×10^{-7}	7	—	—	3.5×10^{-8}	1
12.0	1.2×10^{-8}	1	—	—	—	—	1.2×10^{-8}	1

Table 8. Best Fit Parameters to Luminosity Functions[a]			
Class	Range of Fit	log γ	β
Total	$10^{10}L_o - 10^{12}L_o$	$18.2^{+1.3}_{-1.7}$	-2.1 ± 0.2
Interacting	$4\times10^{9}L_o - 10^{12}L_o$	$6.8^{+3.0}_{-2.5}$	-1.15 ± 0.30
Interacting + Ambiguous	$4\times10^{9}L_o - 10^{12}L_o$	12 ± 3	$-1.5^{+0.2}_{-0.4}$
Non-Interacting[b]	$10^{10}L_o - 6\times10^{11}L_o$	18^{+3}_{-2}	$-2.1^{+0.1}_{-0.3}$
Non-Interacting[c]	$10^{8}L_o - 10^{10}L_o$	$5.3^{+1.7}_{-3.3}$	$-0.90^{+0.45}_{-0.25}$
Non-Interacting + Ambiguous[b]	$10^{10} - 6\times10^{11}L_o$	$20.0^{+2.5}_{-2.0}$	$-2.35^{+0.70}_{-0.25}$
Non-Interacting + Ambiguous[c]	$10^{8}L_o - 10^{10}L_o$	$12.1^{+2.7}_{-3.1}$	-1.60 ± 0.5

Notes for Table 8:

[a]Fit to power law functional form $\phi(L) = \gamma L^{\beta}$ where ϕ is in units of Mpc^{-3} mag^{-1} and L is in solar units. The quoted uncertainties are 68% joint confidence levels (Avni 1976).

[b]Excluded the bin at log $L(60)/L_o = 12.0$. This bin is due to IRAS 03521+0028, using an estimated redshift.

[c]Excluded the bin at log $L(60)/L_o = 7.6$. The galaxies in this bin are nearby (v < 500 km/s), and therefore the luminosities derived assuming Hubble flow are uncertain.

Class	B	W	X	Y	χ^2_ν
Total	1.62	0.80	24.3	5.94	0.50
Interacting	3.24	0.57	24.9	6.95	0.18
Non-Interacting[b]	2.82	0.55	24.1	7.04	0.54
Interacting + Ambiguous[b]	3.26	0.76	24.8	7.00	0.24
Non-Interacting + Ambiguous[b,c]	2.74	0.57	24.1	6.99	0.47

Table 9. Best Fit Parameters to Visibility Functions[a]

Notes for Table 9:

[a]Fit to hyperbolic functional form $\log\left\{\Psi\right\} = Y - \left\{B^2 + \left\{\frac{\log L - X}{W}\right\}^2\right\}^{1/2}$ where Ψ is in units of $Jy^{1.5}$ and L is in units of W/Hz (Condon 1984).

[b]Excluding the bin at log $L(60)/L_o = 7.6$. The galaxies in this bin are nearby (v < 500 km/s), and therefore the luminosities derived assuming Hubble flow are uncertain.

[c]Excluding the bin at log $L(60)/L_o = 12.0$. This bin is due to IRAS 03521+0028, using an estimated redshift.

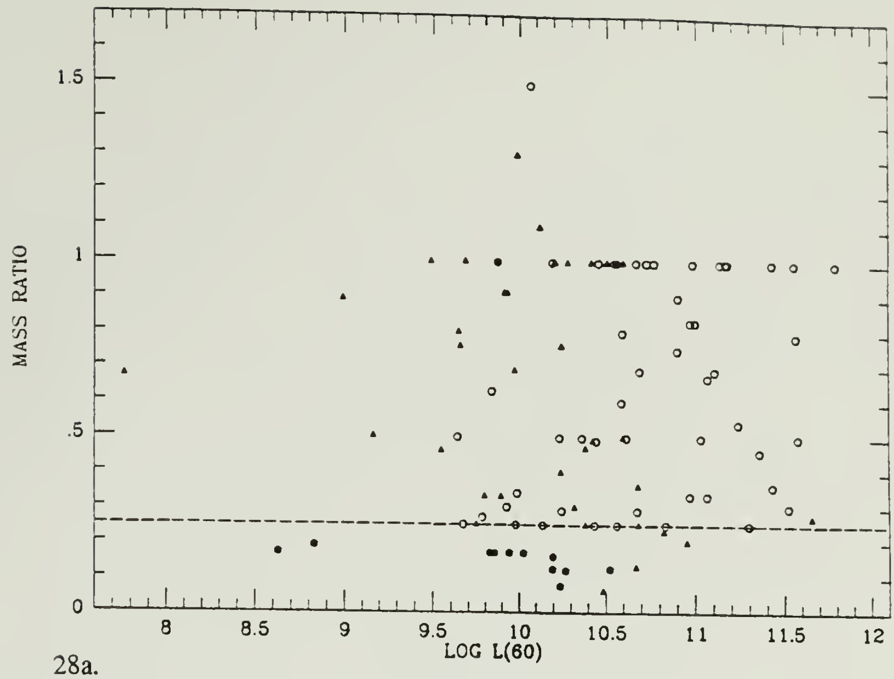

28a.

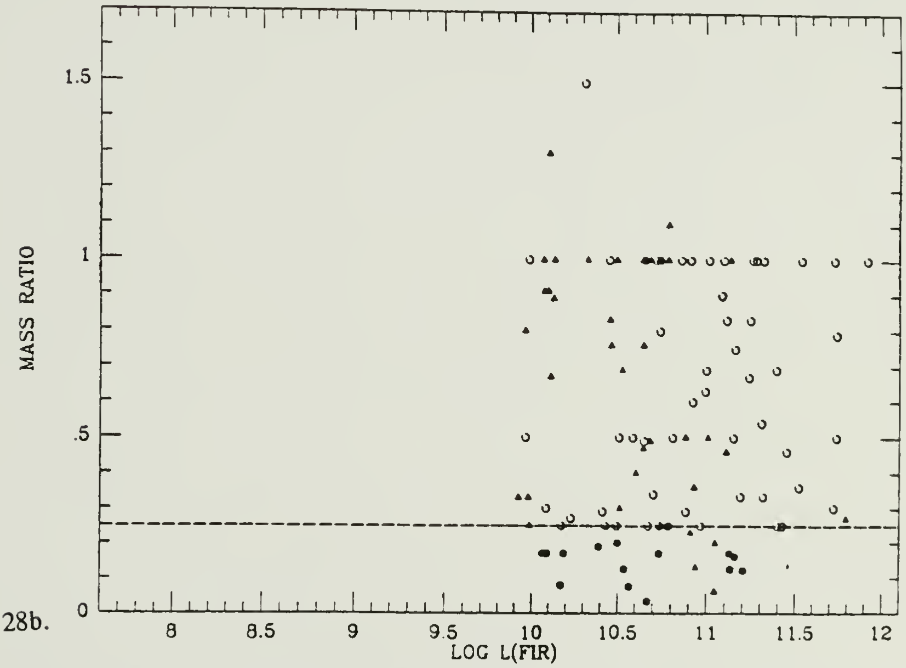

28b.

Figure 28. Mass ratio vs. 60 μm luminosity and total far-infrared luminosity. Figure 28a is the plot of mass ratio (I-band luminosity ratio) vs. 60 μm luminosity. Figure 28b is the plot of mass ratio vs. FIR luminosity, as defined by Lonsdale *et al.* (1985). The mass ratio is m_1/m_2, where m_1 = the mass of the companion, and m_2 = the mass of the infrared galaxy. The open and filled circles are galaxies with companions closer than or equal to 3 times the radius; open circles represent galaxies defined as interacting in this study, because they lie on or above the dashed line at $m_1/m_2 = 0.25$. Filled triangles are wider pairs. The filled circles and the filled triangles represent galaxies which are defined as non-interacting in this study. Pairs of galaxies with $\Delta v > 500$ km/s and ambiguous galaxies are excluded from this Figure.

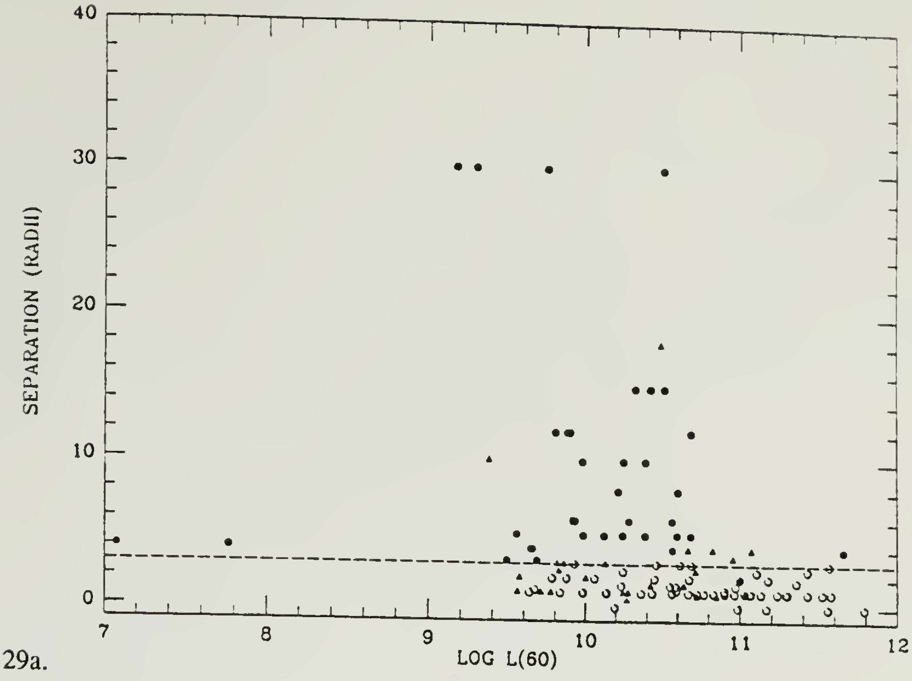

29a.

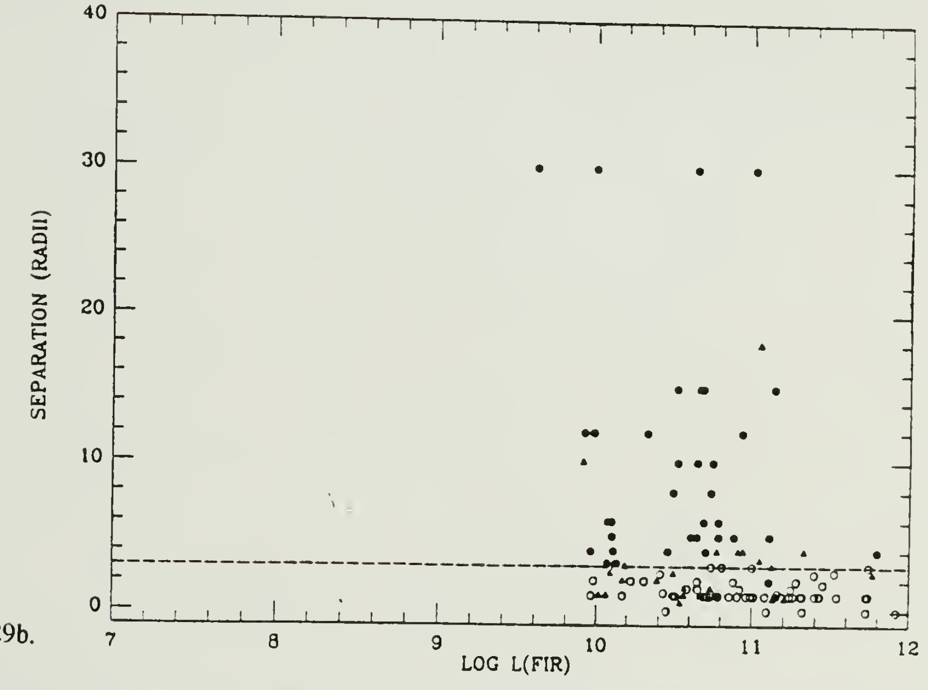

29b.

Figure 29. Separation vs. 60 μm luminosity and total far-infrared luminosity. Figure 29a is the plot of separation vs. 60 μm luminosity. Figure 29b is the plot of separation vs. FIR luminosity, as defined by Lonsdale *et al.* (1985). Open and filled circles are galaxies with companions of mass ≥ 1/4M; open circles represent galaxies defined as interacting in this study, because they lie on or below the dashed line at D = 3R. Filled triangles are galaxies with less massive companions. The filled circles and the filled triangles represent galaxies which are defined as non-interacting in this study. Pairs of galaxies with Δv > 500 km/s are excluded, as are ambiguous galaxies.

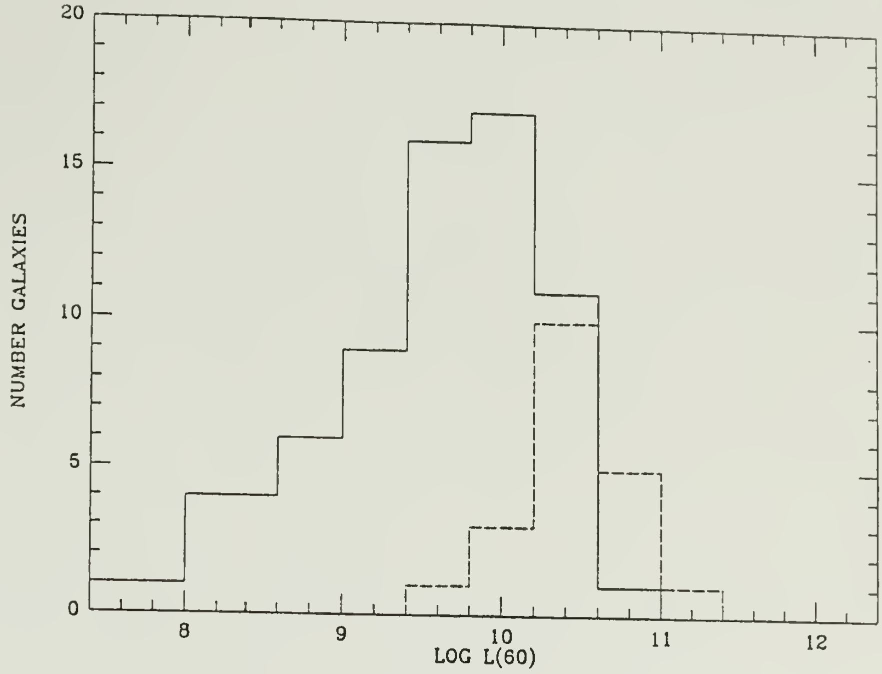

Figure 30. The 60 μm luminosity distributions of distorted and symmetrical galaxies. The dashed histogram represents the 60 μm luminosity distribution of the 20 galaxies in the sample which fail the interaction criteria, yet show obvious signs of gravitational distortion from a companion. The solid histogram shows the luminosity distribution of the galaxies which are seen to be symmetrical spirals on the I-band image.

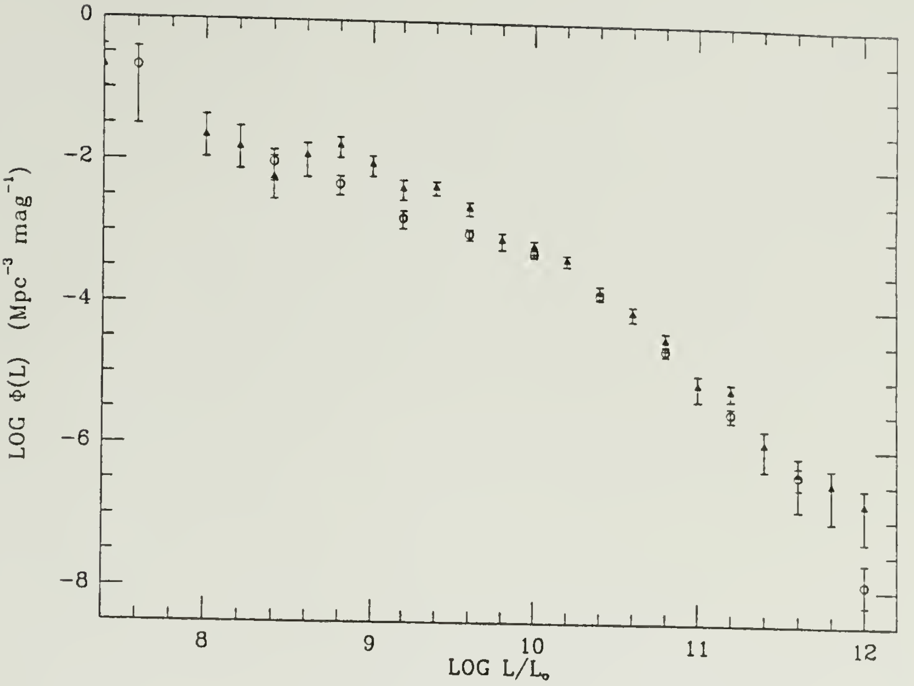

Figure 31. The luminosity function of the entire sample. The open circles are from this study; the filled triangles are from SKHL; the star symbols represents values from Soifer *et al.* (1987). The error bars are proportional to $\sqrt{N}$. The open circle at Log L = 12 is due to IRAS 03521+0028, using an redshift estimated from the blue magnitude, and is uncertain. The data from Soifer *et al.* (1987) has been converted to H_o = 100 km/s/Mpc and this definition of L(60).

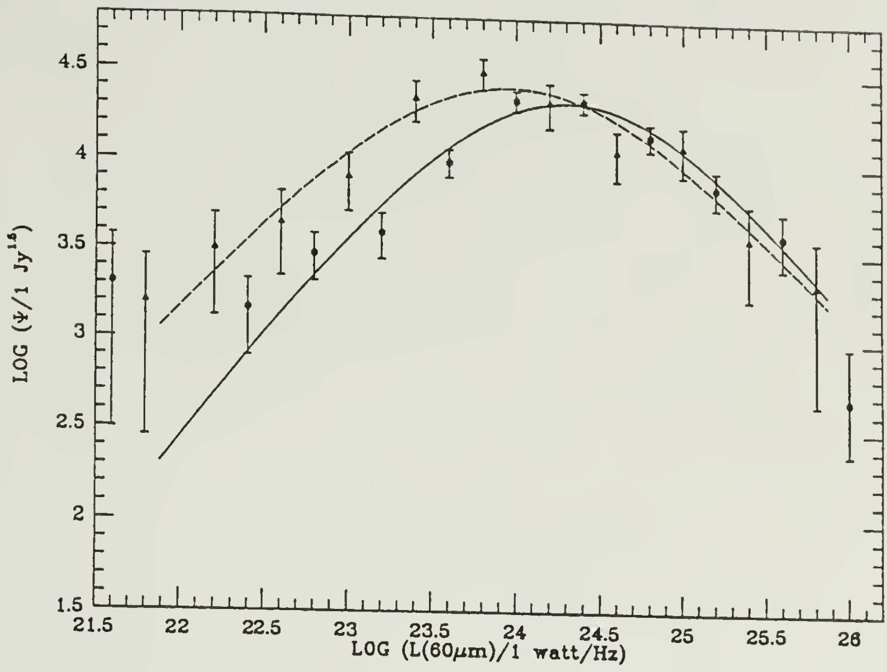

Figure 32. The total visibility function. The filled triangles are the points from Soifer *et al.* (1987); the asterisks are the data from this study. The two curves are the best fit hyperbolae.

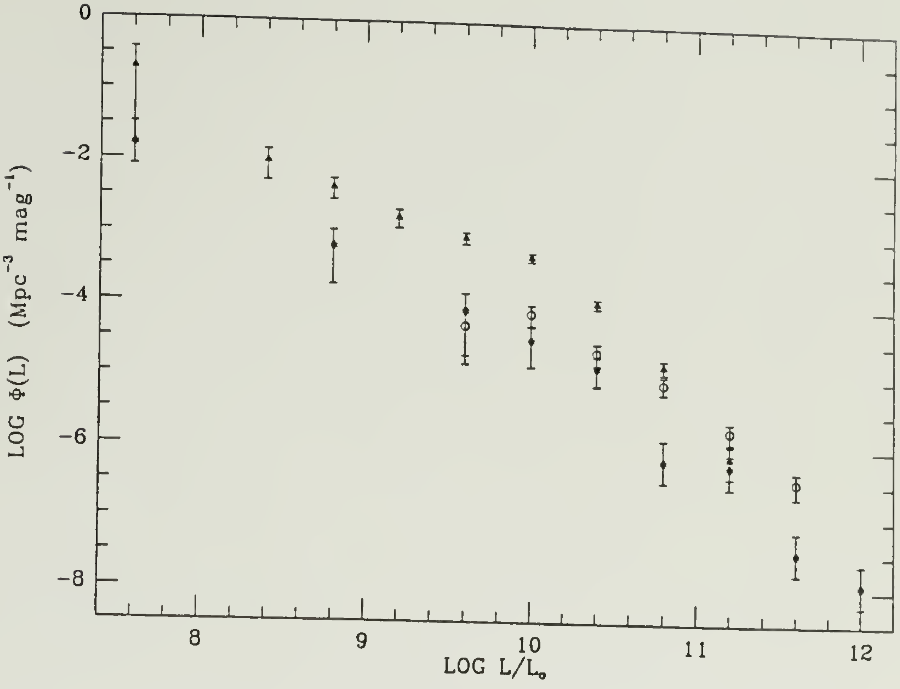

Figure 33. Separated luminosity function. Filled triangles represent the luminosity function of non-interacting galaxies; open circles represent interacting galaxies; and asterisks represent ambiguous galaxies.

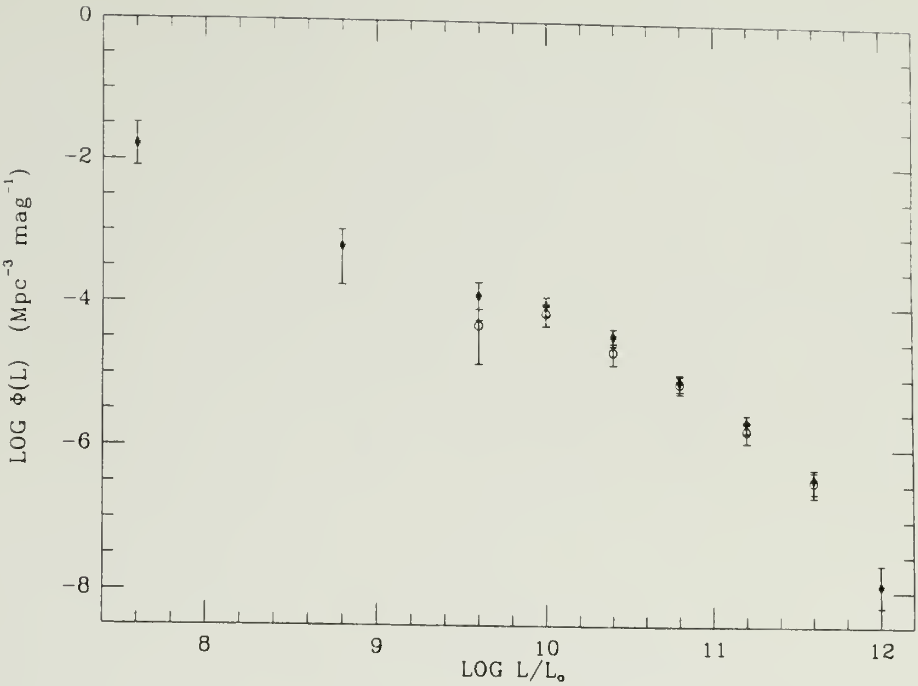

Figure 34. The luminosity function of the combined group of interacting and ambiguous galaxies, plotted with the original interacting galaxy luminosity function. The asterisks represent the luminosity function of interacting and ambiguous galaxies, while the open circles represent the luminosity function of interacting galaxies. These two functions show that the ambiguous galaxies make little difference to the luminosity function of interacting galaxies.

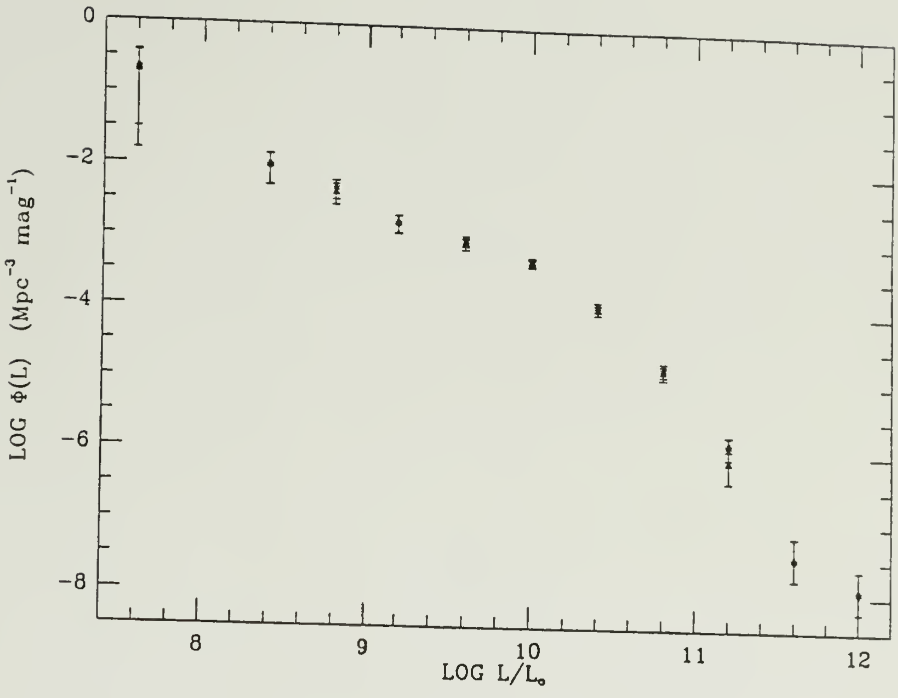

Figure 35. The luminosity function of the combined group of non-interacting and ambiguous galaxies, plotted with the original non-interacting galaxy luminosity function. The asterisks represent the luminosity function of the combined group of interacting and ambiguous galaxies, the filled triangles is the original luminosity function of non-interacting galaxies. These two functions show that the ambiguous galaxies make little difference to the luminosity function of non-interacting galaxies, except for the point at Log L(60) = 12, which represents IRAS 03521+0028.

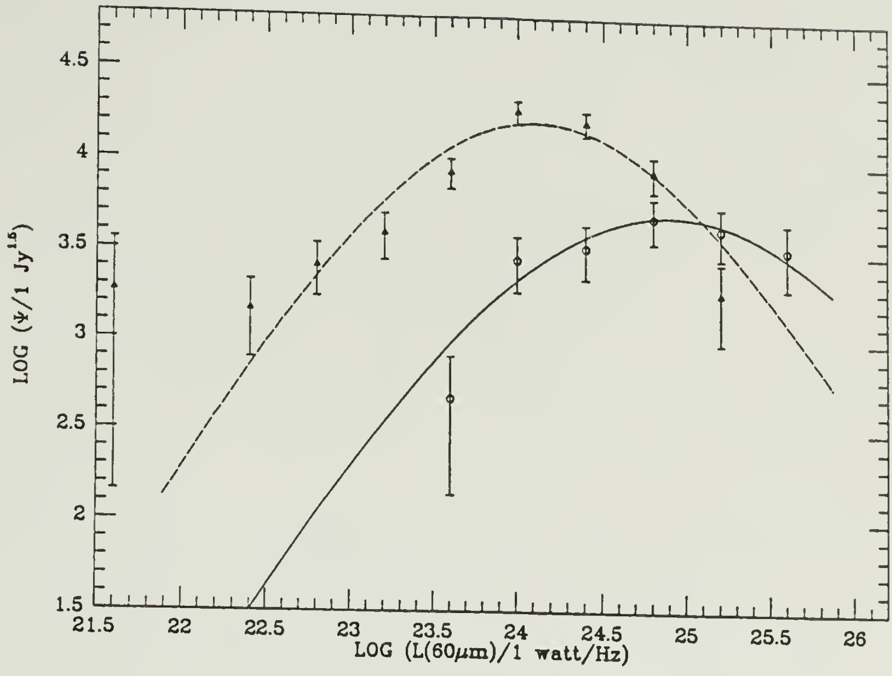

Figure 36. The visibility functions for interacting and for non-interacting galaxies. Interacting galaxies are represented by open circles; non-interacting galaxies are represented by filled triangles. Also shown are the best fit hyperbolae to the data.

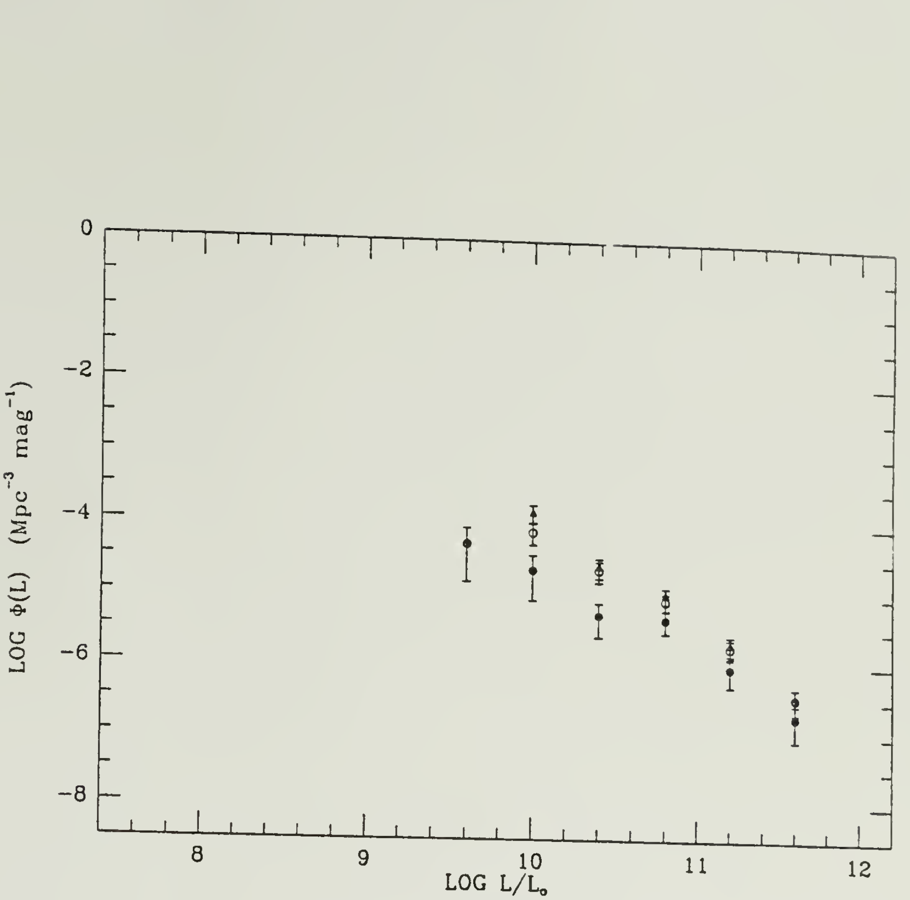

Figure 37. Variations in the luminosity function of interacting galaxies as a function of limiting mass ratio. These are all constructed using a maximum distance separation of 3 times the radius and maximum velocity difference of 500 km/s. Open triangles represent the luminosity function of interacting galaxies derived using a mass ratio limit of $m_1/m_2 \geq 0.1$; open circles, ≥ 0.25; filled circles, ≥ 0.667, where m_1 = the mass of the companion, and m_2 = the infrared galaxy. This Figure shows that there is little difference in the luminosity function derived with $m_1/m_2 \geq 0.1$ or 0.25, however, there is a significant difference between that derived with $m_1/m_2 \geq 0.25$ and that derived with $m_1/m_2 \geq 0.667$, especially at luminosities less than $4 \times 10^{10} L_o$.

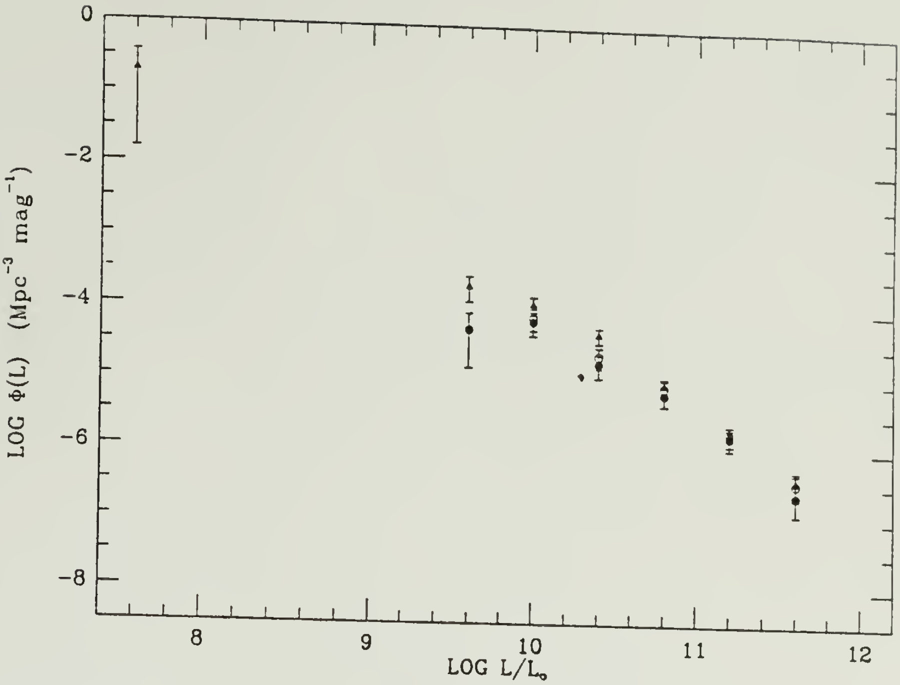

Figure 38. Variations in the luminosity function of interacting galaxies as a function of limiting separation distance. These are all constructed using a minimum mass ratio of 1/4 and maximum velocity difference of 500 km/s. Filled triangles represent the luminosity function of interacting galaxies derived using a separation limit of $D \leq 2R$; open circles, $\leq 3R$; filled circles, $\leq 10R$. This Figure shows that the luminosity function of interacting galaxies does not vary much in a limiting separation range of $2R \leq D \leq 10R$.

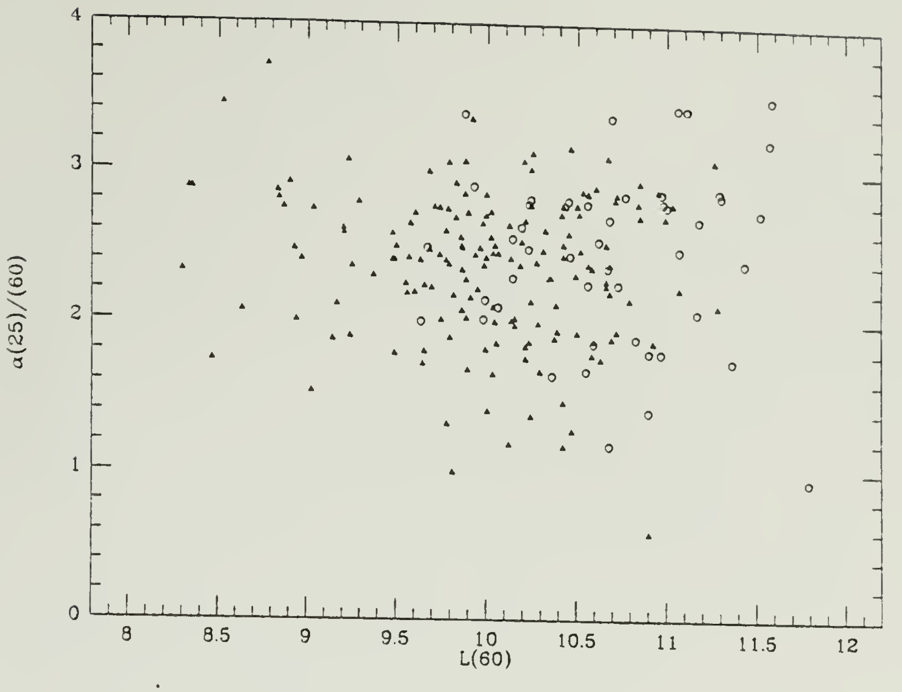

Figure 39. The spectral index α(25/60) vs. 60 μm luminosity. The open circles are interacting galaxies, and the filled triangles are non-interacting galaxies.

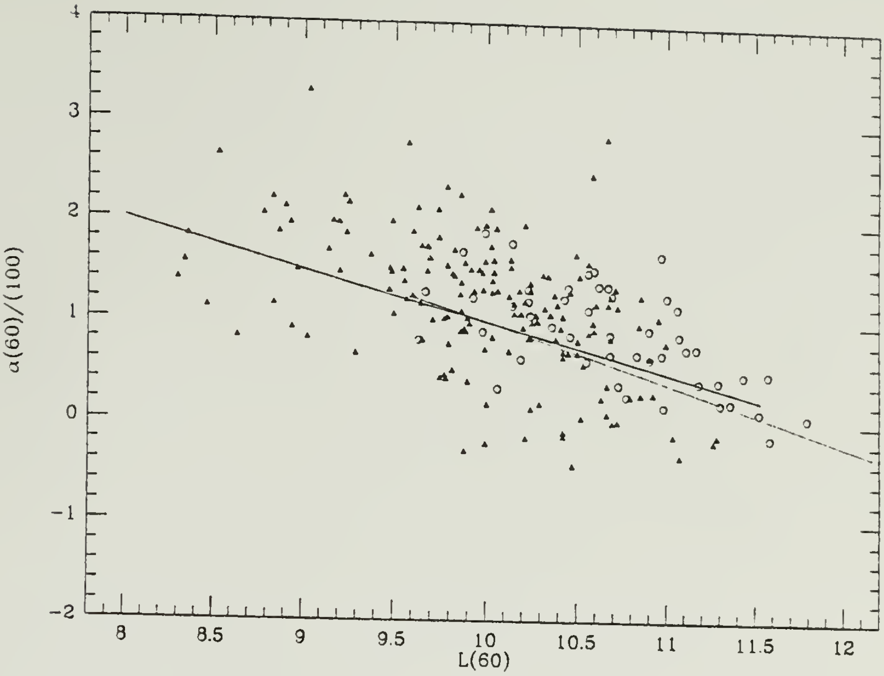

Figure 40. The spectral index α(60/100) vs. 60 μm luminosity. The open circles are interacting galaxies, and the filled triangles are non-interacting galaxies. The solid line is the best fit to the non-interacting galaxies, The dotted line is the best fit to the interacting galaxies.

CHAPTER V

MODEL OF THE DEEP FAR-INFRARED SOURCE COUNTS

A. Introduction

The evolutionary model used for this study is a revision of the model developed by Condon (1984) to account for the observed surface density of radio sources. Condon (1984) modeled the extragalactic source counts at 0.408, 0.61, 1.4, 2.7, and 5 GHz, assuming that the sources were quasars, spirals, and elliptical galaxies. These sources reach to redshifts of ~3. The program provides 60 μm source counts as a function of flux density, using the basic theoretical relationships between the source counts and the luminosity function given in Condon (1984). These are reviewed in Section B of this Chapter.

This routine had since been revised by HCH for use at 60 μm, to model the deep IRAS source counts derived by Hacking and Houck (1987). The deep source counts, described in Chapter I, extend to 50 mJy at 60 μm (10 times fainter than the PSC). This corresponds to a redshift of ~0.15 for a galaxy with 60 μm luminosity of $10^{10}L_o$.

For the current study, the 60 μm version of this model was revised again, to account for different evolution of interacting and non-interacting galaxies. The current study differs from that of HCH in that they assume that the entire luminosity function evolves in the same manner, while in this study it is assumed that only the interacting component of the luminosity function evolves rapidly. The original source code for the computer program was kindly provided by J.J. Condon. The 60 μm visibility functions $\phi(L)$ of non-interacting and interacting galaxies derived in Chapter IV of this thesis are used for the current study, along with the infrared color–60 μm luminosity relationships.

In this study, four different models are used to describe the evolution of the 60 μm luminosity function of interacting galaxies. The choices of models are consistent with those used by HCH. The models used include one in which it is assumed that no evolution occurs, two in which it is assumed that the density (but not the luminosity) of galaxies evolves, and one in which it is assumed that only the luminosity evolves. Pure density evolution assumes that only the density of galaxies varies with redshift; the luminosities, spectral energy distributions, and the shape of the luminosity function do not change. The density evolution models assume that $\phi(L,z) = \phi(L,z{=}0)(1+z)^n$, where n = 6 and 7, respectively. A choice of n = 6 is deduced from a collision model with relative velocities between galaxies that remain constant with time, and n = 7 is derived from a collision model where relative velocities decrease with the expanding universe (HCH). The best-fit evolutionary model to radio galaxy source counts from Condon (1984), is nearly pure luminosity evolution, that is, the luminosity varies with redshift, but the shape of the luminosity function does not change. This is expressed by $\phi(L,z) = \phi(\frac{L}{(1+z)^n},z{=}0)$, where n = −4. (The best fit values to the evolution of radio source counts required some density evolution at high redshifts.)

B. Derivation of Source Count Equations

This section gives a review of the derivation by Condon (1984) and Hacking (1987) of the theoretical relationship between source counts and the luminosity function. In this model, the shape of the spectral energy distribution is assumed to be a power law, $F_\nu \propto \nu^{-\alpha}$, where F_ν is the flux density at frequency ν, and α is the spectral index.

Source counts are given in differential values, that is, in terms of $n(F_\nu,\nu)dF_\nu$, the number of sources per steradian with flux densities between F_ν and $F_\nu + dF_\nu$, at frequency ν. The normalized differential source count, $F_\nu^{5/2}n(F_\nu,\nu)$, is the goal of this derivation.

The number of sources $\eta(F,z,\alpha,\nu)dF_\nu d\alpha$ over the whole sky, at frequency ν and redshift z, with flux densities between F_ν and $F_\nu + dF_\nu$ and spectral indices between

$$\eta(F_\nu,z,\alpha,\nu)dF_\nu d\alpha = \rho(L,z,\alpha,\nu)dLd\alpha(4\pi D^2 dr),$$

$$D = \left(\frac{c}{H_o}\right)\left\{\frac{q_o z+(q_o-1)((2q_o z+1)^{1/2}-1)}{q_o^2(1+z)}\right\}$$

$$dr = \frac{cdz}{H_o(1+z)(1+2q_o z)^{1/2}}$$

The function $\rho(L)$ is the density of galaxies with luminosities between L and L + dL, and is defined by $\rho(L)dL = \phi(L)d(mag)$. Therefore, $\rho(L) = \frac{1.086}{L}\phi(L)$ (van Hoerner 1973).

The luminosity L is $L = 4\pi D^2 F_\nu(\text{rest frame}) = 4\pi D^2(1+z)^{(1+\alpha)}F_\nu$ (Hacking 1987), and $dL = 4\pi D^2(1+z)^{(1+\alpha)}dF_\nu$. Substituting these into the equation for $\eta(F_\nu,z,\alpha,\nu)dF_\nu d\alpha$, along

$$\eta(F_\nu,z,\alpha,\nu)dF_\nu d\alpha = \frac{cF_\nu^{-5/2}}{D(4\pi)^{1/2}}\frac{\Psi(4\pi D^2F_\nu(1+z)^{(1+\alpha)},z,\alpha,\nu)dF_\nu d\alpha}{H_oD(1+2q_oz)^{1/2}(1+z)^{(5/2+3\alpha/2)}}.$$

$$F^{5/2}n(S,\nu) = \int_{-\infty}^{\infty}\int_{0}^{\infty} F^{5/2}\eta(F,z,\alpha,\nu)dzd\alpha.$$

These are the basic relations used to derive $F^{5/2}n(S,\nu)$ from the luminosity function.

C. Spectral Index Dependence of the Visibility Functions

It is also necessary to determine the α dependence of Ψ. As in HCH it is assumed in this study that $\Psi(L,z,\alpha,\nu)=\Psi(L,z,\nu)U(L,z,\alpha)$, where $U(L,z,\alpha)$ is the spectral index distribution at a given L and z. The simplest form of the distribution, a Gaussian, is

$$U(L,z,\alpha) = \frac{1}{(2\pi)^{1/2}\sigma(L,z)}e^{-\frac{1}{2}\left\{\frac{\alpha-\langle\alpha\rangle(L,z)}{\sigma(L,z)}\right\}^2}$$

where $\langle\alpha\rangle$ is the mean spectral index at L and z, and σ is the dispersion in α.

In this model, the relation between spectral index and luminosity in the local Universe (derived in Chapter IV) are used: it is assumed that these relationships are invariant with redshift in the rest frame of the galaxy. However, the observed values

$$\langle\alpha(L,z)\rangle = \alpha(25/60)(z{=}0)$$

$$\langle\alpha(L,z)\rangle = \alpha(25/60)(z{=}0)\left\{\log(1+z)/\log 1.41\right\}$$

$$+\alpha(60/100)(L,z{=}0)\frac{\log\left\{1.41/(1+z)\right\}}{\log 1.41}$$

D. Comparison with Previous Model Results

1. Evolving the Total Luminosity Function

First, to ascertain the effect of variations in the local luminosity function on the outcome of the evolutionary models, the results of evolving the *total* luminosity function from this sample are compared with the original model results from HCH, which use the luminosity function derived by Soifer *et al.* (1987). As in HCH, the four different evolutionary models are designated models 1–4, where model 1 is a non-evolving model, model 2 is a density evolution model, with $\phi(L,z) = \phi(L,z{=}0)(1+z)^6$, model 3 is a density evolution model with $\phi(L,z) = \phi(L,z{=}0)(1+z)^7$, and model 4 is the luminosity evolution model. The results are shown in Figures 41a, b, c, and d (solid curves), along with the original curves from HCH (dotted lines). This plot gives the predicted normalized source counts $F^{5/2}n(S,\nu)$ at 60 μm as a function of flux density. There are factors of ~1.5, 1.5, 1.4, and 1.2 difference between the two predicted source count curves at 100 mJy, for models 1, 2, 3, and 4, respectively. At a flux density of ≥ 30 Jy, the two sets of models reach source count values of a factor of ~1.3 apart. As noted previously, the surface density of galaxies in the Soifer *et al.* (1987) sample a density 1.8 times that of the present 2 Jy survey, suggesting that the difference is at least partially due to inhomogeneities in the local Universe.

For comparison, the deep infrared data from Hacking and Houck (1987) is also shown in Figure 41. At low flux levels, the data points fall between models 3 and 4; the data do not favor one of these models more than the other. The large error bars in the data are a consequence of the relatively small sample size. The scatter in the data is probably due to inhomogeneities in the galaxy distribution at these lower levels. Preliminary results from a redshift survey of the galaxies in this survey (Hacking, private communication) show that there is a spike in the distribution of redshifts at z~0.09, indicating that there may be a cluster at this redshift. Thus, this data is not the ideal database for this study.

However, there is a new survey, the IRAS Faint Source Catalog (1988; hereafter FSC), in preparation at the Infrared Processing and Analysis Center, which may reduce these problems. This survey covers a much larger area, thus minimizing inhomogeneities and enlarging the sample size (several 10's of thousands of galaxies). This survey is being derived by co-addition of the survey data that went into the PSC. It will reach to a flux level of ~100–200 mJy, so a $10^{10}L_{o}$ galaxy will be detected at a redshift of ~0.2–0.35.

2. Evolving only the Luminosity Function of Interacting Galaxies

Figure 42a, b, and c show the results of evolving only the luminosity function of interacting galaxies, for models 2, 3, and 4, respectively. Model 1 remains the same. In these plots, the solid curves are the four model predictions of source counts due to evolution of the total luminosity function, using the total visibility function derived in this study. The dotted and dashed lines are the upper and lower limits of the predicted source counts for each model, assuming that isolated galaxies do not evolve. The dashed lines are the predicted source counts when the ambiguous galaxies are all assumed to be interacting galaxies. The dotted lines are the predicted results when it is assumed that the ambiguous galaxies are non-interacting. Thus the regions between the dotted and dashed curves show the uncertainty in the model results, due to the ambiguous galaxies.

The difference between evolving the total luminosity function and evolving only the luminosity function of interacting galaxies is a factor of ~1.25, 1.25, and 1.75 at 100 mJy for models 2, 3, and 4, respectively. The ambiguous galaxies give an uncertainty in the model results of only a factor of 1.1 at 100 mJy.

E. Conclusions

These results show that, if only interacting galaxies are assumed to evolve, the predicted source counts are 60–80% of those determined if all galaxies evolve. The uncertainty in the predicted source counts due to the ambiguous galaxies is ~10%.

However, differences in the local luminosity function of galaxies, due either to local inhomogeneities or deviations from Hubble flow, cause differences in predicted source counts of a factor of 1.2 to 1.5.

These differences in the local luminosity function could be resolved by a full sky redshift survey of bright 60 μm galaxies, with a larger number of galaxies, with distances to nearby galaxies determined without recourse to the Hubble relation. Such a study is already in progress (Strauss and Huchra 1988; Yahil 1987). Difficulties in predicting deep source counts due to inhomogeneities in the local Universe can be partially resolved by the use of the Faint Source Catalog. Further, when redshifts become available for a sample obtained from the Faint Source Catalog, the evolution can be measured directly.

Figure 41. Predicted source counts, assuming the total luminosity function is evolved. Figures 41a, 41b, 41c, and 41d show results from models 1, 2, 3, and 4, respectively. This plot shows the difference in results, depending on the input visibility functions. The solid curves, labeled (a), are the Hacking, Condon, and Houck (1987) results for the 4 models. The dotted curves, labeled (b), are the results obtained if the local total visibility function derived in this study is used. The source counts shown are from Hacking, Condon, and Houck (1987). The filled circles are values from the Hacking and Houck (1987) survey, and the open circles were determined by Hacking, Condon, and Houck (1987) from the PSC, for galaxies with $|b^{II}| \geq 50°$.

Figure 41. Predicted source counts, assuming the total luminosity function is evolved. Figures 41a, 41b, 41c, and 41d show results from models 1, 2, 3, and 4, respectively. This plot shows the difference in results, depending on the input visibility functions. The solid curves, labeled (a), are the Hacking, Condon, and Houck (1987) results for the 4 models. The dotted curves, labeled (b), are the results obtained if the local total visibility function derived in this study is used. The source counts shown are from Hacking, Condon, and Houck (1987). The filled circles are values from the Hacking and Houck (1987) survey, and the open circles were determined by Hacking, Condon, and Houck (1987) from the PSC, for galaxies with $|b^{II}| \geq 50°$.

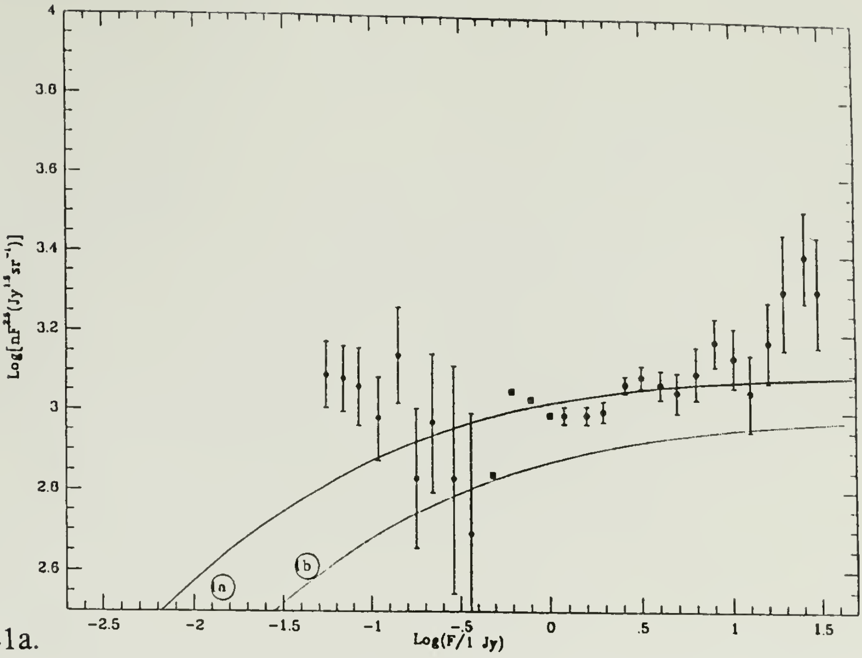
4
3.8
3.6
3.4
3.2
3
2.8
2.6
Log[nF^2.5(Jy^1.5 sr^-1)]
a
b
-2.5
-2
-1.5
-1
-.5
0
.5
1
1.5
Log(F/1 Jy)

41a.

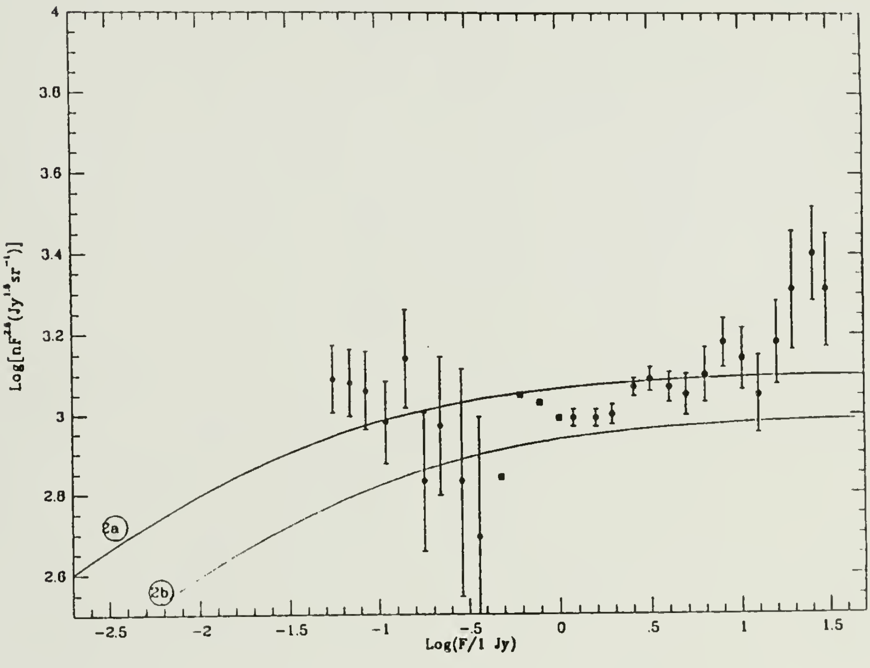
4
3.8
3.6
3.4
3.2
3
2.8
2.6
Log[nF^2.5(Jy^1.5 sr^-1)]
2a
2b
-2.5
-2
-1.5
-1
-.5
0
.5
1
1.5
Log(F/1 Jy)

41b.

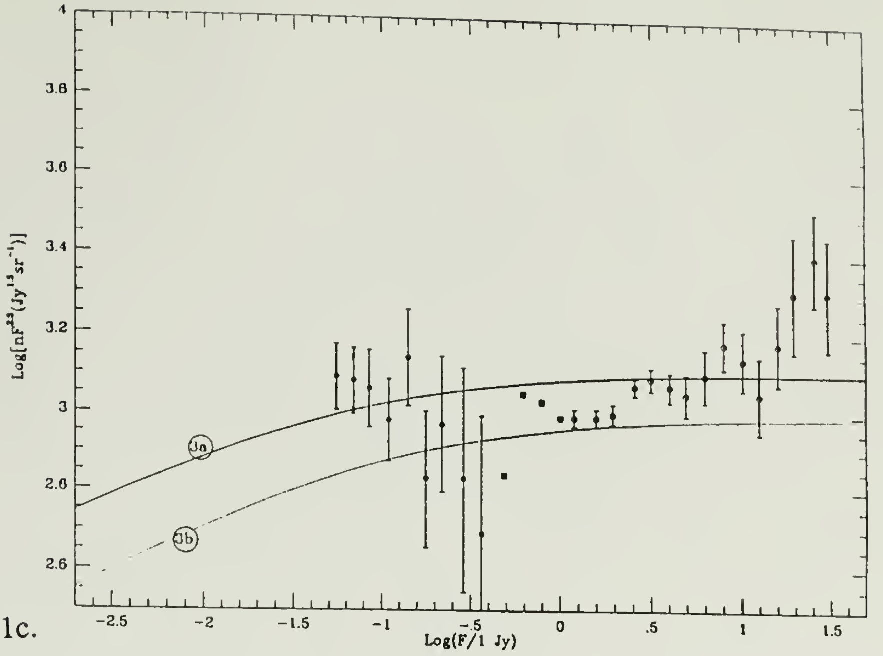

41c.

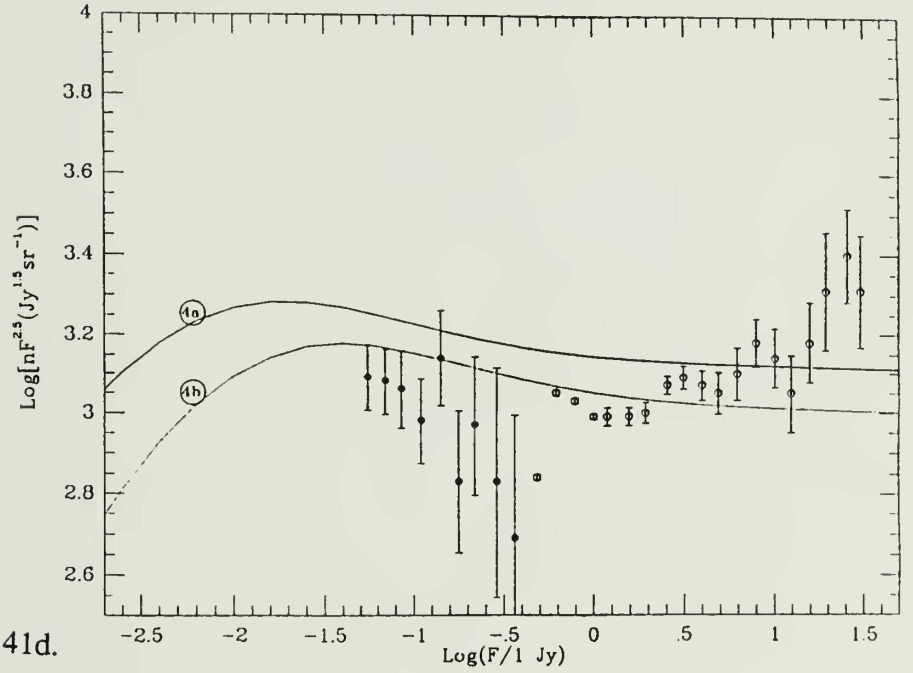

41d.

Figure 41. (Continued).

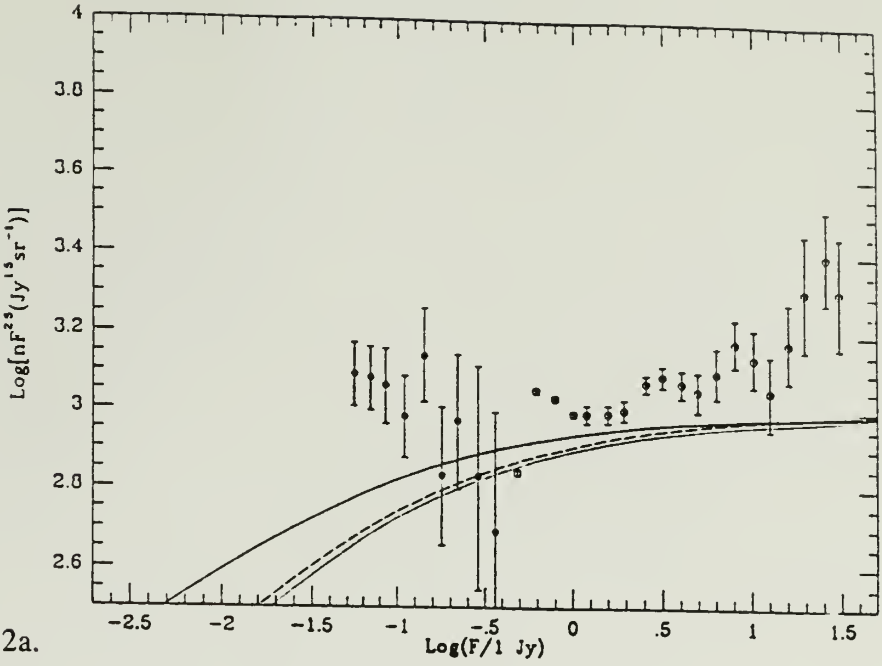

42a.

Figure 42. Evolutionary model results. The solid curves are the results of modeling by evolving the total luminosity function, using the total visibility function derived for this study (curves (b) in Figure 40). The dotted and dashed curves give the predicted source counts if the luminosity function of non-interacting galaxies is kept constant, and the luminosity function of interacting galaxies is evolved. The dotted curves are the result of adding the ambiguous galaxies to the non-interacting galaxy sample; the dashed curves are the result of adding the ambiguous galaxies to the interacting galaxy sample. The regions between the dotted and the dashed curves thus show the uncertainty in the model results because of the ambiguous galaxies. Figure 41a shows results for model 2; 41b shows results for model 3; 41c shows results for model 4. Model 1 does not change. The source counts shown are from Hacking, Condon, and Houck (1987). The filled circles are values from the Hacking and Houck (1987) survey, and the open circles were determined by Hacking, Condon, and Houck (1987) from the PSC, for galaxies with $|b^{II}| \geq 50°$.

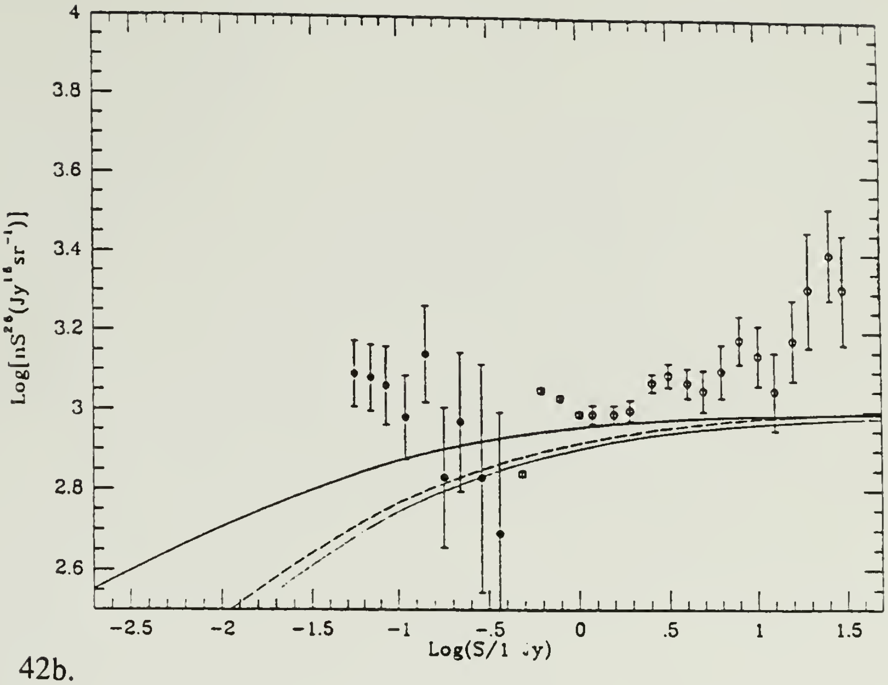

42b.

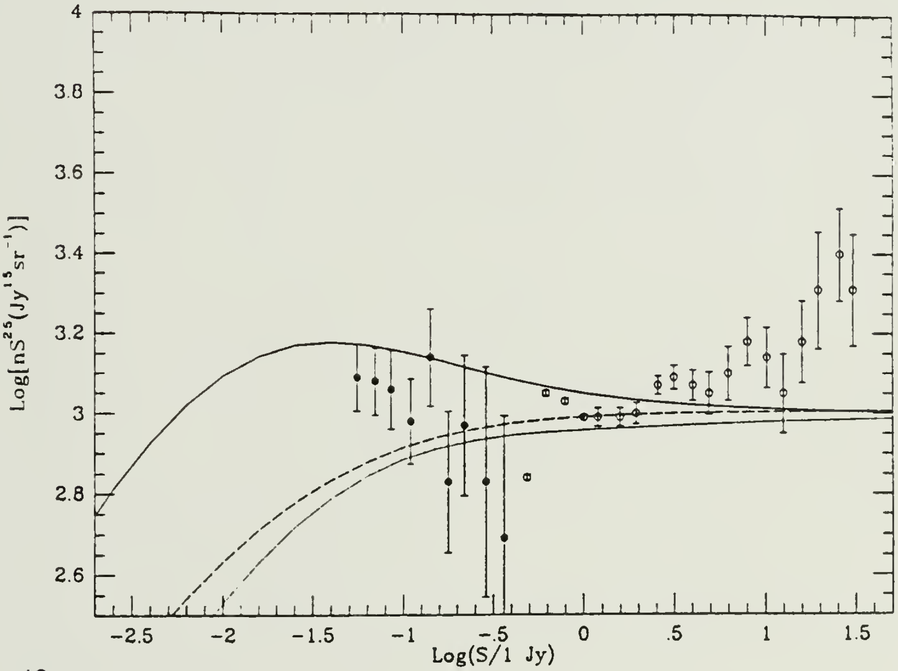

42c.

Figure 42. (Continued).

CHAPTER VI

CONCLUSIONS

A. Interacting Galaxies

In this thesis, the relationship between gravitational interactions and 60 μm luminosity has been explored by means of an I–band imaging survey of 275 galaxies in a 60 μm flux-limited sample. These images were obtained using the Kitt Peak 2.1m telescope. From these images, the galaxies were classified as interacting or non-interacting, using a definition of: the companion galaxy must have a mass of at least 1/4 that of the infrared galaxy, the separation must be less than or equal to 3 times the radius, and the velocity difference must be less than or equal to 500 km/s. It was found that 56 (20%) fit the interaction criteria, 198 (72%) were non-interacting, and 21 (8%) were unclassifiable. The percentage of interacting galaxies is somewhat smaller than the 37% found by Lonsdale *et al.* (1984) for another 60 μm flux-limited sample. Presumably, this difference is due to the fact that this study used more stringent criteria to define interaction. Many of the galaxies classified as non-interacting show clear evidence for gravitational distortion from a companion, however, the companion was either too distant or of too low a mass for the pair to be classified as interacting in this study.

The amount of enhancement of the 60 μm and total far-infrared luminosity in pairs of galaxies with different interaction parameters was then statistically estimated, and found to be consistent with the theoretical results. Galaxies which fit the interaction criteria were found to have ~6 times the 60 μm luminosity of the galaxies without bound companions, consistent with Noguchi and Ishibashi's (1986) results. Further, the mean luminosity of all the pairs of galaxies with $D > 3R$, regardless of mass ratio, is similar to the value for galaxies without bound companions, and the mean luminosity of the galaxies with separations just greater than the cut-off value, $3R < D \leq 5R$, with high mass ratios (> 1/4), is again similar to that of the galaxies without bound companions. This supports the choice of 3R as an appropriate cut-off value for defining interacting galaxies, and is consistent with the Noguchi and Ishibashi (1986) galaxy interaction model results, which show that passages at distances > 3R do not greatly enhance the star formation rate.

Close pairs ($D \leq 3R$) in the mass ratio range 1/10 – 1/4 show an average 60 μm luminosity of only ~2 times that of field galaxies, compared with the factor of ~6 enhancement for the galaxies with $m_1/m_2 \geq 1/4$, supporting the choice of 1/4 as a mass ratio cutoff for interacting galaxies. Thus, the galaxies just outside the mass ratio criteria show some enhancement, while those just outside the separation criteria of 3R do not. The more rapid drop-off in enhancement with increased separation is consistent with the MD^{-3} proportionality of tidal force.

B. The 60 μm Luminosity Functions

The 60 μm luminosity functions of interacting and of non-interacting galaxies differ. Non-interacting galaxies dominate the space density of galaxies at low infrared luminosities, while interacting galaxies dominate at high luminosities. The two luminosity functions are equal at $L(60) \sim 10^{11} L_{o}$. The luminosity function of non-interacting galaxies drops off fairly steeply at $L > 10^{10} L_{o}$ ($\phi(L) \propto L^{-2.1}$), while that of interacting galaxies is flatter ($\phi(L) \propto L^{-1.2}$). No interacting galaxies were found with $L < 4 \times 10^{9} L_{o}$. There are ~5 times as many non-interacting galaxies as interacting galaxies with $L(60) > L_{\mathrm{MILKY\ WAY}}$, and ~100 times more for $L(60) > 2 \times 10^{8} L_{o}$.

The classification of ambiguous galaxies as interacting or non-interacting makes little difference to the luminosity function of either set. Also, changing the definition of interaction slightly does not make much difference, except in the case of increasing the mass ratio cutoff from 1/4 to 2/3. Alternative separation cut-off values of 10R and 2R would change the luminosity function by less than a factor of 2, implying that the luminosity function is not particularly sensitive to the limiting separation value, in the range 2R – 10R. Changing the mass ratio limit to 2/3 would decrease the luminosity function to ~30% of its value, while changing it to 1/10 would increase it by less than a factor of 2.

C. Evolutionary Results

The luminosity functions derived here were then used in the HCH evolutionary models to predict 60 μm source counts of galaxies. The results show that separating the luminosity function and evolving only the luminosity function of interacting galaxies gives predicted source counts which are 60–80% those determined from evolving the total luminosity function. The uncertainty in the predicted source counts due to the ambiguous galaxies is ~10%. However, differences in the local luminosity function of galaxies, due either to local inhomogeneities or deviations from Hubble flow, cause differences in predicted source counts of a factor of 1.2 to 1.5. A comparison of the model results with the deep source counts of Hacking and Houck (1987) was inconclusive, due to the large uncertainties on the source counts and the probability of clustering in this field.

D. Future Studies

Future research on infrared-bright galaxies can proceed in several directions from this point. First, this study has provided, for the first time, high spatial resolution optical images of a large number of galaxies, many of which were previously uncataloged prior to IRAS. Many of these show structural evidence for gravitational interactions. Detailed studies of individual galaxies in this sample by use of broad band emission line mapping and near and far-infrared spectroscopy would give insights into the interaction/merger process, and how it affects star formation and nuclear activity.

Second, the question of non-thermal nuclear activity and how it is related to interactions and far-infrared emission was not addressed in this thesis. However, this sample would provide a good set for statistical comparisons of optical spectral characteristics with interaction parameters, to search for clues as to what kinds of interactions trigger non-thermal activity, and on what timescales. Further, near- and mid-infrared spectroscopy of individual galaxies in this study may provide evidence for obscured non-thermal nuclear activity in infrared-bright galaxies(*c.f.*, DePoy 1986; Becklin and Wynn-Williams 1986; Roche *et al.* 1986).

Lastly, the question of the evolution of the far-infrared luminosity function of galaxies can be further addressed by, first, a full-sky redshift survey of PSC IRAS galaxies, to reduce the uncertainty in the local luminosity function, and to determine the amount of clustering seen in IRAS galaxies. Such a survey is already underway (Strauss and Huchra 1988; Yahil 1988). Secondly, the IRAS Faint Source Catalog, which is in preparation at the Infrared Processing and Analysis Center, will provide statistics from a full-sky survey which reaches somewhat less deep as the Hacking and Houck (1986) sample, but with a much larger sample size. The source counts from this catalog will provide a more useful comparison for the evolutionary model results presented in this thesis. Further, a redshift survey of the 60 μm sources in the Faint Source Catalog will provide a more direct measure of the change in the 60 μm luminosity function as a function of redshift, without need for modelling. It would also provide a measure of the tendency of IRAS galaxies to cluster at deeper redshifts. Finally, when the next infrared astronomical satellite, the Space Infrared Telescope Facility (SIRTF), is launched, it will provide much greater sensitivity (a factor of 100 to 1000 over IRAS), a larger range in wavelength (2 – 700 μm), and higher spatial resolution.

APPENDIX

This Appendix outlines the method used to correct the IRAS flux densities to the rest frame of the galaxy, (K-corrected), and corrected for the shape of the spectral energy distribution within the IRAS 60 μm bandpass (color-corrected). The color-corrections account for the fact that the flux densities listed in the IRAS catalogs were calculated assuming an intrinsic spectral energy distribution of λ^{-1} within the bandpass. However, for galaxies, the spectral energy distribution is better approximated by a blackbody of temperature of 30K < T < 80K. This Appendix is a revision of the Appendix in SKHL.

The corrections applied in this paper were determined in a four-step process:

(1) The *total* flux in each of the 4 IRAS bands was computed by integrating the energy distribution that was assumed in the derivations of the IRAS flux densities,

$$F_i = S_i \lambda_i \int_0^\infty \frac{R(\lambda)}{\lambda} d\lambda,$$

where S_i is the uncorrected flux density and $R(\lambda)$ is the spectral response function.

(2) A look-up table of the total flux expected for blackbody sources of various

$$H_i = \int_0^\infty \frac{B(\frac{\lambda}{1+z}, T)}{(1+z)} R(\lambda) d\lambda,$$

where B = the Planck function.

(3) From the ratios of integrated flux densities, for a source at a known redshift with the look-up table, three color temperatures, T_1, T_2, T_3, corresponding to F(12)/F(25), F(25)/F(60), and F(60)/F(100), were deduced.

(4) The flux densities in the rest frames of the sources are then evaluated on the assumption that the spectral energy distributions in adjacent bands match those of

$$S_i = \frac{B(\lambda_i, T_i) F_i}{H_i}$$

where S_i is the flux density at the effective wavelength of band i in the rest frame of the source, and the temperatures T_i are T_1 for λ = 12 μm, $(T_1 + T_2)/2$ for λ = 25 μm, $(T_2 + T_3)/2$ for λ = 60 μm, and T_3 for λ = 100 μm.

BIBLIOGRAPHY

Arp, H.C. 1966, *Atlas of Peculiar Galaxies* (Pasadena: California Institute of Technology).

Avni, Y. 1976, *Ap.J.*, **210**, 642.

Becklin, E.E. 1986, in *Proceedings of "Star Formation in Galaxies" Conference*, ed. C.J.L. Persson, (Pasadena: California Institute of Technology), p. 753.

Becklin, E.E. and Wynn-Williams, C.G. 1986, in *Proceedings of "Star Formation in Galaxies" Conference*, ed. C.J.L. Persson, (Pasadena: California Institute of Techology), p. 643.

Boroson, T.A., Strom, K.M., and Strom, S.E. 1983, *Ap.J.*, **274**, 39.

Bothun, G.D., and Mould, J.R. 1987, *Ap.J.*, **313**, 629.

Bushouse, H.A. 1986, Ph.D. Dissertation, University of Illinois.

Butcher, H., and Oemler, A. 1978, *Ap.J.*, **219**, 18.

Butcher, H., and Oemler, A., 1984, *Ap.J.*, **285**, 426.

Chester, T.J. 1985, in *IRAS Conference Proceedings: Light on Dark Matter*, ed. F.B. Israel (Dordrecht, Holland: D. Reidel), p. 3.

Christian, C.A., Adams, M., Barnes, J.V., Butcher, H., Hayes, D.S., Mould, J.S., and Siegel, M. 1985, *Pub.A.S.P.*, **97**, 363.

Condon, J.J., Condon, M.A., Gisler, G., and Puschell, J.J., 1982, *Ap.J.*, **252**, 102.

Condon, J.J. 1984, *Ap.J.*, **287**, 461.

de Jong, T., *et al.* 1984, *Ap.J.(Letters).*, **278**, L67.

DePoy, D.L. 1986, in *Proceedings of "Star Formation in Galaxies" Conference*, ed. C.J.L. Persson, (Pasadena: California Institute of Technology), p. 701.

de Vaucouleurs, G., 1977, in *The Evolution of Galaxies and Stellar Populations*, ed. B.M. Tinsley and R.B. Larson, (Yale University Press: New Haven), p. 43.

de Vaucouleurs, G., de Vaucouleurs, A., and Corwin, H.R. 1976, *Second Reference Catalogue of Bright Galaxies*, (Austin: University of Texas).

Devereux, N. 1987, Ap.J., **323**, 91.

Dressel, L.L. and Condon, J.J. 1976, *Ap.J.Supp.*, **31**, 187.

Eisenhart, P.R.M., and Lebofsky, M.J. 1987, *Ap.J.*, **316**, 70.

Farouki, R.T., and Shapiro, S.L., 1982, *Ap. J.*, **259**, 103.

Franceschini, A., Danese, L., DeZotti, G., and Xu, C., 1987, preprint.

Gioia, I.M., *et al.* 1984, *Ap.J.*, **283**, 495.

Hacking, P. 1987, *Ph.D. Dissertation*, Cornell University.

Hacking, P. and Houck, J.R. 1987, *Ap.J. Supp.*, **63**, 311.

Haynes, M.P., and Herter, T. 1988, *A.J.*, **96**, 504.

Houck, J.R. 1984, *Ap.J.(Letters)*, **278**, L63.

Houck, J.R. 1985, *Ap.J.(Letters)*, **290**, L5.

Hacking, P., Condon, J.J., and Houck, J.R. 1987, *Ap.J.(Letters)*, **316**, L15.

Huchra, J.P. 1976, *A.J.*, **81**, 952.

Huchra, J.P., Davis, M., Latham, D., Tonry, J. 1983, *Ap.J.Supp.*, **52**, 89.

Huchra, J.P., and Geller, M.J. 1982, *Ap.J.*, **257**, 423.

IRAS Explanatory Supplement. 1986, eds. Beichman, C.A., Neugebauer, G., Habing, H., Clegg, P.E., and Chester, T.J., (Washington D.C.: U.S. Government Printing Office).

IRAS Faint Source Catalog. 1988, in preparation.

IRAS Point Source Catalog. 1985, Joint IRAS Science Working Group, (Washington D.C.: U.S. Government Printing Office).

IRAS Small Scale Structures Catalog. 1986, prepared by Helou, G. and Walker, D., (Washington D.C.: U.S. Government Printing Office).

Joseph, R.D., and Wright, G.S. 1985, *M.N.R.A.S.*, **214**, 87.

Joseph, R.D., Meikle, W.P.S., Robertson, N.A., and Wright, G.S. 1984, *M.N.R.A.S.*, **209**, 111.

Joy, M. 1986, *Ph.D. Dissertation*, University of Texas.

Keel, W.C., Kennicutt, R.C., Hummel, E., and van der Hulst, J.M. 1985, *A.J.*, **90** (5), 708.

Kennicutt, R.C., and Keel, W.C. 1984, *Ap.J.(Letters)*, **279**, L5.

Kleinmann, S.G., Cutri, R.M., Young, E.T., Low, F.J., and Gillett, F.C., *IRAS Serendipitous Survey*.

Kojoian, G., Elliot, R., and Tovmassian, H. 1981, *A. J.*, **86**, 811.

Koo, D.C. 1985, *A.J.*, **90** (3), 418.

Koo, D.C. 1986, Ap.J. **311**, 651.

Kron, R.G., Koo, D.C., and Windhorst, R.A. 1985, *Astron. Ap.*, **146**, 38.

Krumm, N., and Salpeter, E.E., 1977, *Astron. Ap.*, **56**, 465.

Larson, R.B., and Tinsley, B.M. 1978, *Ap.J.*, **219**, 46.

Lawrence, A., Walker, D., Rowan-Robinson, M., Leech, K.J., Penston, M.V. 1986, *M.N.R.A.S.*, **219**, 687.

Lebofsky, M.J., and Eisenhardt, P.R.M. 1986, *Ap.J.*, **300**, 151.

Longair, M.S. 1978, in *Observational Cosmology*, ed. A. Maeder, L. Martinet, and G. Tammann (Geneva Observatory), P. 125.

Lonsdale, C.J., and Hacking, P.B., 1988, *B.A.A.S.*, Vol. 19, No. 4, p. 1074.

Lonsdale, C.J., Helou, G. Good, J.C., and Rice, W.L. 1985, *Cataloged Galaxies and Quasars Observed in the IRAS Survey*, (Washington: US Goverment Printing Office).

Lonsdale, C.J., Persson, S.E., and Matthews, K. 1984, *Ap.J.*, **287**, 95.

Low, F.J., *et al.* 1984, *Ap.J.(Letters)*, **278**, L19.

Lynds, R., and Petrosian, V. 1972, *Ap.J.*, **175**, 591.

MacKenty, J.W., and Stockton, A. 1984, *Ap.J.*, **283**, 1984.

Markaryan, B.E., and Lipovetskii, V.A. 1971, *Astrofizika*, No. 2., 155.

Marshall, H.L., Avni, Y., Braccesi, A., Huchra, J.P., Tananbaum, H., Zamorani, G., and Zitelli, V., 1984, *Ap.J.*, **283**, 50.

Miley, G.K., Neugebauer, G., and Soifer, B.T. 1985, *Ap.J.*, **293**, L11.

Miller, R.H., and Smith, B.F., 1980, *Ap. J.*, **235**, 421.

Neugebauer, G., *et al.* 1984, *Ap.J.(Letters)*, **278**, L1.

Neugebauer, G., Soifer, B.T., and Miley, G.K. 1985, *Ap.J.Letters*, **295**, L27.

Nilson, P. 1973, *Uppsala General Catalog of Galaxies*, (Uppsala Astr. Obs. Ann., Vol. 6).

Noguchi, M., and Ishibashi, S. 1986, *M.N.R.A.S.*, **219**, 305.

Noguchi, M. 1987, submitted to *Astron. Ap.*

Palumbo, G.G.C., Tanzella-Nitti, G., and Vettolani, G., 1983, *Catalogue of Radial Velocities of Galaxies*, (New York: Gordon and Breach Science Publishers).

Peterson, S.D. 1973, *A. J.* **78**, 811.

Persson, C.J.L., and Helou, G., 1986, *Proceedings of "Star Formation in Galaxies" Conference*, ed. C.J.L. Persson, (Pasadena: California Institute of Technology), p. 153.

Press, W.H., and Schechter, P. 1974, *ApJ.*, **187**, 425.

Pierce, M.J., and Tully, R.B. 1988, *ApJ.*, **330**, 579.

Rice, W., Lonsdale, C.J., Soifer, B.T., Neugebauer, G., Kopar, E., Lloyd, L., de Jong, T., Habing, H.J. 1988, *Ap. J. Supp.*, submitted.

Rieke, G.H., *et al.* 1985, *ApJ.*, **290**, 116.

Rieke, G.H., and Lebofsky, M.J. 1979, *Ann. Rev. Astr. Ap.*, **17**, 477.

Rieke, G.H., and Lebofsky, M.J. 1986, *ApJ.*, **304**, 326.

Roos, N. 1981, *Astron. Ap.*, **95**, 349.

Roos, N. 1985a, *ApJ.*, **294**, 479.

Roos, N. 1985b, *ApJ.*, **294**, 486.

Rowan-Robinson, M., *et al.* 1984, *ApJ.(Letters)*, **278**, L7.

Sanders, D., Soifer, B.T., Elias, J.H., Madore, B.F., Matthews, K., Neugebauer, G., and Scoville, N.Z. 1988, *ApJ.*, **325**, 74.

Sandage, A., and Tammann, G.A. 1981, *A Revised Shapley-Ames Catalog of Bright Galaxies*, (Washington D.C.: Carnegie Institute of Washington).

Scalo, J.M., and Struck-Marcell, C. 1986, *ApJ.*, **301**, 77.

Schechter, P. 1976, *ApJ.*, **203**, 297.

Schild, R. 1984, *ApJ.*, **286**, 450.

Schmidt, Maarten, 1972a, *Ap.J.*, **176**, 273.

Schmidt, Maarten, 1972b, *Ap.J.*, **176**, 289.

Schmidt, Maarten, 1972c, *Ap.J.*, **176**, 303.

Schmidt, Maarten, and Green, Richard, F. 1983, *ApJ.*, **269**, 352.

Schombert, J.M., and Wallin, J.F. 1987, *A. J.*, **94**, 300.

Schweizer, F. 1976, *ApJ. Supp.*, **31**, 313.

Schweizer, F., and Seitzer, P. 1988, *Ap.J.*, **328**, 88.

Smith, B.J., Kleinmann, S.G., Huchra, J.P., and Low, F., 1987, *Ap.J.*, **318**, 161.

Soifer, B.T. *et al.*, 1986, *ApJ.(Letters)*, **303**, L41.

Soifer, B.T., Sanders, D.B., Madore, B.F., Neugebauer, G., Danielson, G.E., Elias, J.H., Lonsdale, C.J., and Rice, W.L. 1987, *ApJ.*, **320**, 238.

Solomon, P.M., and Sage, L.J. 1986, submitted to *ApJ.*

Stocke, J.T. *et al.* 1983, *ApJ.*, **273**, 458.

Stockton, A., and Bertola, F., 1980, *ApJ.*, **235**, 37.

Strauss, M.A., and Huchra, J.P. 1988, *A.J.*, **95**, 1602.

Tokunaga, A.T. 1986, *IRTF Photometry Manual*, (Honolulu: University of Hawaii, Institute for Astronomy).

Toomre, A. 1977, in *The Evolution of Galaxies and Stellar Populations*, ed. B.M. Tinsley, and R.B. Larson (Yale University Press: New Haven), p. 401.

Toomre, A., and Toomre, J. 1972, *Ap.J.*, **178**, 623.

Tully, R.B., and Fisher, R. 1977, *Astron. Ap.*, **54**, 661.

Tyson, J.A., and Jarvis, J.F. 1979, *Ap.J. (Letters)*, **230**, L153.

Vader, J.P., and Simon, M. 1986, *Proceedings of "Star Formation in Galaxies" Conference*, ed. C.J.L. Persson, (Pasadena: California Institute of Technology).

von Hoerner, S., 1973, *Ap.J.*, **186**, 741.

Weedman, D.W., Feldman, F.R., Balzano, V.A., Ramsey, L.W., Sramek, R.A., and Wu, C. *Ap.J.*, **248**, 105.

White, S.D.M. 1979, *M.N.R.A.S.* **189**, 831.

Wolstencroft, R.D., Clowes, R.G., Kalafi, M., Leggett, S.K., MacGillivray, H.T., Savage, A. 1986, in *Proceedings of Light on Dark Matter Conference.*

Wright, A.E. 1972, *M.N.R.A.S.*, **157**, 309.

Yahil, A. 1987, in *Proceedings of the Vatican Study Week on Large Scale Motions in the Universe.*

Yahil, A., Walker, D., Rowan-Robinson, M. 1986, *Ap.J. (Letters)*, **301**, L1.

Young, J.S., Kenney, J., Lord, S.D., and Schoerb, F.P. 1984, *Ap.J.*, **287**, L65.

Young, J.S., Kenney, J.D., Tacconi, L., Claussen, M.J., Huang, Y.-L., Tacconi-Garman, L., Xie, S., Schloerb, F.P., 1986, *Ap.J. (Letters)*, **311**, L17.

Young, J.S., Kleinmann, S.G., and Allen, L. 1988, submitted to *Ap.J.*

Young, J.S., Schloerb, F.P., Kenney, J.D., and Lord, S.D. 1986, *Ap.J.*, **304**, 443.

Young, J.S., Xie, S., Kenney, J.D., and Rice, W.L. 1988, submitted to *Ap.J.*

Zwicky, R., Karpowicz, M., Kowal, C., Herzog, E., and Wild, P., 1961-1966, *Catalog of Galaxies and of Clusters of Galaxies*, (Pasadena: California Institute of Technology), Vols. 1–6.